duplicate

Glaser

Schwan

12TH ANNUAL CONFERENCE ON ELECTRICAL TECHNIQUES IN MEDICINE AND BIOLOGY

NOV. 10-11-12, 1959

DIGEST OF TECHNICAL PAPERS

HOTEL SHERATON, PHILADELPHIA 3, PA.

Sponsored by: Institute of Radio Engineers,

American Institute of Electrical Engineers and Instrument Society of America

Glaser

12TH ANNUAL CONFERENCE ON ELECTRICAL TECHNIQUES IN MEDICINE AND BIOLOGY

DIGEST OF TECHNICAL PAPERS

First Edition

November, 1959

Publisher: Lewis Winner, New York 36, N. Y.

12th Annual Conference on Electrical Techniques in Medicine and Biology

Digest of Technical Papers

PRINTED IN THE UNITED STATES OF AMERICA

Preface

THE ANNUAL conferences on electrical techniques in medicine and biology have traditionally covered a wide range of topics, all concerned with the area between electrical engineering, medicine and biology. A particularly strong activity in this total field is the interaction of electronics with the biomedical area, thus defining what may appropriately be called "Biomedical Electronics". However, we must point out that areas in electrical engineering other than electronics have also in the past contributed to the general field of interest to us. An important example is presently available X-ray equipment and associated instrumentation, with its long established major role in both the diagnostic and therapeutic medical area. Other major areas associated with electrical techniques, as applied to medicine and biology, can readily be formulated.

In all such cases it is possible to differentiate between two major areas: The development of electrical instrumentation for either therapeutic or diagnostic purposes and biological research, and the application of scientific principles concerned with electricity and magnetism to medical and biological problems. While the importance of the former is obvious, the latter is often not clearly recognized. A careful investigation shows that the establishment of basic principles is found to be a prerequisite to the successful development of instrumentation. Thus, the detailed knowledge of the factors which determine electrical characteristics of biological matter is most helpful in order to "match" instrumentation to the biological object.

It has been a good custom during these conferences to concentrate on major themes. These themes could concern either primarily instrumentational topics or more basic problems. Since in the past the former have been usually of primary interest, we decided to continue a pattern which in good part was set during the successful Minneapolis meeting of 1958. Since it has not been the subject of any major symposia or previous meetings, it was decided this year to concentrate particularly on the interaction of various forms of predominantly non-ionizing radiation with biological matter. This involves both acoustic and electromagnetic radiation, in the second case extending from radio frequencies to ultraviolet. The papers are related in part to the interaction of the physical agent with biological matter and in part with the utilization of such interaction for analytical purposes. Pertinent instrumentation plays, of course, a major role. In addition, we have, as customary, the "general" sessions which have been organized from that part of the contributed papers which does not fall in above mentioned categories. They form always an important part of the annual conferences in keeping with our tradition of providing a forum for presentation of all material in the borderline area between the biomedical and electrophysical fields. Thus, we hope that the present meeting fulfills its traditional purposes of being of interest to biologists, medical doctors, physicists and electrical engineers, and encouraging cross fertilization among the various fields.

H. P. Schwan
Conference Chairman

Table Of Contents

Tuesday, Nov. 10, 1959: 10:00 A.M.

SESSION I: Ultraviolet Radiation I

West Ballroom

SESSION II: Cardiovascular I

Independence-Constitution Rooms

Tuesday, Nov. 10, 1959: 2:00 P.M.

SESSION III: Ultraviolet Radiation II

West Ballroom

SESSION IV: General I

Independence-Constitution Rooms

Wednesday, Nov. 11, 1959: 9:00 A.M.

SESSION V: Microwave Radiation I

West Ballroom

SESSION VI: Ultrasonic Radiation I

Independence-Constitution Rooms

Wednesday, Nov. 11, 1959: 2:00 P.M.

SESSION VII: Microwave Radiation II

West Ballroom

SESSION VIII: Ultrasonic Radiation II

Independence-Constitution Rooms

Thursday, Nov. 12, 1959: 9:00 A.M.

SESSION IX: Infrared Radiation I

West Ballroom

SESSION X: General II

Independence-Constitution Rooms

Thursday, Nov. 12, 1959: 2:00 P.M.

SESSION XI: Infrared Radiation II

West Ballroom

Index to Authors

SESSION I: Ultraviolet Radiation I

Chairman, J. Schultz,
The Institute for Cancer Research, Philadelphia, Pa.

1.1: General Problems of Absorption Measurements in the Cell

B. Thorell, Karolinska Institutet, Stockholm, Sweden.

Absorption Measurements in the cell aim at the *in-loco* analysis and quantitation of different biological substances. Ultimately, records of changes in the states or amounts of these substances during physiological conditions will enable us to investigate reactions within the single, living cell or parts thereof. The principal difficulties are encountered by the small dimensions of the cell structures and the complex distribution pattern of their reactive substances.

The lower limit of the size of structures to be analyzed by absorption measurements in the optical part of the spectrum is set by the resolving power of the energy-collecting system which is given by $\lambda/2\,NA$, where λ is the wavelength and NA represents the numerical aperture of the optics used.

The smallest amount of a substance to be quantitated by absorption measurement is set by the absorption coefficient of the substance at the wavelength used (k), its actual concentration (c) and the length of absorbing path (l) within the object. This is expressed in the law of *Lambert-Beer*: $E = k \cdot c \cdot l$, where E (the extinction or optical density) can be measured within the range of 0.001—1.0, with maximal accuracy occurring at 0.3.

To determine the absorption constants within small objects with magnifying instruments which include dioptric or catoptric systems, the distribution of the intensity in the image given by the lenses or mirrors shall correspond to the distribution of the intensity in the object. A microscopic lens produces a true image of an illuminated object, only if it has an aperture large enough to transmit the whole diffraction pattern produced by the object (grating). It can be shown that for a numerical aperture (*N. A.*) equal to 1.5 and a grating with a slit width of 2λ, 99% of the light intensity participates in the image formation.

In cell material, however, particle sizes smaller than the value of 2λ are often encountered. The light-scattering effect displayed by such, often complex and polydisperse, particle systems may be impossible to express in general terms and may thus introduce errors. A monodisperse system of spherical particles can be treated according to *Mie*'s theory, where the total radiation field of the spherical particles is represented by dipoles or higher poles having the center of sphere as their origin. When the particle size is small ($r<1/10\,\lambda$) the scattered radiation is reduced to *Rayleigh*'s expression, represented by Figure 1*A*. As the particle size is increased, the scattered radiation is more in the "forward" direction (Figure 1*B*) and the energy which falls outside the collecting microscope optical system may finally be negligible. Interestingly, as has been pointed out by *Caspersson*, the treatment according to the *Abbe* diffraction theory of the microscopic image formation as well as the *Mie*'s theory of light scattering give essentially the same results; absorption measurements of radiant energy can be performed on objects the size of which is more than 2 times the wavelength used.

Light scattering together with multiple reflection may give rise to varying optical path length through absorbing cell structures. Figure 2 shows such a phenomenon in a model experiment. Some other complications of absorption measurements in the cell will be discussed more briefly, as they are met with only in rather special material. Anomalous dispersion around absorption maxima may occur when substances having a large k are present in high concentrations. Orientation and dichroism as shown by the long chains of some high molecular substances will introduce a systematic error, depending on the ratio of transmission between the different components of the incident light.

Refraction and reflection phenomena due to the gross shape of the cell or boundaries within the cell (nuclear membranes, etc.) can sometimes cause considerable "unspecific" losses of light. Media with matching refractive index might be employed to minimize such effects. These can in most cases also be treated with ordinary geometrical optics.

In addition to these general physico-optical problems, the microspectroscopist will also face problems of a more technical nature. The use of magnifying optical systems with large apertures leads to very small amounts of radiation energy per surface unit in the plane of the image. High sensitivity receptors with enough stability must therefore be used to record the light intensities. The cell-material itself also presents varying conditions for the measuring technique. Biological substances may be present in high concentration in which case absorptions between 10 and 90% have to be measured. Or substances may be present at "enzyme" concentrations which requires quite another range of maximum sensitivity of the energy-recording system. Examples are presented in Figures 3 and 4.

Figure 5 illustrates the general setup of a recording microspectrograph. In the photomultiplier-amplifier system, dynode-feedback and measuring circuits can be adapted for measurements of small photocurrents at rather high signal-to-noise ratios. Recent development of these techniques has made possible studies of the kinetics of enzyme reactions within small parts of the single, living cell.

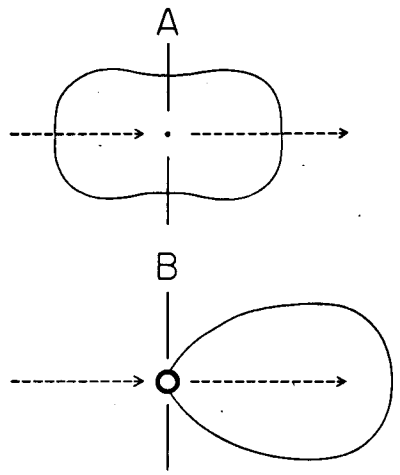

Figure 1—distribution of radiation around an infinitely small particle (A) and a large particle (B). The figures show longitudal sections of the "radiation bodies" or isointensity envelopes of emergent light around the incident light beams represented by the arrows.

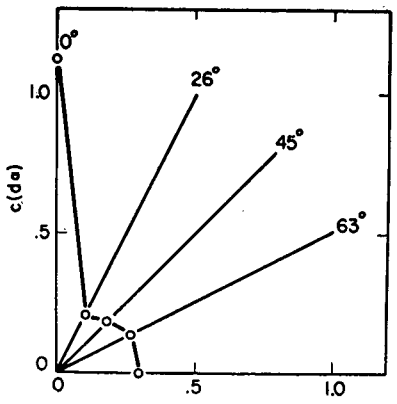

Figure 2—The effect of multiple scattering on the light absorption maximum of a hemoglobin solution which is made turbid by mastic. The incident light bundle (cross section area 0.1 mm²) fell perpendicular to the axis of a cylinder cuvette (diameter 10 mm). Light intensity measurements were made at angles varying from 0° to 90° to the plane of the incident beam; c = concentration, d = thickness of absorbing layer, and α = absorption coefficient. The apparent absorption coefficients were calculated from the ratios of the light intensities scattered from the cuvette with and without hemoglobin in the scattering liquid. The results (in polar coordinates) show changes in absorption up to 5 times those calculated from the measurements at 0°.

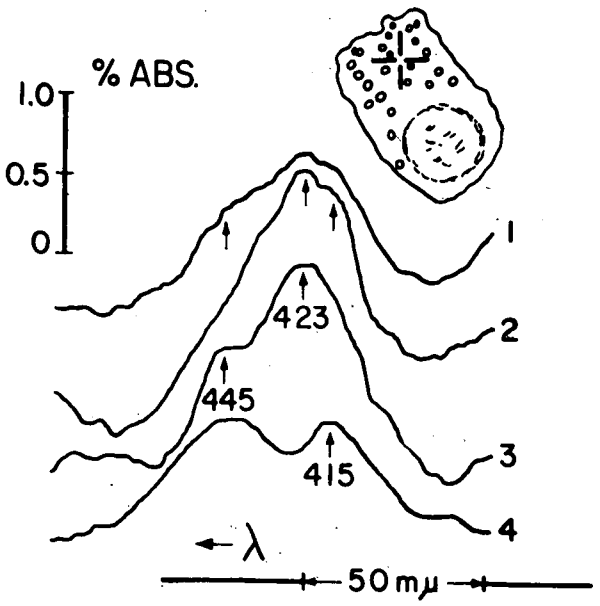

Figure 4—Absorption spectra from adjacent sites in the cytoplasm of an anaerobic kidney cell. The location of the four different areas measured correspond approximately to the four arms of the cross. Absorption maxima of respiratory pigments present at "enzyme concentrations."

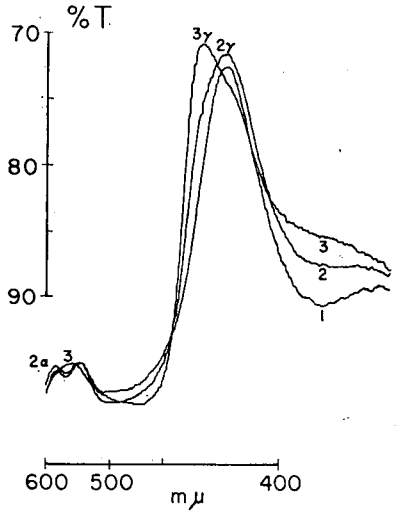

Figure 3—Group of absorption spectra taken during the reduction of the hemoglobin (concentration about 30%) in a single red blood cell.

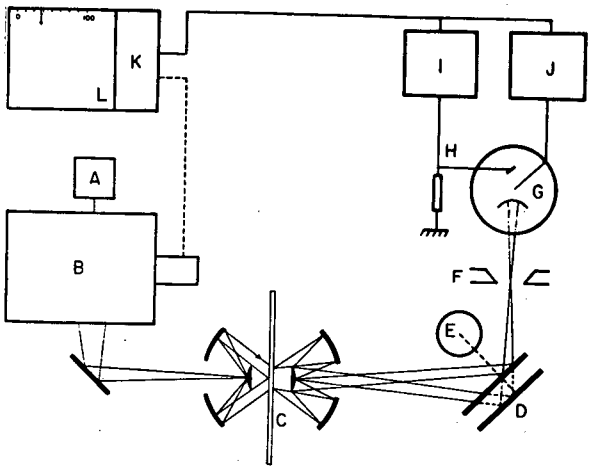

Figure 5—Scheme of a recording microspectrophotometer: *A*, light source; *B*, monochromator; *C*, microscope optics; *E*, vibrator connected to the plane mirrors (*D*) vibrating in a plane perpendicular to the paper; *F*, slit system shielding off the reflected, alternating "measurement" and "blank" parts in the microscopic image; *G*, photomultiplier; *H, I, J*, dynode-feedback and measuring-amplifier system; *K, L*, recorder.

SESSION I: Ultraviolet Radiation I

1.2: The Application of Ultraviolet Absorbance Measurement to Problems in Cell Biology

George Rudkin, The Institute for Cancer Research, Philadelphia, Pa.

SINCE RADIATION must be absorbed to have an effect, it has been possible to identify those substances damaged by ultraviolet radiation by comparing absorption spectra with action spectra. A study of the distribution of the target substances within cells, in relation to the known functions of the organelles within which they are found, may yield a new insight into a function as well as the radiation damage to that function. Both types of analysis are possible in the ultraviolet between 230 and 400 millimicra where nucleic acids have a broad absorption band near 260 millimicra and many proteins absorb, but much more weakly, at 280 millimicra. The problem of measuring absorption will be considered in this paper.

The instrumentation problem centers around the measurement of the absorption of radiation by a cell structure that may be several microns in any dimension, but which is typically made up of smaller sub-units. It is necessary to drive enough energy in the form of monochromatic radiation through an area of about one square micron to obtain an acceptable signal-to-noise ratio in the detection system, after the inevitable losses have been incurred in the optical path. We still consider only instruments based on conventional microscopes in which the specimen is illuminated through a condenser and imaged onto a detector. Special sources of high *UV* output are used, most of which utilize elements whose emission spectra are rich in *UV* lines, but the recently developed xenon arc, provides a high intensity continuum down to 240 millimicra. Suitable monochromators are available, even specifically designed for illuminating ultraviolet microscopes. Microscope optics are still a problem; one has a choice between high-aperture quartz refractors corrected at a single wavelength and reflecting type lenses that have lower aperture, transmission and resolving power, and also have the central beam obscured, but which possess the tremendous advantage of being achromatic. Refracting achromats are being developed. Several types of detection system are in current use. The photographic plate and the photomultiplier tube are old standbys, while the newer television type detectors, the vidicon and the image orthicon, have been recently put to use in the *UV*. Focussing and centering the object in the measuring beam have been made both easy and precise by the vidicon, and most recently by a less expensive *UV*-image converter tube. An extremely wide variety of data presentation has been designed, the simplest being a meter reading proportional to intensity and the most complex an electronic computer that types out the absorbance values for hundreds of points in the object.

Given a working instrument, it is necessary to show that optical conditions within the object to be measured will not introduce errors.

Caspersson's original application of the method was to show that the absorption spectra of cellular organelles *in situ* could be derived by summation of the spectra of compounds isolated from cells and measured *in vitro*. He could then show where in the cell the nucleic acids and the proteins were distributed. By digesting away the protein with specific enzymes, he confirmed the spectrophotometrically-determined distribution. Analogous methods have since been used to study nucleic acid metabolism. However, quantitative analysis of absorption curves has met with the difficulty that the required constants, the absorptivities of the compounds *in situ*, have not been determined. Rough analyses based on constants determined *in vitro* are subject to errors which may easily be as high as 100 per cent in the calculation of the nucleic acid-protein ratio. However, absorption curve analyses may prove useful as a tool for studying the molecular interactions between compounds complexed into the different intracellular structures.

In those rare cases in which an organelle is homogeneous and has a simple geometric shape, the total absorbance of the structure can be calculated from the absorbance determined at a single spot on it and its volume. In general, however, it is necessary to scan the object with a narrow probe of radiation and sum the values over its entire area. Three systems are in current use: *1)* scanning the image with a detector, *2)* moving the object while the rest of the system remains stationary, and *3)* scanning the object with a moving pencil of radiation. Used in one of these ways at a single wavelength, the microphotometer becomes an instrument for microassay.

Notes

SESSION I: Ultraviolet Radiation I

1.3: Evaluation of Radiation Change in the Ultraviolet Microscopy of Living Cells

Jerome J. Freed and James L. Engle, The Institute for Cancer Research, Philadelphia, Pa.

THE PARTICULAR ADVANTAGE of the ultraviolet microscope, as compared to the phase and interference microscope systems, lies in the possibility of using it to obtain quantitative estimations of cell constituents by the method of absorption spectrophotometry (cytospectrophotometry); it is thus tempting to consider the use of the ultraviolet cytospectrophotometric method in studies on living cells. The recent development of electronic, and especially of television, techniques of ultraviolet-image detection has increased the sensitivity of the ultraviolet microscope to a point which permits study of individual living cells by the time-lapse film method. Such a system used as a cytospectrophotometer might permit direct sequential study of physiological processes within individual cells if these involved changes in amount or distribution of ultraviolet absorbing compounds e.g., the synthesis of deoxyribonucleic acid in the interphase nucleus. The main problem in carrying out such measurements is that of obtaining a sufficiently high signal-to-noise ratio without inducing artifacts caused by radiation damage.

Radiation-induced artifacts of importance for this work may be considered to be of two types: structural and physiological. The first type is observed with rather high radiation doses, and may be defined as a change induced by radiation which results in the destruction of the object being studied. For example, ascites tumor cells in slide cultures, when irradiated, show severe blebbing followed by swelling. The latter effect represents a complete loss of cellular integrity; it is irreversible. Similarly, grasshopper spermatocytes irradiated at the first meiotic metaphase apparently undergo a complete destruction of the spindle, so that the chromosomes move at random in the cell and no division occurs.

With lower doses of radiation, typical of the level required for television systems, physiological artifacts are more likely to occur. These involve interference with physiological processes of the cell without apparent structural change. For example, prophase cells of newt heart endothelium will return to an interphase condition if exposed to radiation doses which are apparently without effect on interphase cells. Moderate irradiation of newt-heart cells in interphase may result in the cessation of pinocytosis and the inhibition of normal cell movement on the substrate.

Variation in susceptibility to radiation-induced artifacts may be influenced by changes inherent in the cells themselves. In ascites tumor slide cultures large cells, probably polyploid in nature, are considerably more radiation sensitive in the interphase than are the cells of normal size. Also, cells obtained a few days after inoculation are rather more susceptible than cells removed at the end of ten days. These latter cells are cytologically indistinguishable from the former. Finally, it may be pointed out that the sensitivity of the cells varies greatly depending upon the ultraviolet wavelength employed, following the action spectrum of the particular inactivation process which is involved.

It is thus apparent that it may be impossible to design a microscope system safe for all work with all living cells in the ultraviolet. If there is no general threshold level, then the possibility of artifact must be carefully controlled by parallel experiments using the phase contrast or interference microscopes, or by the use of unirradiated cells in the experimental preparation as controls.

The feasibility of absorption spectrophotometry of living cells in the ultraviolet thus depends strongly on the use of a microscope system of the highest possible efficiency. Efficiency may be defined as the factor relating the signal-to-noise ratio obtained to the dose incident on the cell. Of the various television systems proposed for use in ultraviolet microscopy, the flying-spot system offers the highest efficiency, together with relative simplicity of the associated circuitry for obtaining absorption measurements. The main disadvantage of presently-available flying-spot systems lies in the shortcomings of ultraviolet-scanner tubes, which permit little control of wavelength and spectral resolution. If the flying-spot principle is retained, but a mechanical-raster generator is used with a conventional source consisting of arc lamp and monochromator, this disadvantage may be overcome. Such a system is now being constructed, and will be evaluated for use as a cytospectrophotometer.

Notes

SESSION II: Cardiovascular I

2.1: Phase Space Display of Vectorially-Resolved Electrocardiograms

Otto Schmitt, University of Minnesota, Minneapolis

CONSIDERABLE ATTENTION has recently been devoted to the orthogonalization and normalization of electrocardiographic lead systems and to analyses of the influences of position and orientation of contributory dipole-current moment sources on the normal and abnormal electrocardiograms recorded in these various leads. Less attention has been paid to evolving displays of the electrocardiogram, which will automatically emphasize features of the potential variation in a selected lead, or leads which are rich in clinical diagnostic and theoretical significance.

Drawing upon the concept of a phase space which has been so productively used in theoretical physics and in the engineering analysis of feedback systems, a series of electrocardiographic displays is being developed which promises to offer more intuitively obvious insight into heart function.

Basically, the concept of a phase space assigns to a chosen number of spatial coordinates the attributes of a similar group of variables, so that each point in the phase space becomes identified with a specific value of each of the coordinate variables. In our *ECG* case we have chosen a phase space of three orthogonal coordinates, which is convenient because it can easily be identified with a conventional *Cartesian* space and because a display of potential in such a coordinate system can conveniently be seen in our *SVEC* stereoscilloscope and can be spatially reresolved with the conventional *SVEC* resolver.

As an initial effort we have assigned to the three coordinate axes, respectively, the electrocardiographic potential function itself, its time derivative, and its time integral, thus yielding a space similar to that in which servomechanism function loci are studied. The rationale behind this choice, beyond the formal mathematical attractiveness of the system, depends upon the simple physiological significance that can be assigned to the variables.

In simple language, the derivative function can be thought of as identifying, along the function variable, the points where changes occur, while the integral represents cumulative processes to any specified point. Indeed some cardiologists attribute substantial importance to the "ventricular gradient" integral.

Experimentally, the space figures representing this primitive phase display show highly characteristic patterns quite sensitive to many of the detailed pattern features of the electrocardiogram ordinarily measured. A sample set of patterns (not all plotted to uniform scale) is shown for basic illustration. The electrocardiogram chosen for illustration is an SVEC III X-lead from a normal healthy young man; Figure 1. This is an orthogonalized horizontal lead. The loop patterns, Figures 2 and 3, are not vector cardiograms in the ordinary sense, but are patterns displaying, respectively, the derivative against function and function against integral. The two loop patterns thus give projections on two principle planes of the spatial phase diagram. Further study will show the range and kinds of variability in these phase displays for populations of normal and abnormal individuals and the sensitivity with which clinical abnormality is evidenced.

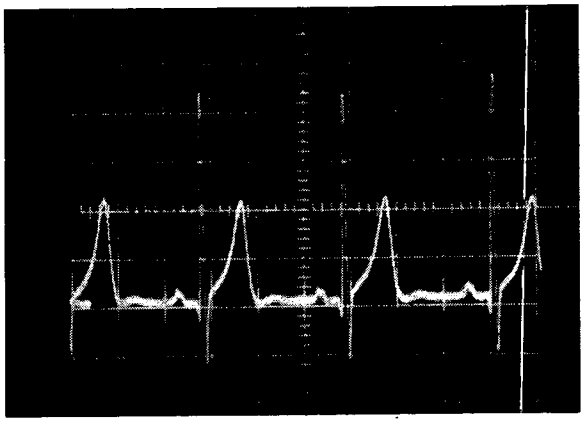

Figure 1—Electrocardiogram SVEC III X-lead from a normal healthy young man.

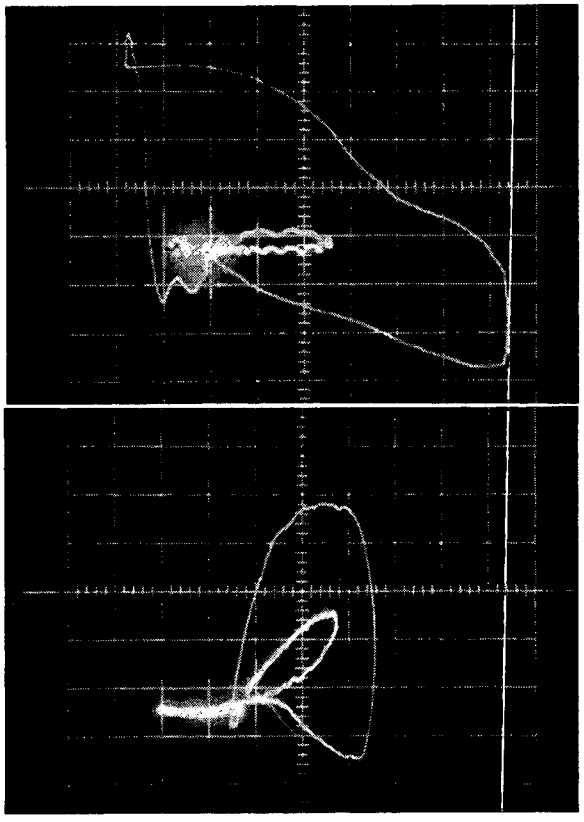

Figures 2 and 3—Patterns displaying, respectively, the derivative against function, and function against integral.

SESSION II: Cardiovascular I

Chairman: Robert L. Bowman,

National Heart Institute, National Institutes of Health, Bethesda, Md.

2.2: A Comparison of the Arrival in the Cerebral Hemispheres of Intravenously Injected Radioisotope

W. H. Oldendorf, Veterans Administration Center, Los Angeles, California

A TECHNIQUE has been devised in which the radioisotope concentration in each cerebral hemisphere is monitored by a collimated detector for 60 seconds after injection of radioisotope into an arm vein. Radioiodine labeled *Diodrast* is used because it is rapidly excreted in the urine and virtually all of the injected material can be voided at the end of one hour. This limits the total body radiation to about ten milliroentgens for the dose we use. It also allows frequent repetition of the test. The test is simple to administer, quite painless and extremely safe.

The test produces a pair of curves representing the volume of blood flow in one cerebral hemisphere relative to the other. That such a test might be of clinical value was suggested by analysis of multiple exposure serial cerebral angiography. These studies have shown that, in addition to the displacement and abnormal structure of vessels in the brain, there is a considerable alteration in rate of filling of the brain in many disease processes. Thus, a technique which had poor spatial resolution might still be of considerable value if it could differentiate one cerebral hemisphere from the other and could document the rate of blood flow in each. On this supposition, this technique was developed and a preliminary evaluation carried out.

It was shown that an intravenous injection of radioisotope into a distended arm vein, with subsequent sudden release of venous obstruction, resulted in a bolus of radioisotope which remained discrete enough to be clinically valuable after passing through the heart, lungs and great vessels to the head.

When performed on five normals, the curves were very similar. Compressing the common carotid artery on one side during the test resulted in a redistribution of blood flow which was clearly evident in the curves. Spontaneous carotid occlusion in three cases studied is well demonstrated. One arteriovenous malformation in which there was a greatly increased flow showed markedly asymmetrical curves, much higher on the abnormal side. One large aneurysm and one intracerebral hematoma have also been documented.

It is anticipated that several other conditions will commonly show abnormalities in this test. Some of these are unilateral neoplasms, subdural and extradural hematoma, arteriovenous malformations and major vessel occlusions.

The test will be of value primarily as a screening test for cerebral angiography because of its simplicity, safety and repeatability.

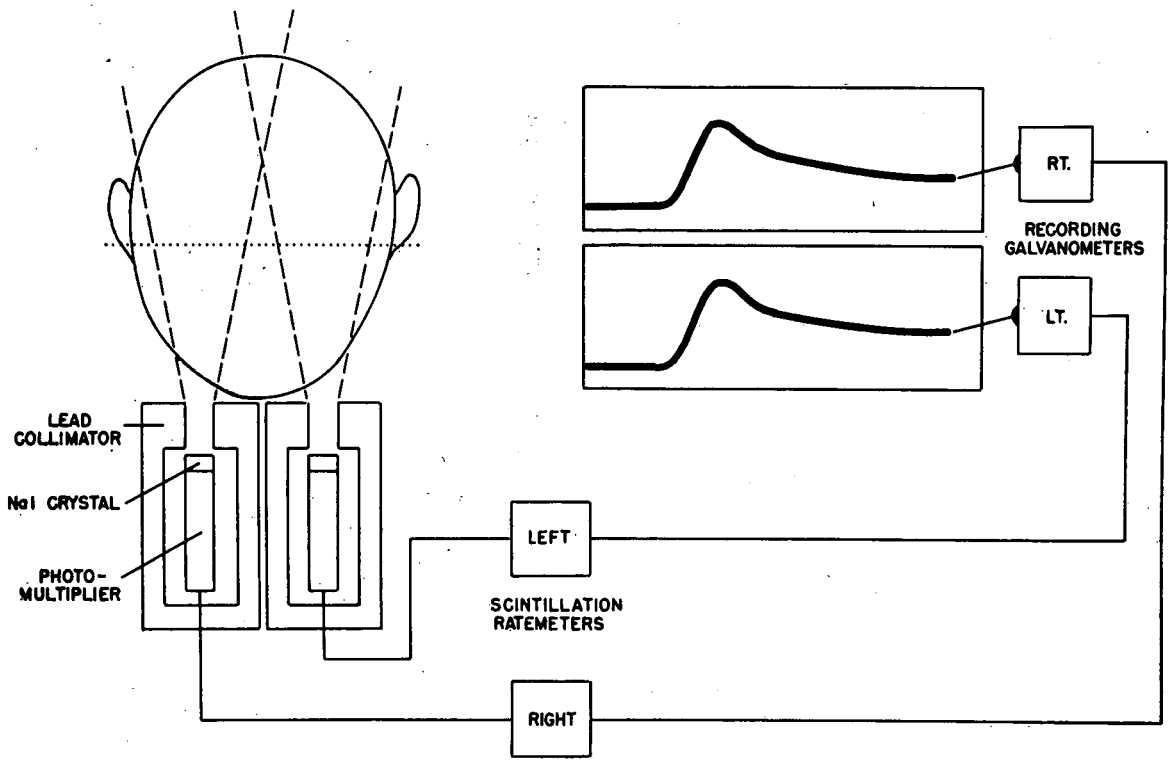

SESSION II: Cardiovascular I

2.3: Blood Flowmeter Utilizing Nuclear Magnetic Resonance

Robert L. Bowman and Vsevolod Kudravcev, Laboratory of Technical Development, National Heart Institute, Bethesda, Md.

THIS PAPER will present a consideration of the use of nuclear magnetic resonance for the measurement of blood flow; preliminary experimental results encourage a belief in the feasibility and relative simplicity of the projected method.

The principle of *NMR* may be briefly described as follows: When a substance is placed in a combined *dc* magnetic field and perpendicular *rf* field, it will absorb *rf* energy of a characteristic frequency if it contains atoms whose nuclei have magnetic moments (such as hydrogen). This absorption is due to induced transitions between energy levels of the spinning nuclei in the magnetic field and will occur at a frequency determined by the product of the *dc* field strength and the gyromagnetic ratio (defined as the magnetic moment of the nucleus divided by its angular momentum). The hydrogen nucleus gives an especially strong *NMR* signal which is suitable for observation in biological systems and occurs in a convenient frequency range, about 5 to 30 megacycles for practical magnetic field strengths.

The times required for interaction between the applied fields and the nuclei may vary in liquids from about a millisecond up to several seconds, depending principally on such things as the presence of paramagnetic molecules, temperature, viscosity and molecular composition. Conditions can be arranged so that these times are comparable to the time required for a nucleus in a flowing liquid to pass through the resonance region, so that the degree of interaction is limited by flow rate.

For use in *NMR* blood-flow measurements, an instrument was constructed consisting of two basic units; a magnetron magnet containing in its gap a glass flow-tube inside an *rf* coil, and an electronics unit having high sensitivity and stability. The electronics unit consists of an oscillator-detector, low-frequency function generator, modulation amplifier, regulated power supply, and control panel. The oscillator-detector is a multi-purpose device designed to be capable of measuring flow under a variety of conditions by several different *NMR* methods: resonance absorption desaturation, or nuclear induction (emission) at a fixed point downstream, or variations of these methods. It can be operated from 1 to 30 Mc as a crystal-controlled *rf* generator or a marginal oscillator or a super-regenerative oscillator, and includes automatic frequency and *rf* level controls. A transistorized form of the entire flowmeter is shown in Figure 1.

The overall performance of the apparatus is such that a strong and relatively stable signal is obtained over the range from a small fraction of 1 cc/minute up to 350 cc/min of liquid flow through a tube of 1-cm diameter. Adjustment of the various circuit parameters, from the control panel, allows one to obtain maximum sensitivity of *NMR* signal response to flow rate, under a variety of conditions, while retaining high enough reproducibility to permit the use of calibration curves directly without appreciable error.

The exact nature of the relationship between the *NMR* absorption signal and the flow rate depends on saturation effects, relaxation processes, and to some extent on the geometrical arrangement of coils and magnetic field. Under one set of conditions, where static saturation has been achieved in the sample by a high *rf* level, the *NMR* signal may *increase* (Figure 2) as the flow rate increases. Under another set of conditions, where the *rf* level has been adjusted to give maximum signal with no flow, the signal may decrease (Figure 3) as the flow rate increases. For practical purposes, the important thing is that there exists, for any particular set of circuit parameters, a reproducible relationship between the flow rate and the *NMR* absorption signal.

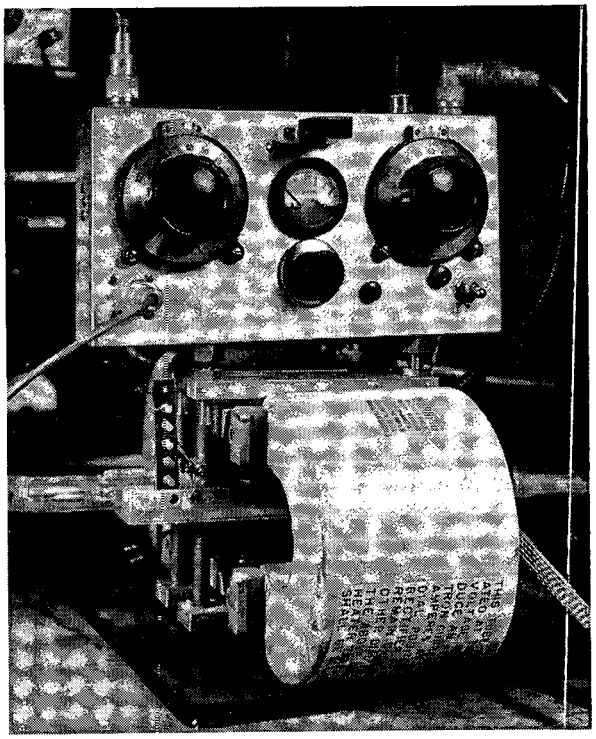

Figure 1—Transistorized version of *NMR* flowmeter.

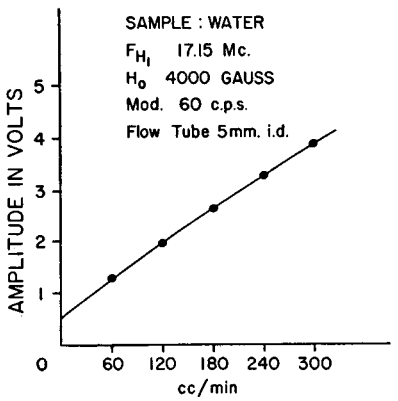

Figure 2—Increase of *NMR* signal with increasing flow rate (high *rf* level).

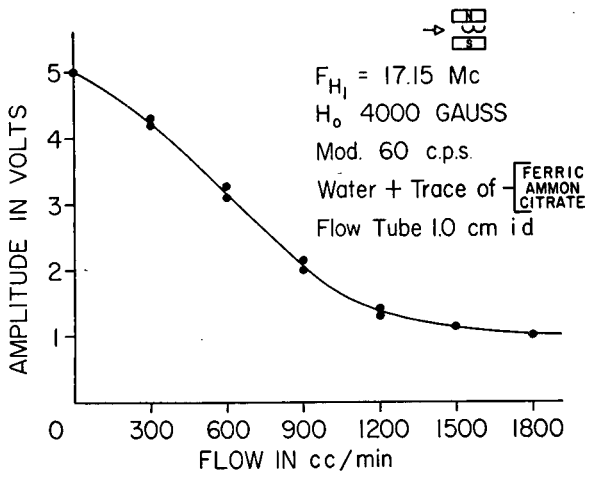

(*Right*)
Figure 3—Decrease of *NMR* signal with increasing flow rate (*rf* level adjusted for maximum signal at zero flow).

SESSION II: Cardiovascular I

2.4: Application of Magnetic Resonance Phenomena to Biological Problems Including Measurement of Blood Flow

J. R. Singer, Division of Electrical Engineering, University of California, Berkeley, Calif.

THE LONGITUDINAL RELAXATION time of nuclei or electrons observed in paramagnetic resonance experiments is phenomenologically described by the *Bloch* equations[1]. *Bloch* introduces a characteristic time T_1 which denotes the time needed for a set of paramagnetic spins to reach within 1/3 of the equilibrium magnetization. The present paper is concerned with observations of flowing fluids. In such a situation, the paramagnets will not, in general, spend sufficient time in the magnetic field to achieve a static (non-flowing) equilibrium magnetization. Therefore observations upon such flowing fluids provide an "apparent relaxation time" $(T_1)'$ which is shorter than the static relaxation time.

The interest in these relaxation time measurements stems from several sources: *(1)*—The flow rate of fluids may be measured by the difference in relaxation time, *(2)* — the static relaxation time may be accommodated to more simple measurement techniques. The author is mainly interested in flow rate measurements. Such measures are of considerable importance in accurately measuring human and animal blood flow velocities without breaking the skin. In addition, the system may be used for many other industrially important flow measures where non-interference with the normal channel is required.

Amplitude Effects of Flow

One procedure consists of measuring the relaxation time indirectly by determination of the saturation parameter. This scheme provides a very fast measurement, and is particularly useful when the flow rate varies with time since the variation may then be measured. In particular, the method has important application to measuring blood flow at much faster intervals than the heart pump rate. This may be accomplished by the method described below.

When measuring magnetic resonance absorption with an *rf* level sufficient to approach saturation levels, the absorption level is reduced by a factor Z given by

$$Z = [\,1 + (1/2)\,\gamma^2 H_1^2 T_1 g(\nu)\,]^{-1} \qquad (1)$$

where γ is the gyromagnetic ratio of the spins, H_1 is the *rf* magnetic field, $g(\nu)$ is the shape function of the resonance line, and T_1 is the longitudinal relaxation time. For convenience we define

$$Z = [\,1 + sT_1\,]^{-1} \qquad (2)$$

with obvious relationships to equation *(1)*.

If the observed material is a flowing fluid, the saturation factor is

$$Z = \left[1 + \frac{sT_1L_r}{L_r + T_1\bar{V}}\right]^{-1} \qquad (3)$$

where L_r is the length of flow channel in the effective *rf* field, and $\bar{V}$ is the average flow velocity. Consequently, the amplitude of a partially-saturated signal is increased with more flow velocity. If the amplitude of the resonance absorption without flow is denoted by A, and that with flow by A_f, a convenient equation to describe the flow velocity is

$$\frac{A_f - A}{A} = \frac{s\left[1 - \dfrac{L_r}{L_r + \bar{V}T_1}\right]}{1 + s\left[\dfrac{L_r}{L_r + \bar{V}T_1}\right]} \qquad (4)$$

Certain assumptions are implicit in this equation; these will now be explicitly enumerated:

(1) The flowing spins are in the magnetic field long enough to reach their equilibrium magnetization before entering the resonance absorption region. (Otherwise a comparison of amplitudes requires a more complicated expression.)

(2) No extraneous material exhibits resonance absorption, i.e., the measurement involves only the absorption due to a fluid at rest and then in motion.

In the case of biological measurements, the second assumption is not always justifiable. If we consider proton absorption, the normal water in the tissues provides absorption which leads to inaccuracies when measuring the static absorption amplitude. Consequently, the most practicable blood flow use for *(4)* is a comparative measure. For example, one may find the average flow velocity on the same subject when subjected to various physiological or psychological stimuli and compare relative flow rates. In this case, the "noise" due to water in the tissues will cancel out.

Equation *(4)* may be simplified to

$$\frac{A_f - A}{A} \approx \frac{\bar{v}T_1}{L_r} \qquad (5)$$

if s is much larger than unity. The amplitude comparisons for blood flow rates may readily be performed by measuring the resonant absorption amplitude with a tourniquet to obtain A and with tourniquet removed to observe A_f. Since the same region is observed in both measurements, extraneous water in the tissues only alter the denominator. If the subject is now perturbed and the relative change in flow velocity is to be measured, this is achieved by using

$$\frac{(A_f - A)_1}{(A_f - A)_2} = \frac{\bar{V}_1}{\bar{V}_2} \qquad (6)$$

Thus, relative measurements of flow may be achieved with considerable sensitivity and precision. Furthermore, changes in flow rate are immediately apparent from changes in the *rf* absorption amplitude curves.

Experimental observations were obtained upon blood flow velocity in mice tails. These will be discussed in detail.

---

[1]F. Bloch, "Nuclear Induction," *Physical Review*, Vol 70, pp. 460-474; October, 1946.

SESSION II: Cardiovascular I

2.5: A Square-Wave Electromagnetic Flowmeter of High Sensitivity Suitable for the Measurement of Low Flows of Blood in Unopened Vessels

William M. Chardack, University of Buffalo School of Medicine and Veterans Administration Hospital, Buffalo, New York, and Francis A. Giori, Cornell Aeronautical Laboratories, Buffalo, New York.

For Some Years, our group has been interested in the various surgical possibilities of bringing new blood supply into the heart muscle when the latter is involved with chronic obstruction of its own arterial system. The details of the experimentation done along those lines are not germane to this discussion; suffice it to say that the need arose to measure the flow of blood in various types of arterial and venous grafts which are embedded into the heart muscle in order to create new and additional channels. It was important for us to know the pulsatile characteristics as well as the magnitude and direction of flow without cannulation of the vessels involved. We knew that the peak velocities during each pulsation might be moderately high, but we also had reasons to expect that the net forward flow into the heart would be extremely small, measuring from perhaps 3 to 20 or 30 ccs a minute at the most.

It appeared to us that an electromagnetic flowmeter would be a suitable instrument for our investigation. Electromagnetic flowmeters have been used for many years and time does not permit us to present a history of its development and the numerous contributions which have been made in this field. Very briefly, the principle rests upon the fact that as a conductor moves through a magnetic field and cuts its lines of force, a voltage is generated which is proportional to the velocity of the motion, the magnetic field and the length of the conductor. The blood is the conductor and the generated voltage is lead off by electrodes from the surface of the blood vessel and is then electronically amplified and recorded.

A most important contribution to the field was made by *Denison* and *Spencer* who introduced the square-wave electromagnetic flowmeter. The magnet is energized by a square-wave current periodically reversed in polarity. An instrument based upon their design is commercially available and has been extensively used by numerous investigators as well as by us and produces perfectly good recordings for most experimental situations.

Unfortunately, our particular experimental setup required the measurement of extremely low flow rates, the objective being to be able to resolve clearly a flow of only 3 cubic centimeters per minute. This had to be done close to the heart; in other words, in a mechanically highly unstable situation and in an area where a considerable interference arises from the voltages generated by cardiac contraction which are huge in comparison to the flow signals.

The electromagnetic flowmeter principle was considered most promising for our purposes and all development effort was devoted to extending the range of this type of flowmeter. In particular, the so-called square-wave concept, introduced by *Spencer* and *Denison,* was selected because it appears capable in principle of allowing the longest data sampling interval reasonably free of noise or quadrature signal.

Noise pulses, several orders of magnitude larger than the desired signal appear in the input of any flowmeter of the square-wave type as a result of switching the polarity of the magnetizing current. These switching pulses are ultimately gated out of the signal; nevertheless, the early stages of amplification (prior to the sampling gate) must accommodate the switching transients with negligible interaction on the desired signal. In order to minimize such interaction, a balanced-input direct-coupled preamplifier is used, and the signal sampling function is performed after only one stage of amplification. At the selected gating point, the desired signal is of the order of a few microvolts. Therefore, it was necessary to utilize a special, low-noise, mechanical chopper to perform the gating function.

A small amount of the induced voltage transient will always remain in the input signal. These voltages are balanced out against similar out-of-phase noise voltages in the probe input circuitry. Stable baseline, in this instance, requires extremely regular sampling intervals relative to the probe excitation interval. Sampling stability was achieved by using a high-frequency master oscillator and a succession of vacuum-tube flip-flops in a frequency-divider circuit. The original oscillator operates at twice probe excitation frequency and is synchronized to the power line.

The convenience of center-tap excitation of the probe magnetizing coil was relinquished in favor of energizing the entire coil simultaneously. This excitation method assures symmetry of probe flux wave shape, without depending on precisely balanced winding and magnetic circuit construction. With full coil excitation, adjustment also can be provided for capacity balance between the probe excitation windings and the signal leads.

A flowmeter satisfying these criteria was constructed and has been in use by our group since June, 1959. The results to date indicate a sensitivity which permits resolving flow differences of the order of 3 cc per minute, a noise level equivalent to about 1 cc per minute (at 40 cycles bandwidth setting) and a zero point drift equivalent to about 1 cc per minute. Cardiac voltages are barely discernible at maximum sensitivity settings.

Pertinent features of the circuits will be discussed and samples of actual flow records will be shown.

SESSION II: Cardiovascular I

2.6: The Theory of Electromagnetic Waves and Arterial Pulsations

Harry Lobel, Omaha, Neb.

THIS PAPER will deal with Womersley's application of electromagnetic wave theory to arterial pulsations, and his anticipation of an anatomical discovery by mathematical reasoning.

The wave theory finds application in all branches of the physical sciences. It has aided reasoning in the fields of astro-physics and nuclear-physics. It has accelerated the practical application of abstract concepts. It has facilitated the transfer of knowledge from one field to another. It is the basis of analog computations and has led to the prediction of impending scientific discoveries.

As examples of the latter, Maxwell developed the mathematics of radio waves twenty years before they were discovered. Leverrier predicted the presence of the planet Neptune years before it was observed.

In applying the wave theory to the cardiovascular system, these questions might be raised: What is the relationship between a reciprocating force pump and the heart? What principles governing the ocean tides apply to arterial pulsations? Can characteristics protecting the arteries from hydrodynamic stress have aeronautical applications?

"Conventional" cardiovascular research is based on theories that dietary fats are in some way implicated in the causes of arterial degeneration. This form of arterial degeneration has persisted for thousands of years. Studies of Egyptian mummies show an incidence or arteriosclerosis the same as today[8]. The Pharaoh of the Exodus suffered from this disease[4].

In 1956, after a study of over 5,000 cases, the Cleveland Clinic Foundation, Harvard University, and the University of Pittsburgh, published a joint report discrediting the claim that high blood cholesterol levels indicate impending heart failure[1,2].

Actually, as a normal function of the arterial wall, fat may act as a lubricant. Irritants, such as virus infections and eddy currents in the blood, may disturb this protective mechanism, eventually leading to a deposition of fat.

In 1955, the late J. R. Womersley, a British mathematician, successfully correlated the engineers' theory of hydraulic surges with the dynamics of the wave theory. His analog treated pulsations as electromagnetic waves, conduits as wave guides, rate of flow as electrical current, and frequencies dependent on the ratio of diameter/wall-thickness (equivalent to elasticity). This analog built a bridge between the fields of hydraulics and arterial physiology[5].

In many instances, arterial pulsations have to pass from a low-frequency, into a high-frequency branch, such as from the aorta, into the renal artery. The relatively rigid renal artery should act as a "high pass filter"[6], reflecting much of the wave energy due to hydraulic "impedance". Actually, from the viewpoint of the wave theory, the efficiency of wave transmission is too high. The arterial system works better than the engineering system.

To reconcile this discrepency between physiological and theoretical performance, Womersley introduced a mathematical correction factor. He postulated a favorable area-ratio between the aorta and its branches[7]. This is significant, in that, arterial function was reconciled to the wave theory; and not the converse.

By a remarkable coincidence, prior to receiving Womersley's letter, healthy arteries were being examined with the view of designing more efficient aeronautical hydraulic components. Several features, which contribute to the efficiency of wave transmission between the aorta and its branches, were discovered. The most obvious of these features is the structure and design of the points of arterial bifurcation.

At the mouths of arteries branching from the aorta, are funnel-shaped structures. These serve to increase the area of the bifurcation. Microscopic examination reveals muscle fibers. On stimulation, the renal artery, for example, is seen to adjust its contour to streamline varying flows of blood.

The mathematical correction factor of Womersley seems to describe the function of these funnel-shaped structures. They act as impedance couplings between the low frequency aorta and the relatively high frequency branches. Malfunction results in eddy currents and hydrodynamic stress. This is the first clue to coronary occlusion based on an anatomical discovery.

One significance of Womersley's work lies in its anticipation of physiological developments by mathematical reasoning. Womersley was on the verge of finding the solution to a problem he could not know existed, and implied the presence of an anatomical discovery, which at that time, had not been publicized.

[1]Gofman, John W., et al, *Circulation*, 14:691; Oct. 1956.
[2]Page, I. H., *Jour. Am. Med. Assoc.*, 163/6; Feb. 9, 1957.
[3]Ruffer, M. A., *Cairo Sci Jour.*, 4:3; 1910.
[4]Shattock, S. G. *Lancet*, 1:319; 1909.
[5]Womersley, J. R.:
[6]Personal communication, 1956.
[7]WADC TR 56-614, Wright-Patterson Air Force Base; 1957.
[8]*Physics in Med. and Biol.* 2:313; 1958.

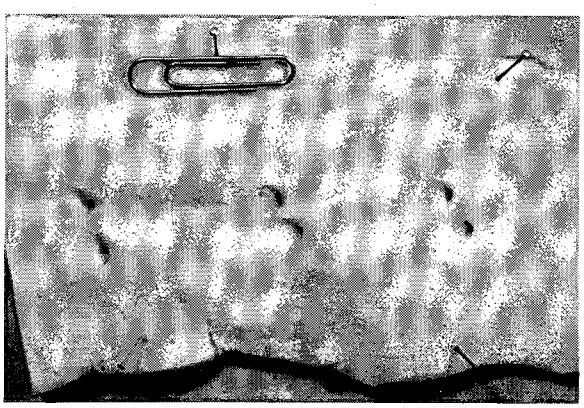

Figure 1—Inner wall of aorta, showing funnels at mouths of arterial branches.

SESSION III: Ultraviolet Radiation II

Chairman: George Z. Williams,

National Institutes of Health, Bethesda, Md.

3.1: Biological Effects of Ultraviolet Radiation

Max R. Zelle, Division of Biology and Medicine, Atomic Energy Commission, Washington, D. C.

ANY REVIEW of the biological effects of ultraviolet radiation must necessarily be concerned with only a very small portion of the entire field, because of the diversity of effects which have been studied in many different cells and organisms. Because ultraviolet is so readily absorbed by protoplasm, most studies of the biological effects have utilized individual cells or single-celled organisms to circumvent difficulties of penetration. The recent development of quantitative-tissue-culture techniques will permit extension of investigations to a wide variety of mammalian and other cells.

Interest in the biological effects of ultraviolet stems in large part from the selective absorption in different molecules. This is the basis of action spectroscopy in which, by means of observed similarity between the relative efficacy of various wavelengths in producing a particular biological effect and the absorption spectra of biologically important molecules, clues are gained as to the molecular systems involved. For example, action spectroscopy has been instrumental in identifying the oxygen-transporting enzyme in yeast and gave one of the first indications, through the implication of nucleic acids in the survival and mutation of microorganisms, that deoxyribonucleic acid might possess genetic specificity.

Although a number of different types of action spectra have been identified, most interest centers on the nucleic acid type (a maximum at 2600Å, a minimum about 2500Å, increasing at shorter wavelengths) and the protein with aromatic amino acids type (a maximum about 2800Å, a minimum between 2500-2600Å, increasing at shorter wavelengths). For example, nucleic acid action spectra have been observed for lethality in bacteria, protozoa, fungi and viruses; for mutation production in fungi, bacteria, protozoa, maize, and drosophila; for the induction of virus production in lysogenic bacteria; for the production of cytoplasmic mutants in yeast; and for chromosome breakage in Tradescantia pollen. Protein-type action spectra include the inactivation of various enzymes; inactivation of paramecin, the killing substance of paramecia; immobilization and vesiculation of paramecia; loss of hemagglutination in influenza virus; and paling of chromosomes following microbeam irradiation.

In the past decade, a number of post-irradiation treatments such as variation in media and temperature have been shown to influence the amount of ultraviolet effects. Especially important is photoreactivation or the apparent reversal by exposure to visble light of a substantial portion of ultraviolet effects involving damage to the nucleus or nuclear constituents including mutation induction. Wavelengths from 3400-4000Å are most effective in producing photoreactivation.

The modification by post-irradiation treatments indicates that a major proportion of ultraviolet effects are indirect and hence, that action spectroscopy identifies only the molecules absorbing the energy, which are not necessarily the molecules in which the observed effect is produced.

An understanding of ultraviolet effects and the mechanisms whereby they are produced is important in contributing to our knowledge of high energy radiation effects. Thus, studies of additivity of ultraviolet and X-ray effects and of the mitigation of X-ray damage in yeasts by pre- or post-treatment with ultraviolet suggest an appreciable overlap in damaged sites. X-ray induced cytogenetic effects in drosophila and plants are modified by ultraviolet.

In recent years, ultraviolet radiation has proven to be a powerful tool in the analysis of complex biological systems. A good example is afforded by ultraviolet microbeam irradiation of parts of dividing cells in which a wide variety of effects have been observed. For example, cytoplasmic irradiation will inhibit spindle formation, irradiation of the centromere causes the loss of directed movement of the chromosome, and irradiation of the nucleolus will permanently inhibit mitosis in grasshopper neuroblast cells. Perhaps the best example is the significant contribution to the knowledge of bacteriophage reproduction and genetics made by the analysis of multiplicity reactivation of ultraviolet inactivated phage, of crossreactivation in which genetic markers of inactivated particles are rescued in mixed infections with normal phage, and of the inactivation of phages during intracellar reproduction and maturation.

Except for the microbeam studies, most of the results discussed have been obtained by use of relatively simple equipment. Even more important findings should result as more sophisticated instruments such as the microbeam combined with monochromatic light sources and the flying-spot microscopes are perfected.

Notes

SESSION III: Ultraviolet Radiation II

3.2: The Use of Television in Scanning Techniques for Ultraviolet Irradiation of Cells

P. O'B. Montgomery, University of Texas Southwestern Medical School, Dallas, Texas

In 1912, Tschachotin devised an ultraviolet microbeam for the purpose of irradiating selected areas of living protoplasm. This ultraviolet microbeam was brought to focus by the use of refracting lenses and was rather crudely positioned on the specimen. In 1954, *Uretz, Bloom* and *Zirkle* reported a much improved method for ultraviolet-microbeam irradiation of living protoplasm.

In 1956, *Montgomery, Roberts* and *Bonner* announced the development of the ultraviolet flying-spot television microscope and a new tool for the study of ultraviolet irradiation effects came into being. The more technical aspects of the design and operation of the ultraviolet flying-spot television microscope will be covered elsewhere at this meeting by the author's colleague, *Lee Hundley*, in his paper on *Flying-Spot Techniques in Microscopy.*

In brief outline, the ultraviolet flying-spot television microscope utilizes as a light source, an ultraviolet-emitting flying-spot scanner tube. A 250-line raster may be traced upon the face of this tube at variable sweep speeds from one sweep every 10 seconds to one sweep every 1/20th of a second. For intermittent-irradiation studies, the raster may be switched on and off for any integral number of frames following any predetermined number of sweeps. The image of the raster of the ultraviolet-emitting cathode-ray scanner tube is minified by its reflectance in reverse through the optical components of a reflecting microscope. The unabsorbed energy transmitted by the specimen is allowed to strike the photocathode surface of an ultraviolet-sensitive photomultiplier tube. The resulting current generated in the photomultiplier tube is suitably amplified and used to modulate a monitor tube locked in synchrony with the ultraviolet flying-spot scanner tube. In this way, a black and white ultraviolet absorption image of the living specimen is traced out on the monitor tube. Since the spectral characteristics of the ultraviolet emitting cathode-ray scanner tube are centered at 2600Å, the black and white image of the specimen on the monitor tube represents, in the main, a nucleic-acid absorption image of the living protoplasm. By appropriate photographic techniques these images may be recorded by time-lapse motion picture photography.

The use of specially-designed intercept circuitry permits the brightening of selected rectangular areas of the raster of the ultraviolet-emitting cathode-ray scanner tube. A similar brightened area appears on the monitor tube superimposed upon the image of the specimen under the microscope. The brightened area may be easily positioned by visible observation of the monitor tube and its dimensions and configuration may be readily changed to include the entire raster of the ultraviolet emitting cathode-ray scanner tube. The converse of this technique is readily attainable by extinguishing, rather than intensifying the rectangular area on the raster of the ultraviolet-emitting cathode-ray scanner tube.

Recent advances in this laboratory have made it possible to improve the above-outlined techniques and to apply them to living cell studies. The improvements consist of the utilization of a second scanner tube whose emission is in the visible spectrum. This scanner tube is synchronized with the ultraviolet-emitting cathode-ray scanner tube in such a way that the brightened area of the ultraviolet emitting scanner tube is extinguished on the visible-light scanner tube. The resulting image on the face of the monitor tube thus contains components from two wavelengths of light. An extension of this technique permits one to scan sequentially the entire specimen with opposite halves of the ultraviolet-emitting scanner tube and the visible-emitting scanner tube and to present both of the resulting images side by side on the same monitor tube.

This paper will consist primarily of a time-lapse motion picture demonstrating the application of the above briefly-described techniques to living-cell systems:

(1) Continuous, or intermittent, intense differential ultraviolet irradiation of the nucleolus of a living cell with simultaneously obtained ultraviolet absorption images of the remainder of the cell.

(2) Continuous, or intermittent, intense ultraviolet irradiation of the nucleolus of a living cell with a simultaneously obtained visible light image of the remainder of the cell.

(3) Continuous, or intermittent, intense differential ultraviolet irradiation of the nucleus of a living cell with a simultaneously-obtained ultraviolet-absorption image of the remainder of the cell.

(4) Continuous, or intermittent, intense ultraviolet irradiation of the nucleus of a living cell with a simultaneously obtained visible light image of the remainder of the cell.

(5) Continuous, or intermittent, intense ultraviolet irradiation of the cytoplasm of a living cell during which time the nucleus of the cell is entirely excluded from ultraviolet irradiation.

(6) Continuous, intermittent, intense ultraviolet irradiation of the entire living cell with a simultaneously-obtained ultraviolet absorption image or a visible light image of the cell.

(7) Simultaneous presentation of the same image side by side on the same monitor, as seen when illuminated by visible light-dark field and ultraviolet dark field.

(8) Simultaneous side-by-side presentation of the same specimen as seen when illuminated by ultraviolet light and visible light.

SESSION III: Ultraviolet Radiation II

3.3: Flying-Spot Techniques in Microscopy

L. L. Hundley, University of Texas Southwestern Medical School. Dallas, Texas.

THE FLYING-SPOT ULTRAVIOLET MICROSCOPE has been described previously by *Montgomery, Roberts* and *Bonner*. The basic system consists of a sweep-generation system, an ultraviolet-emitting cathode-ray tube, a microscope with quartz and reflecting optics, an ultraviolet-sensitive photomultiplier tube, a video amplifier, and a monitor tube.

A time-lapse camera is used to photograph the monitor tube. The monitor is keyed off and on for a predetermined number of frames for photographic purposes. This is accomplished by the use of two counters and associated gate circuits. A block diagram of this system may be seen in Figure 1.

A technique for spot irradiation of a specimen has been devised and has been described by *Montgomery* and *Bonner*.

The horizontal and vertical sweeps are fed to variable delay, variable pulse-width generators. The pulses thus generated are compared in a coincidence circuit and at the time when both occur, an output from the coincidence circuit modulates the scanner tube grid, causing an intensified spot to appear on the scanner tube. This spot may be moved about on the raster by means of the delay circuit and by varying the pulse widths, the spot size may be varied down to one picture element.

Figure 3 shows the operation of these circuits. The drawings in this figure lettered *A* and *B* show the individual effect of the pulses and their combined effect is shown on the face of the scanner tube.

A recent modification of the equipment now allows simultaneous viewing of the specimen in visible and ultraviolet light. A visible-light tube has been mounted on the equipment at 90° to the ultraviolet tube. This arrangement is shown in Figure 4. A first-surface mirror and beam-splitter arrangement allow the two outputs to be combined optically.

To view a specimen simultaneously in both wavelengths of light, opposite halves of each raster are masked off and the remaining output is brought into optical registration. The first half of the horizontal scan, in the focal plane, is then ultraviolet and the second half is visible light, and the two scan the same area of the specimen. The monitor tube then displays the two images in a side-by-side presentation. This arrangement is shown in Figure 5.

With only the ultraviolet tube available, positioning the intensified spot required that the background intensity be brought up to a level which would allow viewing of the entire field. This would require increasing the video gain to a level that would cause overloading of the video amplifier in the intensified area and a subsequent loss of information. There was also the possibility that the background radiation would cause biological damage to the cells in the field which were to be used as controls.

These difficulties were overcome by applying to the visible-light tube a pulse of opposite polarity to that applied to the ultraviolet tube. The two rasters were brought into optical registration. This allowed the ultraviolet background to be at zero level and the background to be filled in with visible light of the same intensity as the spot. The video system could then be adjusted to the proper level to view the entire field and the danger of ultraviolet damage to the control area was removed. This arrangement is shown in Figure 6.

By reversing the pulse polarities, the converse situation may be achieved. The background is in ultraviolet and a portion of the cell is protected and simultaneously viewed in visible light.

This paper will consist of a more detailed explanation of the equipment involved in achieving the techniques described.

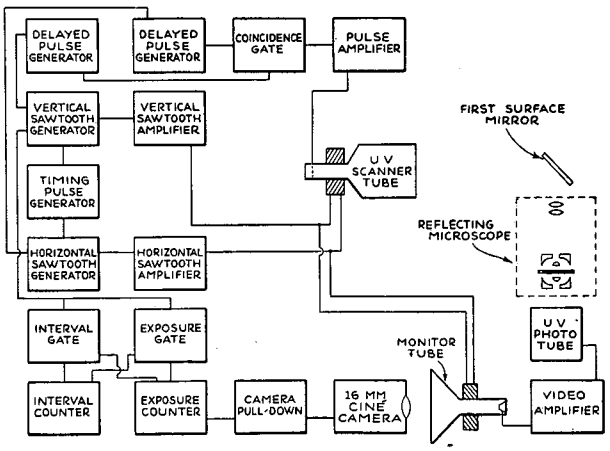

Figure 1—Variable sweep-speed *UV* flying-spot TV microscope.

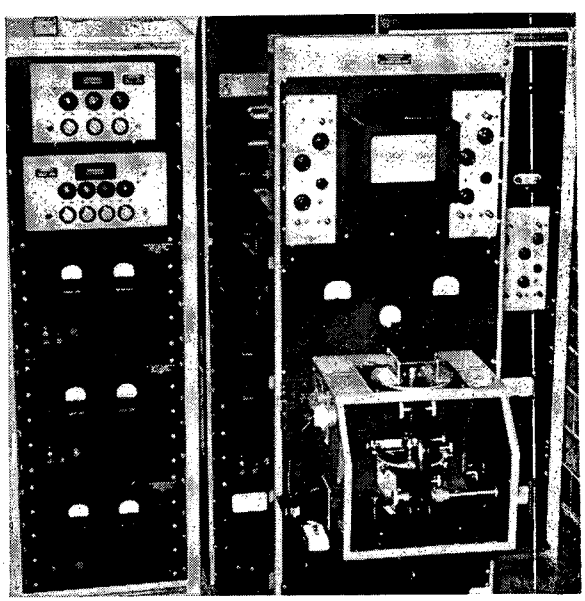

Figure 2—Arrangement of equipment.

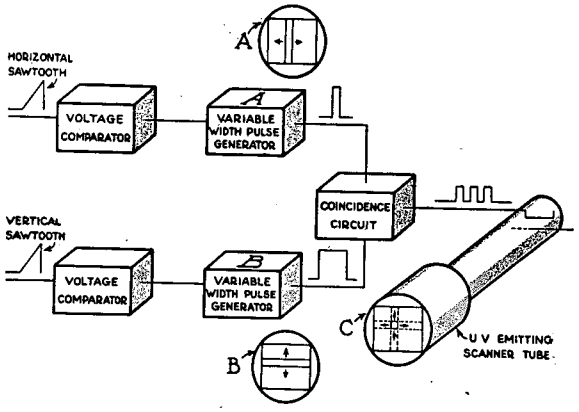

Figure 3—Spot-irradiation technique.

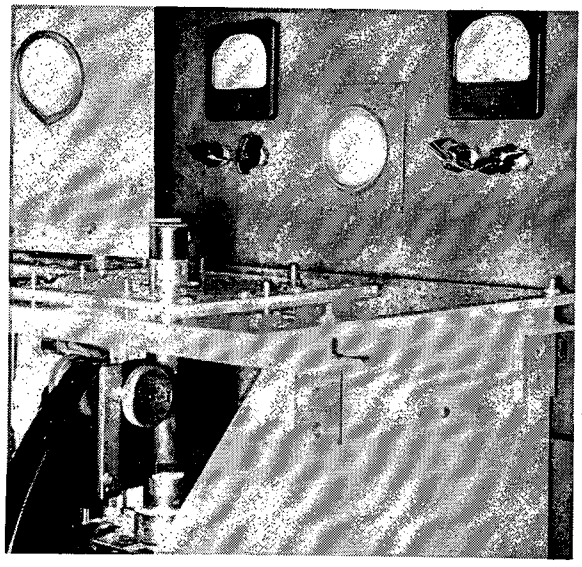

Figure 4—Double scanner-tube arrangement.

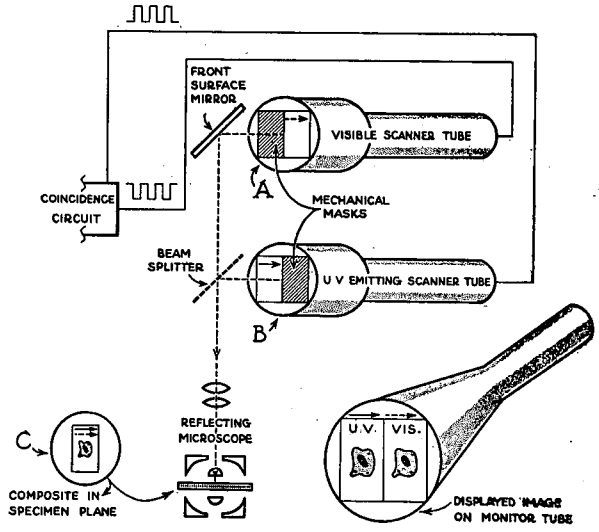

Figure 5—Composite ultraviolet visible light system.

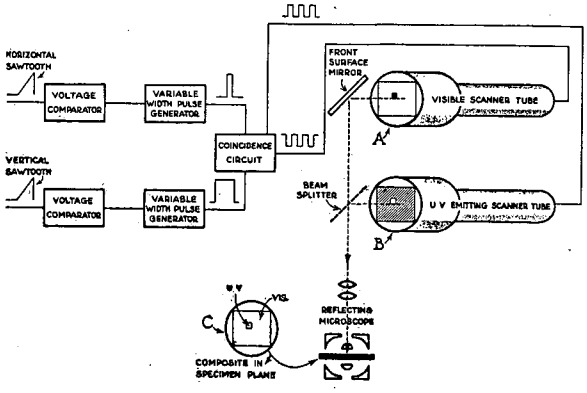

Figure 6—Composite spot background system.

SESSION III: Ultraviolet Radiation II

3.4: Measurements of Reaction Rates in Living Cells by Time-Lapse Ultraviolet Television Microscopy and Oscilloscopy

G. Z. Williams and G. C. Vurek, National Institutes of Health, Bethesda, Md., and R. G. Neuhauser, RCA, Lancaster, Pa.

WE KNOW MUCH of the chemistry of separated cell enzymes, particles and juices. What chemical reactions occur in the intact living cell and what is their relation to specific structure? One approach to the study of living-cell chemistry is ultraviolet microscopy and oscilloscopic measurement of absorption of products in the cell. But *UV* quickly injures cells so very short and interrupted exposures are necessary. Use of the *UV*-sensitive vidicon as an image storage and detection device enables the combination of *UV*-TV microscopy in time-lapse sequence and oscilloscopic measurements to visualize and record absorption images from 1/100-sec exposures.

Instrumentation

A microscope with reflecting optics and a warm-stage perfusion micro-chamber for cells is illuminated by a Xenon arc and quartz prism monochromator. An automatic shutter is interposed in the beam. The image is stored on the vidicon target by blanking the electron scan. At closure of the light shutter the vidicon grid is unblanked and the stored image signal is scanned and transmitted to the monitor and line-selecting oscilloscope. Sensitivity of the vidicon is maintained by white-light illumination during dark phases of each cycle. To provide framing synchronization of the TV monitor picture and film motion-picture camera for time-lapse sequences the picture tube is blanked, except for one full interlaced frame during the open period of the movie camera. An electronic control circuit of pulse and waveform generators[1] and vidicon-grid blanking, *UV* light shutter, film-camera shutter, and picture-tube grid blanking controls* is synchronized with the vertical-drive pulse of the TV system and adjusted to time properly the shutter actions of vidicon and picture-tube blanking pulses and sensitizing lamp. The line-selecting oscilloscope displays a single raster line derived from the vidicon-scan signal and oriented vertically to traverse any desired portion of the *UV*-absorption image. Thus, in sequence, the sensitizing lamp is extinguished, the light shutter opens for 10 ms, exposing the blanked vidicon target to the *UV* light transmitted by the cell; this image is scanned, the film camera shutter opened, one full frame (33 ms) is displayed on the monitor and the selected line on the oscilloscope; the film camera closes and the vidicon sensitizing lamp is energized. This cycle is initiated and repeated by a clock or pulse generator.

Application

Time-lapse movies and photographs of the oscilloscope screen in a sequence, from before to completion, of a cellular reaction which accumulates an absorbing product, provide data for estimating reaction rates. Oscilloscopic voltage deflections from white to black level, V_o, represents 100% transmittance and the image deflection from base black level, V_e, is proportional to the UV transmitted by the cell. Because the system gamma is .96, $\log \frac{V_o}{V_e}$ expresses the density.

Tetrazolium is a useful indicator of certain enzyme-substrate reactions because it penetrates the living cell, is of low toxicity, absorbs little *UV* in solution and becomes insoluble when reduced to formazan which absorbs intensely.

To test the validity of such measurements aliquots of counted washed-mouse liver cells were added to equal amounts of 0.0025 M 2, p-nitro, 3, o-nitro, p-methyoxy triphenyl tetrazolium and incubated at 38° C. At 2.5, 5, 10, 20 and 30 minutes one tube of cells was centrifuged, the formazan extracted and density measured by spectrophotometry. Other liver cells from the same specimen were incubated within the warm stage micro-chamber in the *UV*-TV microscope and background density determined at 300 mu. Then, tetrazolium in like concentration was added and oscilloscopic measurements of the same cell made at 2.5 to 30 minutes.

The results produced a plotted curve of increasing density very similar to that of the gross cell suspensions. Such curves depict the reaction rate of tetrazolium reduction by an enzyme-substrate system in these intact cells.

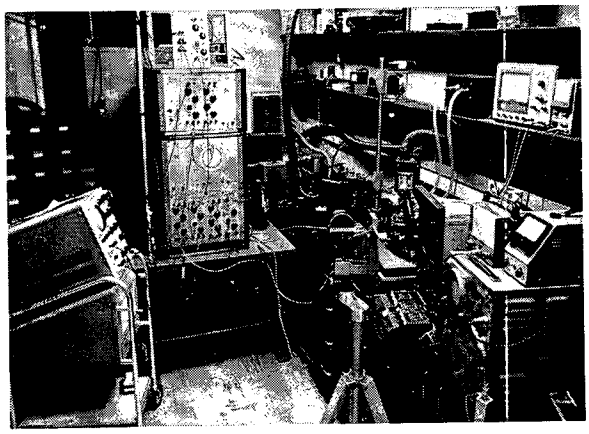

Figure 1—Ultraviolet-television microscope. Left to right: Aligning oscilloscope, cycling control components, Xenon lamp, monochromator, movie camera, warm stage on reflecting-type microscope and vidicon camera above, picture-tube monitor and line-selecting oscilloscope.

[1] Tektronix 160.
* Details of these circuits to be published.

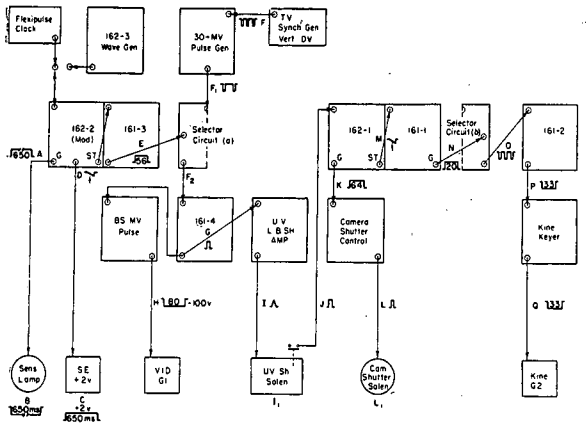

Figure 2—Block diagram of components. Arrows indicate direction of activating pulses and type, polarity and duration as indicated. The 161 series are pulse generators with delay circuits and 162 series are waveform generators with interval adjustments.

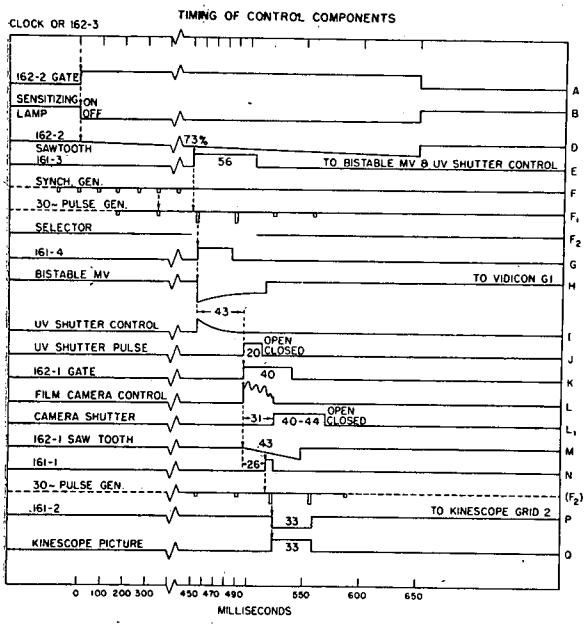

Figure 3—Chart of activating pulses; their alignment and orientation to operation of components of the *UV*-TV microscope-system. Letters designate relations to components in block diagram.

(Right)

Figure 4—Ultraviolet television absorption of isolated liver cell exposed to tetrazolium and substrate; the formazan particles in the cytoplasm and fat droplets absorb at 300 mu.

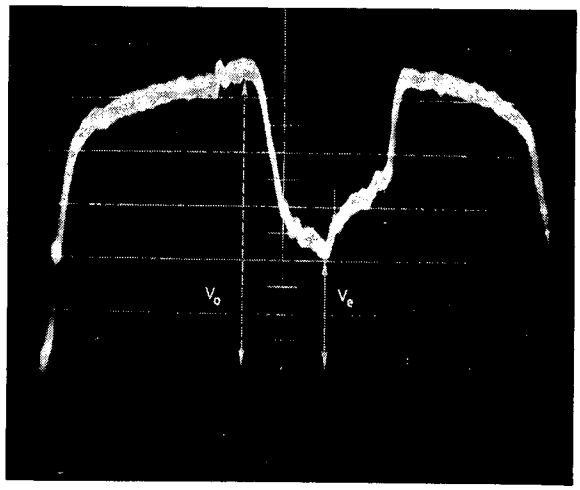

Figure 5—Oscilloscopic tracing of single line through liver cell; Figure 4 *A*. V_o represents black to total transmitted light level, V_e light transmitted by cell at most dense point along *A*. Log V_o/V_e, the density is log 40/16 or .40.

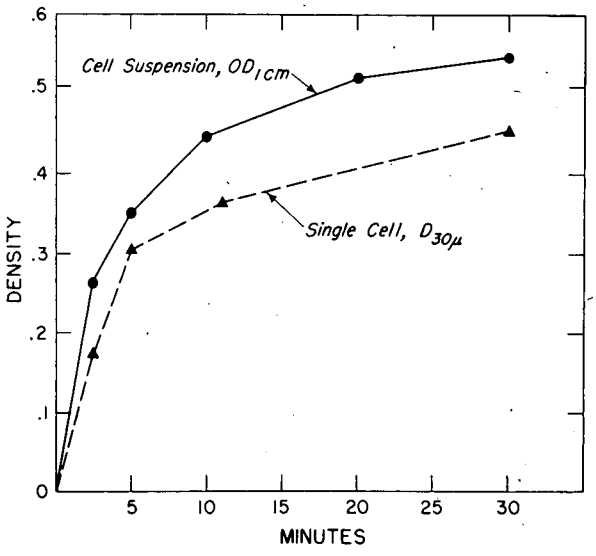

Figure 6—Reaction rate curves: Reduction of tetrazolium to formazan in liver cells. Solid line: Density of formazan produced in cell suspensions measured spectrophotometrically. Dashed line: Density of single cell by *UV*-TV microscopy and oscilloscopic measurements.

SESSION III: Ultraviolet Radiation II

3.5: Television Spectroscopy of Biological Fluorescence

S. S. West and C. N. Loeser, Department of Anatomy, School of Medicine, Western Reserve University, Cleveland, O.

THE FLUORESCENCE of living cells and tissues stained with the *acridine* dyes is of basic interest, because of the vital affinity of the dyes for the nucleic acid components of the cell, to say nothing of the recent diagnostic applications of such study.

For supravital or vital use these dyes are least toxic at low concentrations, but this results in correspondingly low levels of fluorescence. Previous cellular work with these dyes has been limited to the absorption spectrum and recording of the gross fluorescence colors. The lengthy exposure required by photographic recording of the fluorescence spectrum results in cell damage and fading of the fluorescence and the motion inherent in some biological material makes the origin of the recorded spectrum uncertain.

Recently, one of us* suggested that microspectral fluorescence emission recording might be accomplished using high-sensitivity television pickup tubes and the line-selection technique. In these experiments, the image orthicon and the recently-developed intensifier-image orthicon[1] television camera tubes have been used in conjunction with a *high-power* monochromator[2] (exit slit removed) to record the fluorescence emission spectrum from single cells stained with *acridine orange*. The intensifier-image orthicon proved to be about one-hundred times more sensitive than a standard-image orthicon and permitted the recording of the fluorescence emission spectrum of cells stained with $1:10^6$ *acridine orange*. The standard-image orthicon is about one-hundred times more sensitive than film. Exposure to the exciting radiation was limited to approximately one second, but could be reduced considerably without changing the intensity of the exciting radiation.

The method employed here uses a high-pressure mercury vapor concentrated arc lamp[3] with appropriate colored glass filter as the source of exciting radiation. The light passing through the microscope is dispersed by the monochromator (exit slit removed) and the spectrum focussed on the faceplate of the television pickup tube. It was necessary to add a filter to absorb the exciting radiation only in the case of the intensifier image orthicon. The line selector displays the variation of the intensity of the light with wavelength and is photographed. These photographs are then used to generate curves of the fluorescence emission spectrum.

Experimental results obtained show the spectrum of the known bichromatic orange and green fluorescence of *acridine orange*, and the shift to the longer wavelength expected with increasing dye concentration, but also the spectrum has in it an unpredicted continuum through the yellow. The relationship of these colors to *DNA*—dye, *RNA*—dye, and interdye combinations will be discussed, as well as the biologic potentiality of the methods used. These methods should permit the study of other areas of secondary fluorescence, including the spectroscopy of fluorescent carcinogens in living tissues. These high-sensitivity techniques may also permit a more revealing analysis of the autofluorescence of living cytoplasm of various tissues.

---

* S. S. West. [1] RCA. [2] Leitz. [3] Osram HB-107.

Notes

SESSION IV: General I

Chairman: O. H. Schmitt,

University of Minnesota, Minneapolis

4.1: A Transistorized Portable Electronic Hematocrit

Robert H. Okada and Herman P. Schwan, Electromedical Division, The Moore School of Electrical Engineering, University of Pennsylvania, Philadelphia, Pa.

THE RELATIVE VOLUME concentration of blood cells and plasma in human blood is a medical standard of diagnostic significance. It also may serve as an indicator of the amount of absorbed nuclear radiation. The principle of the presently-used technique is to spin a sample of blood in a high speed centrifuge and record the volume concentration by noting the difference in color between the cells and the plasma. Several investigators have recognized that the resistivity of blood is a function of the volume concentration of the cells in blood and one of us has previously shown that this fact may be used to determine electrically the blood cell concentration. An instrument has been developed which utilizes this principle, the construction and performance of which is the subject of this paper.

Blood cells have been found to be nonconducting electrically in comparison with their surrounding fluids (plasma). Hence, for spherical shape of cells, *Maxwell's* equation

$$K = K_s \frac{1-p}{1+p/2}$$

applies (p is the volume concentration of cells in relative units, K is the observed conductivity, K_s is the conductivity of plasma). For nonspherical shape, this equation is to be replaced by

$$K = K_s f(p)$$

where $f(p)$ is a function which deviates only slightly from the *Maxwellian* function $1\text{-}p/1 + \frac{p}{2}$. Hence K is proportional to K_s and $f(p)$, i.e. a strong function of p. The temperature dependance of K is identical with that of K_s in view of the experimentally-verified temperature independance of $f(p)$. It has been investigated in detail by us before and is near +2%/°C. The variability of K_s from sample to sample has been reported by us previously to be quite small, so that variation of K largely reflects corresponding variations of $f(p)$ and thereby p. The above formulated relations have been utilized to develop an instrument which measures essentially the resistance of a small sample of blood and converts this value into its equivalent volume concentration value, p (hematocrit value).

The new instrument is portable and transistorized and is the size of a standard portable voltohmmeter. There is no warmup time and a reading including calibration can be made in a few seconds. The cell contains 0.02 CC of blood which is easily obtained from a finger-prick technique.

Resistance measurements are made using an off-balance bridge excited by a 10-kc oscillator. A thermistor is used in one arm of the bridge to compensate for the temperature dependance of the blood's resistivity. A feedback amplifier, following the bridge, builds up the signal to a sufficient level for a standard detector and meter circuit. The output meter is calibrated directly in per cent blood cell volume.

The transistor oscillator is of the Wien-Bridge type and a complete analysis of this circuit and of the feedback amplifier is available. Figures 1 and 2 demonstrate the instrument and its calibration curve. We are obliged to *Lawrence Sher* for his help in calibrating the instrument.

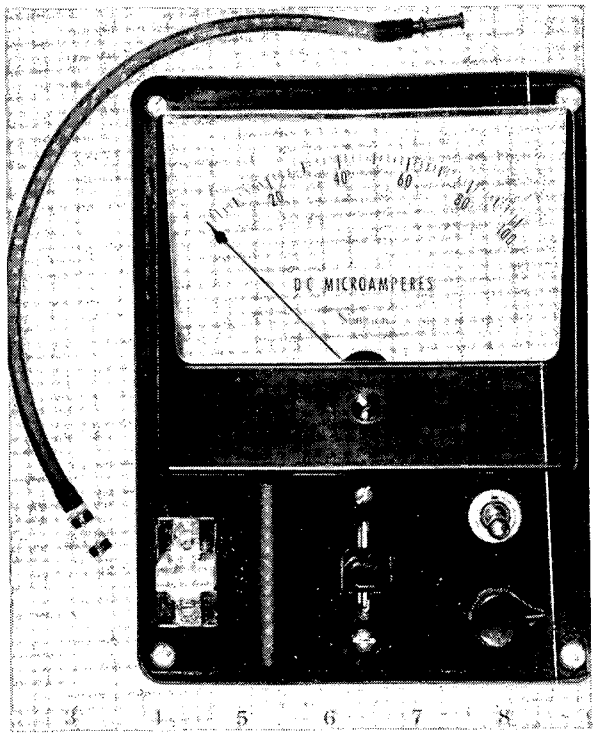

Figure 1—Photograph of electronic hematocrit meter showing cell used in measurement of blood sample.

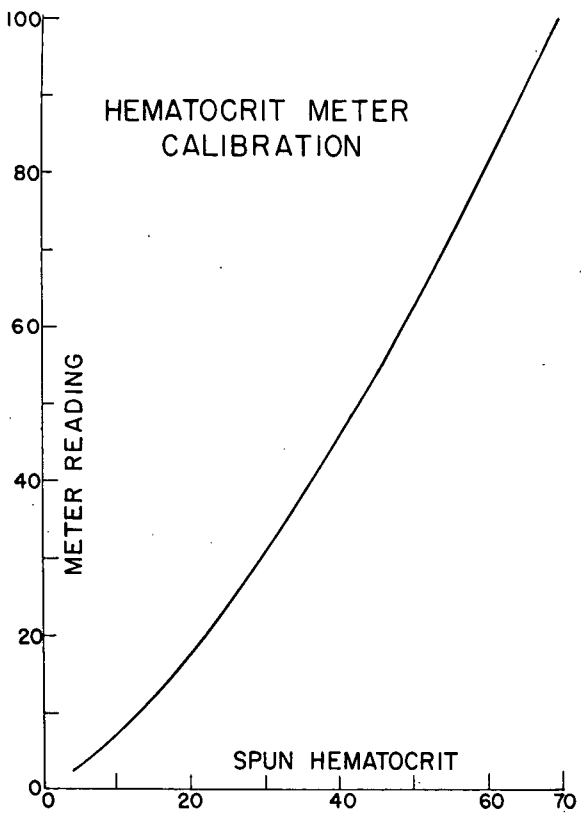

(Right)

Figure 2—Calibration curve of hematocrit readings obtained by centrifuge process versus linear meter scale readings.

SESSION IV: General I

4.2: In-Vivo Radioluminesent Glass Dosimetry*

S. J., Malsky, Veterans Administration Radiophysics Research Section, and New York University Department of Science and Mathematics; C. Amato, Attending Nuclear Physicist V-A, Radiation Physicist-AMF Atomics, Guest Nuclear Physicist, Brookhaven N. L.; B. Roswit, V-A Radiotherapy Service; C. Reid, V-A Radiophysics Research Section; S. Unger, V-A Radiotherapy Service; C. Spreckels, V-A Electronics Engineer, also Bulova Watch Co., and M. Villazon, V-A Radioisotope Service.

THE STUDY of the practicability of radioluminescent glass to medical radiation dosimetry was undertaken due to the unique size of the glass (1 mm in diam. by 6 mm in length). This characteristic would be highly desirable for in-vivo dosimetry of patients undergoing radiation therapy in virtually all conditions encountered in modern therapy practice. Figures 1, 2 and 3 illustrate typical implants of these dosimeters. There are several types of radiation detecting units. These units are ideally suited for calibration and general radiation measurements, but can only serve in a limited way for in-vivo applications of human radiation dosimetry. Prior to the use of these microdosimeters, various physical characteristics were investigated. Several of these characteristics are presented in Table 1:

Characteristic	*Observation and Correction*
1) Energy Dependence	Bare glass must be calibrated for each energy. Employ shield of proper wall thickness.
2) Orientation of glass a) In air b) In scattering Medium	Readings vary by ±40% depending on orientation of glass to beam. Less than 3%. Since the dosimeter will be in body matter, this orientation will not be a problem.
3) Linearity and Accuracy	Slopes vary with energy. Lower energy "saturates" glass. Proper shield will allow for interchangeability for 1 MeV X-rays, Cobalt-60 and Radium.
4) Handling, etc.	Flourescence errors due to oil of hands, etc., require care in handling. Body fluids also affect bare glass. The bare glass will not be affected by body fluids if in shield and in plastic tube.

Table I

Figure 4 is a pictorial representation of the fluorimeter reader. After exposure, the microdosimeter is inserted into the fluorimeter and read. The ultraviolet light causes the silver-activated glass to emit an orange luminescence proportional to the amount of radiation received. The intensity of the orange luminescence is measured by a photomultiplier tube fitted with an orange bypass filter. Since the signal from the photomultiplier tube is of the order of 10^{-8} amperes a balanced-bridge electrometer amplifier is employed. The use of an isolating transformer and variable autotransformer in the input circuit reduces any chance of wide voltage deflections which may result in a discrepancy of readings.

Conclusions

The microdosimeter has an important role in human radiation dosimetry.

The bare glass dosimeter cannot be readily identified unless in a numbered shield.

The selection of an optimum wall thickness of the dosimeter shield permits its use in-vivo when the radiation source has an energy lying between 0.26 and 1.33 MeV, independent of separate calibration tables.

Work In Progress

1) The investigation of a low-Z microdosimeter for possible reduction of the energy dependance of the present glass.
2) The plotting of radiation penumbra with the glass dimensions; it is possible to obtain accurately 1-mm separation distances and readings.
3) The use of the glass dosimeter with various shields thicknesses as gamma-ray absorption spectrometers.
4) The use of the glass dosimeters with beta-ray emitting isotopes.
5) The use of the glass rods to measure gamma radiation in the presence of intense neutron beams.

*From Radiophysics Research Section, Radiotherapy Service, Bronx V.A.H.

**The authors wish to express their sincere appreciation to Dr. Schulman of the Naval Research Lab for his assistance and suggestions throughout this study.

Figure 4 (right)—Pictorial representation of the optical system of the fluorimeter. This reader is based upon a design by Schulman and the U.S. Naval Research Lab.

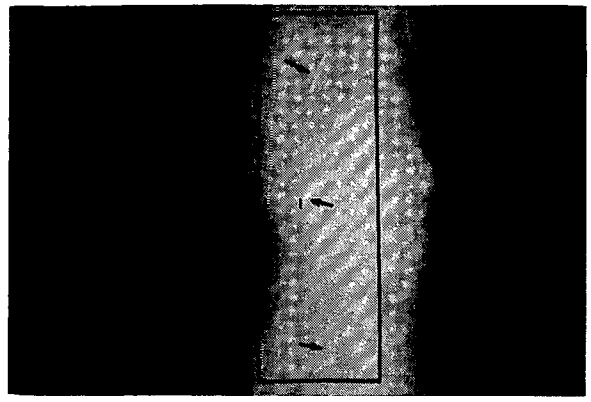

Figure 1—Radiograph of chest illustrating three crystals in gold shields placed within the esophagus to record the dose delivered to cancer of esophagus and adjacent spinal cord.

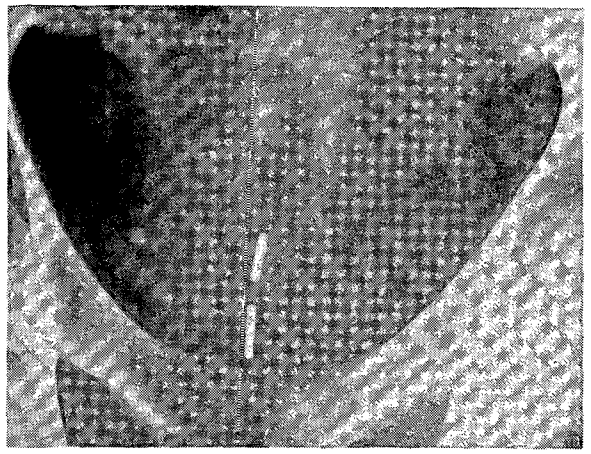

Figure 2—Patient with cancer of bladder receives glass-rod dosimeters via urethral catheter for accurate recording of Cobalt-60 radiation required for cure of his malignant neoplasm.

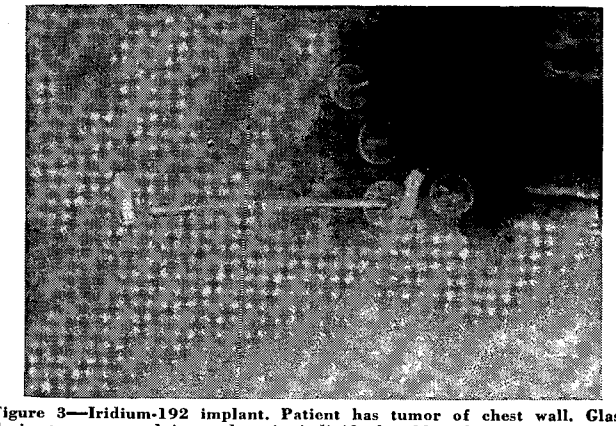

Figure 3—Iridium-192 implant. Patient has tumor of chest wall. Glass dosimeters mounted in tandum in individual gold jackets, positioned in the mid-plane of the two-plane implant.

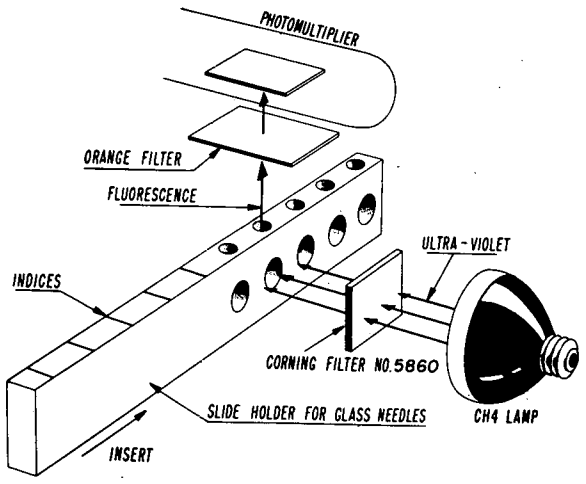

SESSION IV: General I

4.3: Measurements of Pathologically Significant Primary Cosmic Particles*

dePaul J. Corkhill, Aeromedical Field Laboratory, Air Force Missile Development Center, Holloman Air Force Base, New Mexico.

BIOLOGICAL SPECIMENS exposed at high altitudes to primary cosmic radiation have exhibited certain pathological conditions. Primary cosmic particles of specific energies and $30 > Z > 6$ produce these pathological effects by the formation of thousands of ion pairs causing radiation dosages as high as 1000 *REP* to cells 10 μ in diameter. Detail characteristics of cosmic particles causing these effects have been determined to a limited extent using photographic film techniques during ballon flights. Under an Air Force contract[1,2], an electronic system has been developed, which is superior to the film method, because the count rates per unit time can be more readily ascertained, the atomic number and charge can be determined with greater accuracy, and automatic data reduction techniques can be employed. The system defines particles with atomic numbers of 6 through 30 in the energy range from 100 to 300 *MEV*.

Particles are detected in the counter with crystal and plastic scintillators with photomultiplier tubes transducing the light to an electrical value for analysis. This information is analyzed aloft and thereupon telemetered to three telemetry receiving stations both on the ground and in the air. The information is recorded on magnetic tape and returned to *Holloman Air Force Base, Data Reduction Division,* where the tapes will be played back through conventional channel discriminators into a digital computer programmed to solve the pertinent equations, providing a typewritten time history of particles striking the detector. Nuclear track plates flown on these flights are presently being developed, analyzed and scanned by *University of New Mexico* and *Aeromedical Field Laboratory* personnel under an additional Air Force contract. Data from emulsions and the counter will be compared for accuracy.

Prior to launching the balloons for high-altitude flight, complete checkout of telemetry receiving channels was made using a tunable discriminator and a recorder[3]. However, primary cosmic particles are attenuated by the earth's atmosphere and magnetic field; impinging primary-cosmic particles information was not received until the counter reached altitudes of over 90,000 feet.

The two successful flights with a two-million cu. ft. two-mil and three-million cu. ft. 0.75-mil balloon, reached 118,000 and 128,000 feet, respectively. They remained at altitude approximately 12 hours and data were received on all channels during the total flight time. All equipment was recovered in excellent condition.

The ultimate purpose of this detection system is to incorporate it, after further miniaturization, into a compact reliable direct-readout ionizing radiation meter which a pilot could observe at any time, indicating the radiation level received at any given time, as well as the total radiation exposure during the total flight time.

Prior to this miniaturization, plans are being formulated to fly the device in a satellite to measure and differentiate particles at higher altitudes and thereupon the RBE (*Relative Biological Effectiveness*) of each particle could be assigned.

*To be presented by *Horace Castillo.*

[1, 2] Assigned to Chicago Midway Laboratories, University of Chicago, scheduled to issue a Final Report Cosmic Ray Counter.

[3] Brush.

Notes

SESSION IV: General I

4.4: Remote Open-Chamber Method for Breathing Measurements in Hibernation Utilizing Thermistors

Samuel P. Battista, A. D. Little Co., Cambridge, Mass., and Albert R. Dawe, Office of Naval Research, Chicago, Illinois.

In An Ideal Sense, a device to measure respiration rate in animals entering hibernation and remaining in hibernation during an experimental procedure must meet the following unique requirements: *(1)* It must not touch or constrain the body of the animal in any way, since this may affect the animal's entrance into the hibernating state; *(2)* it must be capable of detecting gas disturbances which have a breathing rate range varying from 200/minute in the active state to .2/minute in hibernation; (3) it must measure amplitudes of as little as 0.01 cc of gas exchanged per respiratory cycle; and *(4)* it must be usable in a chamber open to the outer atmosphere, since a sealed chamber in some hibernation experimentation produces environmental variables which modify the results.

A breath detector *D* was developed which met the above performance requirements. It was small enough to be held in the hand; Figure 1. A phone jack connected the output into a suitable amplifier-recorder *E*. Connections were made for circulation of coolant water or brine through the water jacket in the detector.

The sensitivity of the device was noted by the following:

(a) Placed on a table in a room in which air movements are relatively slight, breathing movements of an individual 10 feet from the unit are easily recorded. Air movements caused by the individual moving his arm or leg record. Opening a door produces off-scale deflections.

(b) In a series of experiments with hibernating animals, excellent results have been reported elsewhere[1], which describe the extreme usefulness of the device for detecting otherwise imperceptible respirations.

Method

The operation of the sensing element is based on responses of a thermistor to temperature changes. Although a thermistor's resistance will undergo changes with the periodic warmth of exhalant air from an animal body, such changes are not sufficiently great in the case of a cold hibernating animal. To record respiration in hibernation, *flow* of exhalant gas alone must be detected. To accomplish this, the recording thermistor T_R (Figure 2) is mounted in an airway *A* surrounded by a brine or cold water jacket *J*. T_R is electrically connected into a Wheatstone bridge circuit as one arm of it. When voltage is increased across the bridge, T_R warms. Concurrently, the jacket temperature lowers due to circulating coolant. With extremely small flows of gas or breaths of air through the airway and across the heated thermistor, the amount of heat dissipated thereby (hence the change in resistance) is a non-linear function of air flow. This unbalances the bridge, is amplified and records. Thus, breathing changes are detected at a distance—remote from the animal.

Very great sensitivity was attained by building several novel additional features into the detector:

(a) A balancing thermistor T_B is enclosed in a glass air pocket in the water jacket with access to the airway through a pinhole *H*. Both T_R and T_B change in resistance with fluctuations in water jacket temperatures and with gradual changes in temperature in the airway *not* due to air movements. These resistance changes cancel each other on the bridge, making possible alone detection of those resistance changes which occur at T_R with air movement.

(b) A perforated inlet tube *P* prevents temperature gradient establishment within the jacket.

(c) Jacket coolant, together with the metal box around the device are grounded to a second earth ground *G*.

(d) A gang switch S_G, with proper circuitry permits:

Position 1—coarse bridge balance.

Position 2—thermometry circuit to note airway temperature.

Position 3—recording circuit when airway is O°-15°C.

Position 4—recording circuit when airway is 15°-30°C.

Usefulness

With or without telemetering, both respiration or activity can be recorded at a distance (remotely) in open or closed chambers.

[1] Landau and Dawe, *American Journal of Physiology*, 194 No. 1, 75; 1958.

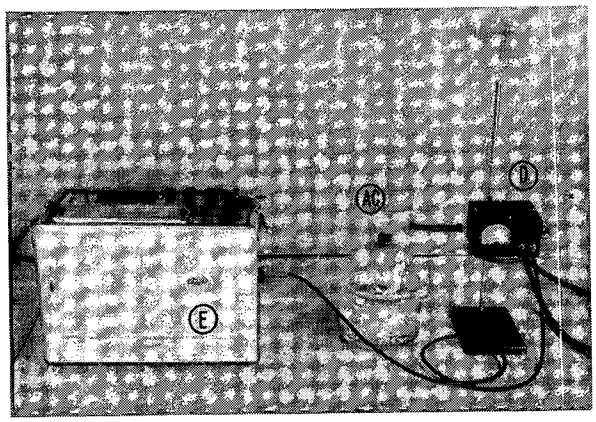

Figure 1—Device in use with 150-gram ground squirrel. D = breath detector, one end of airway connected to animal chamber, other end (obscured, open to atmosphere; AC = animal chamber; E = electrocardiograph amplifier-recorder.

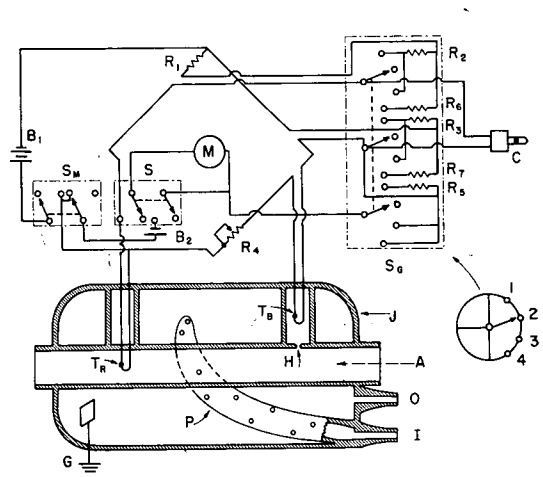

Figure 2—Schematic of breath detector: Resistance: R_1 = 50,000 ohms; R_2, R_3 = 250,000 ohms; R_4 = 25,000 ohms; R_5 = 500,000 ohms; R_6, R_7 = 100,000 ohms. Switches: S = spring, push button, S_M = double-pole-double throw, S_G = gang. M = microammeter, C = phone jack, T_R and T_B = Victory (51A16 less glass) thermistors.

SESSION IV: General I

4.5: Radio Telemetry of Whole Nerve Action Potentials*

Roger M. Morrell, Montreal Neurological Institute, Montreal, Canada

THE PURPOSE OF THESE EXPERIMENTS was to test the hypothesis that nerve impulses can be transmitted and received by an *FM-FM* system of the type commonly used in radio telemetry of pulse-coded data from remote points. To prove that this could be done, it was necessary to integrate certain electronic systems common to the neurophysiological laboratory with those commonly used in telemetry; Figure 1.

A portable checkout station and a complete main telemetry ground station were available for this research. Stimulus pulses were provided by a stimulator[1], and were delivered to whole guinea pig sciatic nerves via non-polarizable (*Ag- AgCl*) stimulating electrodes after being isolated from ground by an *rf* isolation unit. Pulses of 300 microseconds duration at one per second stimuated the nerve which was suspended in paraffin oil. Thresholds for excitation varied from 0.7 — 5.0 *v*. Healthy nerves followed a stimulus repetition rate of up to 400 pulses-per-second. The output of the stimulator was set at 2+, *monophasic* and *pulses*, and with a 5-volt signal received at the paraffin bath (stimulating electrodes) the *dc* resistance of the nerves (at the input probes) was approximately 20,000 ohms in one direction and 5,000 ohms in the other. Resistors (900 ohms) were placed in series with the output leads from the stimulus isolation unit to the stimulus probes. All probe input and output leads were twisted and screened.

The nerve action potential was led into a 40/20-db amplifier[2] through 100,000 ohms at the leads from the recording electrodes. The output of this amplifier terminated in a 3,300-ohm load to the input of a *dc* amplifier[3]. To determine the pickup level at the recording electrodes, a dummy recording circuit was used, as depicted in the insert of Figure 1. The pickup level was 1 millivolt. In paraffin oil, the input resistance at the test meter was greater than 1 megohm, and with a 40-volt input (stimulus at *V1* and *V2*) the output of the *dc* amplifier, after a gain of 2000, consisted of ±5-volt spikes, but there was no pulse and no *rf* superimposed upon a pulse. Spikes only were present at the output of the 40-db amplifier. To transmit a stimulus pulse followed by an action potential, instead of a pickup spike plus a response, the output of the stimulator was fed through a 100,000-ohm variable resistor to the output of the 40-db amplifier. Thus, the signal transmitted by the subcarrier oscillator consisted of the stimulus waveform followed by the response of the nerve. With capacitive artifacts on the stimulus pulse, the response itself might have been lost due to modulation of the subcarrier by the stimulus. For example, if the stimulus were 2 volts and the response were relatively much smaller, it would not be recovered. In these experiments the action potentials were initially negative-going, but the leads to the amplifier versus earth were reversed to get a physiologically-conventional positive-going response with only one capacitive spike.

The output of the *dc* amplifier[4] was fed through a 5,000-ohm potentiometer to the subcarrier oscillator[5] and also through 39,000 ohms in series with a 20,000-ohm potentiometer to feed the signal amplifier of the galvanometer recorder with the transmitted subcarrier-oscillator signal; the 40-kc channel of the subcarrier-oscillator was employed. For an input signal of 1000 microseconds at 0 to +2.5 volts, the deviation was 40—46 kc, or 15 per cent; *rf* deviation of 25 kc.

The transmitter[6] (221 Mc and 2-watts output) and the 26 volt-filament subcarrier oscillator were contained together in the telemetry pack. The transmitted signal was received[7] and fed through a switched bandpass filter for the 40-kc channel; Figures 2-4. For selection of filters, the following ranges were available: 3- 14.5 kc filter, f∞ at -3 db point = 1.1 kc, and 22-40 kc filter, f∞ at -3 db point = 2.1 kc. The receiver contained a multichannel discriminator. The input to the transmitter-subcarrier oscillator and the output from the receiver-filter were fed simultaneously to an oscilloscope[8] with dual and single-trace plug-in units for direct monitoring and measurements. Photographs[9] were made from the oscilloscope (Figure 5), and the same signals were fed to galvanometer-signal amplifiers[10] (with inverter amplifiers), the output of these amplifiers being fed to a 36-channel galvanometer oscillographic recorder through a variable series resistance and a parallel damping resistance. A signal generator[11] provided a timing standard of 1 kc, which was fed to the galvanometer and also through a 1,000-ohm potentiometer to the junction of the 40/20-db and *dc* amplifiers via a 7,000-ohm resistor. The galvanometer circuits were set for a one-inch peak-to-peak deflection at 1 kc. Maximum attainable galvanometer paper-speed was 100 inches-per-second.

With this instrumentation it was possible to record timed nerve action potentials, each preceded by its stimulus, and to compare the waveform of the telemetered action potentials with the directly-amplified response as led from the recording electrodes; Figure 6. Distortion of telemetered responses was sufficiently small to allow the suggestion that this method might be used with confidence in the transmission of data from nerves or other excitable tissue located in orbital vehicles or at other remote points where cable transmission is not feasible.

* The valuable theoretical discussion and technical assistance of George Whyte and Selwyn Bell, Special Weapons Division, Canadair Limited, Montreal, on this project are greatly appreciated.

[1] Grass S4-C [2] Hewlett-Packard 450A.
[3] Electromechanical Research Inc., type 62A.
[4] 62A, CVG 60-1 [5] EMR 83B.
[6] Raymond Rosen 960B. [7] Raymond Rosen 842-C1.
[8] Tektronix type 454.
[9] With a Polaroid camera.
[10] Allegheny Corp. 705A.
[11] Hewlett-Packard 205-AG.

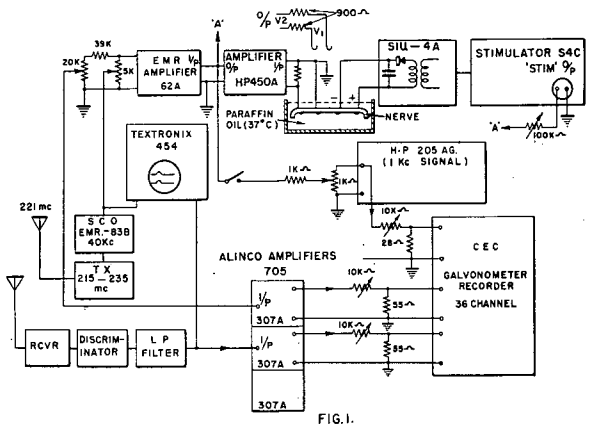

Figure 1—Experimental arrangement. Stimulator output is fed to nerve and amplified response is transmitted *(SCO-TX)* to receiver *(RCVR)*, as well as monitored directly by scope. Insert (above nerve) is circuit used to measure pickup.

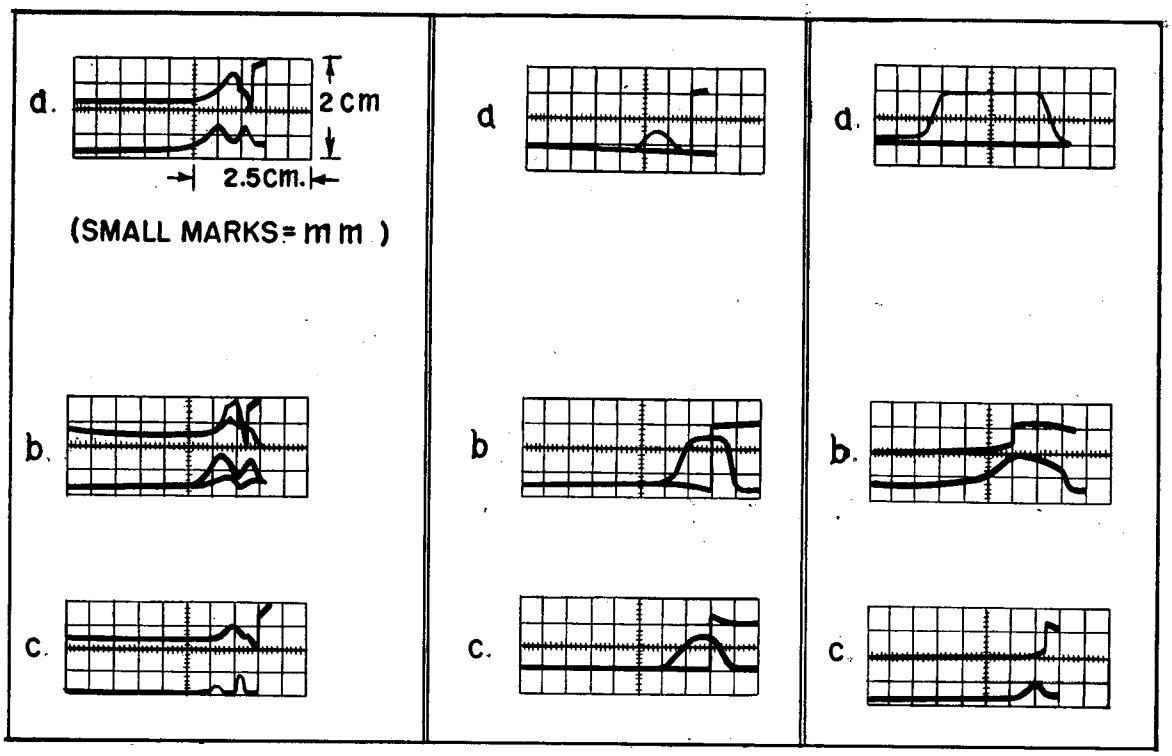

Figures 2, 3 and 4—Figure 2 is a subcarrier oscillator calibration. (*a*): (Top) transmitted subcarrier oscillator response; (below) received signal. Vertical sensitivity (top) 2 volts/cm; (below) 0.5 volt/cm. Time (right to left) 500 microseconds/cm, 150-microsecond stimulus pulse added at subcarrier oscillator. Plot (*b*) = 300-microsecond stimulus (superimposed); (*c*) = 100-microsecond stimulus. Figure 3 is portable ground-station record; traces as in Figure 2. Vertical sensitivity-1 volt/cm. (*a*)=Horizontal sensitivity, 200 microseconds/cm, 100-microsecond pulse, 2-kc filter; (*b*) = horizontal sensitivity 500 microseconds/cm, 1000-microsecond pulse, 2-kc filter; (*c*) = same, 1.1-kc filter. Figure 4 represents main ground-station record; traces as in Figure 2. Horizontal sensitivity = 200 microseconds/cm; vertical 1 volt/cm. (*a*) = 1000-microsecond pulse, 3.3-kc filter; (*b*) = 1000-microsecond pulse, 2.1-kc filter, via electrodes in Elliott's solution; (*c*) = 100-microsecond pulse, 2.1-kc filter, (electrodes).

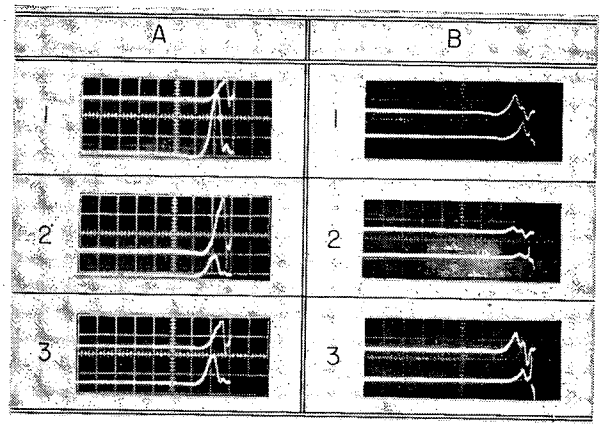

(*Right*)

Figure 5—Oscilloscope record. Horizontal sensitivity (right to left)=1 millisecond/cm; vertical sensitivity 2 volts/cm. *A1* (top), transmitted; bottom, received. Stimulus 1 volt, 220 microseconds. Lower trace has higher gain. Traces in *A2*=sensitivities reversed, *A3*=equal. *B1*=different nerve: top, received; bottom, transmitted. Stimulus=2 volts. Traces in *B2*=stimulus 0.75 volt; *B3*=3 volts.

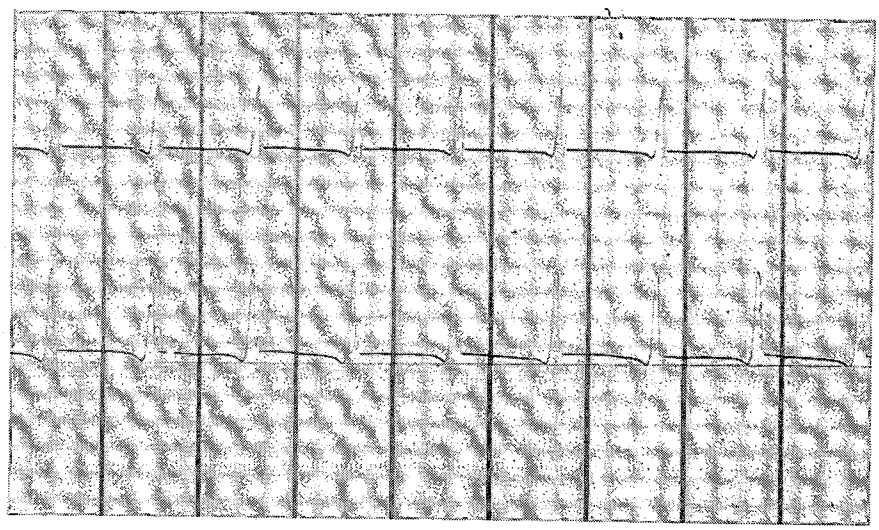

(*Right*)

Figure 6 — Oscillograph record. Top — transmitted signals; middle — received signals; bottom — 1-kc timing waveform. Time: right to left, stimulus followed by response. Paper rate: 100 inches per second, left to right. Lamp voltage, 15.5; stimulus 1 volt at 220 micro-seconds, 100/second.

SESSION V: Microwave Radiation I

Chairman: George M. Knauf USAF, MC

Air Force Missile Test Center, Patrick Air Force Base, Fla.

5.1: Biological-Effects of Microwave Radiation: A Research Progress Report

George M. Knauf, USAF, MC, Patrick Air Force Base, Fla.

9. Biological response - (effects) - needs increased emphasis in transfer from RADC to Scientific Research.

THIS PAPER will present a review of the progress made to date in exploring the problem of hazards to personnel as a result of exposure to the beam of a radar set. Data developed by the various research groups engaged in investigating the several aspects of this problem will be discussed insofar as they can be related to the radar-hazards control problem. No attempt will be made to assay individual research results, but rather an attempt will be made to generalize on these results as safety guide lines. Special attention will be paid to the crystalline lens of the eye as probably the body tissue most susceptible to this energy. Animal experiments establishing the cataractogenic property of this energy will be cited as the basis for a study of human ocular exposures at an electronic research center. A plan to extend this pilot study to include a large group of employees in the electronic industry will be outlined.

The question of sterilization of the male by exposure to this energy will be discussed.

Certain precautionary measures deemed to be effective in avoiding injury as a result of being required to perform certain essential operations in a high-power *rf* field will be discussed.

Finally, the future course of this research program will be discussed, with special reference to the effects of this energy on single cells and the nervous system.

Knauf
1. Beyond 500 ft - not much of a problem
2. 1/100 of a watt, well established; eye estab. as most susceptible.
3. not sure of frequency division, Probably need caution at lower frequencies.
4. Sterility of male - out.
5. Worked with small group of RADC to determine opacity effects of RF radiation on eyes. Above 70% in age groups below 30 years, and between 31-39 years.
6. RADC sponsoring industrial survey to determine further effects on eye, and ways of avoiding hazards.
7. No known serious injury or death as result of exposure.
8. Techniques - shielded passageways, impregnated clothing, metallic mask goggles for eyes

SESSION V: Microwave Radiation I

5.2: Review of Some Recent Research on the Whole Body Effects of Microwaves

Thomas S. Ely, Office of Health and Safety, Atomic Energy Commission, Washington, D. C.

"Specific Effect" of radio-frequency energy on biological materials was an active question a generation ago. *Dalton, Weisz, Nasset, Fenn, Taylor, Coulter,* and others were extolling the pros and cons of the matter during the middle thirties. Those who proposed anything other than a thermal effect seem to have lost the debate, and little more was heard of the matter. Also, it must be remembered that wavelengths were long, and powers were low in those days. World War II brought higher powers of higher frequencies than had ever been broadcast before, by several orders of magnitude, and the postwar years have seen no slackening of the trend, although the recent development has been toward higher powers rather than higher frequencies.

It was inevitable that the question of "Specific Effect" should be reopened. Now we call it "Athermal Effect" as opposed to "Thermal Effect." The low duty cycles found in radar applications have added to the interest in athermal effects, since these might be postulated a result of peak power not masked by thermal effects related to average power. The debate is now as lively as it was in the thirties.

"Thermal orthodoxy," a delightful term used by *Dr. Russell L. Carpenter,* is aptly applied to the thermal school of thought. This line of thinking says that temperature rise in a particular tissue location can be described on the basis of the energy of radio-frequency input, rate of heat dissipation, and time, and that the effect produced in the biological material is related to the temperature and the time.

A simple model of this concept is the structure which gains heat at a constant rate in a constant field, and which loses heat at a rate proportional to its temperature rise. This model can then be said to have a time constant, say the time required to reach ½ or 1/e of the equilibrium temperature following a step change in radiation field. The heating time constant would be identical with the cooling-time constant.

Such thinking was considerably reinforced by much experimentation. Small areas of experimental animals behave with remarkable similarity to the idealized model. Even whole animals, particularly the smaller ones, approximated this case. Time constants for limited portions of the organism were measured in hundreds of seconds, for entire organisms up to hundreds of minutes.

In the practical situation of personnel exposure to microwaves, there are several field periodicities. Smallest in interval would seem to be the individual half-cycle of the fundamental frequency. Next longer is the pulse interval of a pulsed equipment. Next would be the field variations caused by a nutating feed horn, intermittent pulsing, or antenna rotation or sectoring. A very long period is represented by a military man on watch, or a civilian worker on a shift.

Thermal orthodoxy tells us that from the standpoint of effect, we must average the power over the periods much shorter than the biological time constants, but must not average power over the periods much longer than the biological time constants. Thus, we may consider the conventional "average" power, but we don't average a sailor's four hours on watch with his eight hours off watch. Where field period is of the order of biological time constant, an intermediate situation exists.

Research in the field of the biological effects of microwaves today covers work with several fundamental frequencies, pulsed and *cw*, several species of subject, several portions of the body exposed, and many ways of looking for and evaluating biological effect.

Some of the current research on the whole body effects of microwaves will be considered briefly in order of frequency:

At the University of Buffalo, Drs. *Fischer* and *Osborn* have exposed the whole bodies of chick embryos, mice, guinea pigs, dogs, and sheep to 200-megacycle fields, both pulsed and *cw*. The effects produced can be correlated with temperature rise. Rather intense fields were survived by the eggs and mice, presumably because of the relative transparency of objects this small compared to the wavelength. Some burns and subcutaneous damage were found in the dogs and sheep. Death of the larger animals due to hyperthermia could be produced by fields in the order of 200 mw/cm², whereas mice lived and reproduced in fields of 700 mw/cm² of long duration. The interesting fact was noted that more heating occurred in dogs oriented parallel to the plane of polarization than perpendicular to it. This effect would be unlikely with a wavelength small compared to the length of the animal.

Dr. *Richardson* at St. Louis University, Dr. *Howland* at the University of Rochester, and Drs. *Imig* and *Searle* at the State University of Iowa have used microwave exposures to "S" band frequencies. The Rochester equipment is pulsed, the other two are *cw*, and yet experimental results of all three groups are consistent when compared on the basis of average power. Chick embryos exposed in the St. Louis laboratory were not adversely affected, if temperature did not exceed that normal for incubation. Rats exposed by the same group and dogs exposed by the Rochester group have been studied in considerable detail from a physiological and pathological standpoint. Results are consistent with a hyperthermal mechanism. It is interesting to note that although one group uses a continuous wave field and the other a pulsed field with a duty cycle of 1:1400, physiological changes are similar, and are comparable to effects produced by other forms of heating.

The Iowa group has compared head and abdominal radiation exposure in their effect on whole body and localized temperature rise. They found that head irradiation was more effective in raising the rectal temperature than abdominal exposure, presumably because of greater direct heating of the thermoregulatory center. This group also has 10,000-Mc pulsed equipment. With it they made some comparison dog exposures, and found a definite greater penetration of the longer wavelength "S" band energy.

Dr. *Susskind* and his group at the University of California, and Dr. *Nieset* and his group at Tulane University, have conducted whole body exposures to 10,000-Mc pulsed microwave fields. Both laboratories have determined an *LD*50 for mice, and both find that it bears a simple relationship to body temperature. Additional studies by the California group on mice and rats have allowed the development of detailed mathematical models of the heating and cooling characteristics. The Tulane group exposed animals to fields of 10 mw/cm² for prolonged periods, and found no adverse effect as determined by body weight. They have also performed chronic irradiations of cold-blooded animals, and have found no effect at field intensities that would have killed mice.

Dr. *Deichmann* and his group at the University of Miami are studying the effects of the highest frequency under investigation, 24,000 Mc. Their equipment is pulsed. Rats exposed to this energy heat die, as one would anticipate, from thermal considerations. A critical lethal temperature of 43°C was found, which is similar to that developed by several other investigators. In a cycling experiment, in which the transmitter was switched on and off at regular intervals, they found substantial difference from an equivalent average field, even with a cycling period as low as six seconds.

Some of the current research on the whole body effects of microwave irradiation is yielding results that might reasonably have been predicted on the basis of a thermal model. Other research is giving valuable quantitative data on the thermal effects which were predictable only in a qualitative sense. Some investigators are uncovering findings which are disquieting to the thermal orthodoxy devotee. Skin burns are produced in the animals at Rochester and Buffalo in fields which seem incapable of causing that degree of differential heating. The effects of a field switched on three seconds and off three seconds at the University of Miami indicates a structure which has a time constant shorter than suspected. The low penetration of 1.25-cm waves suggests the skin as this structure, and one would expect the skin to have a short time constant. But one would not expect it to prove critical in causing the acute death of the animal.

SESSION V: Microwave Radiation I

5:3 Physical and Electrical Characteristics of a Microwave Hazard

Joseph H. Vogelman, Research and Development, Dynamic Electronics-New York, Inc., Richmond Hill, N. Y.

THE EFFECT on living organisms and humans of radio-frequency energy is a function of the ratio of the size of the exposed organism to the wavelength, the loss tangent and interface characteristics and the average and peak power to which it is exposed. For a material of given resistivity, permittivity, and permeability, the incident field will be partially reflected and scattered, partially absorbed, and partially transmitted.

The "hazard" of a particular field density (watts/1 cm²) is a function only of the power absorbed by the living organism. The power-absorption percentage is a function of the physical dimension of the organism compared to the wavelength of the radio-frequency signal. In any material, the attenuation in decibels per-unit length is proportional to the loss tangent and inversely proportional to the wavelength. Accordingly, for an organism small compared to the wavelength, the total energy absorbed, for a given resistivity, is small. When the wavelength is decreased the absorption percentage increases and the "hazard" increases. The maximum fraction of the incident power density that can be absorbed is limited further by the reflected and scattered energy at the interface between free space and the organism's surface.

An idealized set of curves are shown in Figure I for different combinations of resistivity, permittivity and permeability. For living organisms, the case of a largest dimension-to-wavelength ratio of 0.1 is considered to be the lowest frequency where the effect of radio-frequency energy in space is potentially "hazardous". The area of the effect is a function of the penetration depth. For human or animal tissue, this value is in the order of 1/10 to 1/100 of the wavelength. Some selected frequencies are tabulated below showing smallest size considered important and penetration depth:

Frequency	*Wavelength*	*Minimum Size*	*Penetration Depth*
3 mc	100 m	10 m	1-10 m
15 mc	20 m	2 m	0.2-2 m
3 kmc	10 cm	1 cm	0.1-1 cm
15 kmc	2 cm	2 mm	0.2-2 mm
300 kmc	1 mm	0.1 mm	0.01-0.1 mm

Interfaces within the skin surface of a living organism produce additional reflections which form standing waves inside the organism. The peaks of the power standing wave are "hot spots" producing increased effects.

The effects on living organisms can be divided into thermal and non-thermal effects. The thermal effects are directly related to the average power absorbed from the incident *rf* field. In the case of pulsed systems of large peak to average power ratios, the average power has been found to be the significant factor. This is true only if the time duration of the individual pulse is extremely short compared to the thermal constants of the human organism. Where the pulse duration is a large portion of a second, the peak power effect may cause an effect out of all proportions to the average power in the incident field. Dimensional resonances as well as molecular, electron and nuclear resonances increase the *rf* energy absorbed from the incident field. The non-thermal effects take the form of either alignment of the molecules with the direction of the field or in disassociation of the molecules into their components. These effects have been found in only a few circumstances and are as yet not correlated to the *rf* phenomena; these effects may be related to the peak power rather than the average.

FIGURE 1

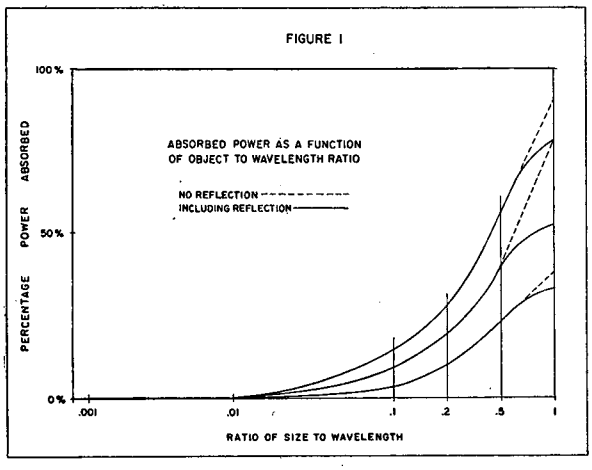

FIGURE 2

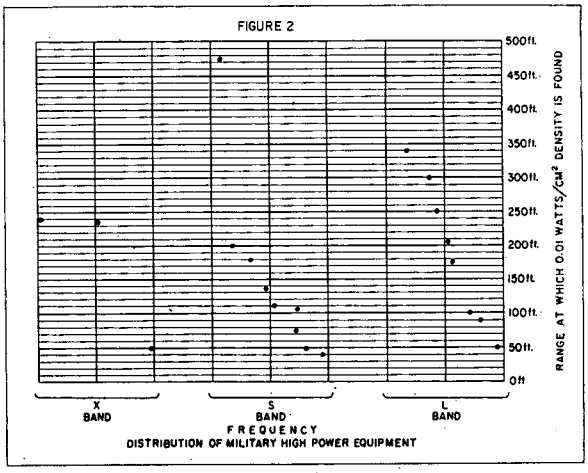

DISTRIBUTION OF MILITARY HIGH POWER EQUIPMENT

Radio-frequency "hazards" are associated with the fields along transmission lines and the radiated fields from antennas. To be effective, a transmission line system cannot radiate any significant portion of the energy carried on it. For most practical transmission lines in use today, the *rf* field external to the transmission line is negligible. Even in open-wire transmission lines, the greatest hazard is from an electrical arc from the transmission line and not from the *rf* field. In the case of extremely large waveguides the possibility of being in the waveguide when the *rf* energy is being transmitted must be avoided.

The Department of Defense has accepted a field density of 0.01 watt-per-square centimeter average as being completely safe regardless of exposure time. This value will be used as the criteria for the existence of a "hazard". The peak and average power associated with the largest currently programmed or developmental transmitters are given below; the power density at the feed horn of the antenna is also given:

Frequency	*Tube*	*Peak Power*	*Average Power*	*Power Density*
9200 Mc	Magnetron	0.75 mw	0.75 kw	234 watts/cm²
5400-5900	Klystron (T)	3.0 mw	3.0 kw	303 watts/cm²
2700-2900	Magnetron	5.0 mw	4.5 kw	155 watts/cm²
	Magnetron (T)	3.5 mw	3.5 kw	120 watts/cm²
	Klystron (T)	5.0 mw	8.0 kw	276 watts/cm²
1250-1350	Magnetron	9.0 mw	10.0 kw	86 watts/cm²
	Klystron (T)	2.0 mw	6.0 kw	52 watts/cm²
	Klystron (T)	10.0 mw	15.0 kw	129 watts/cm²
400-450	Triode (T)	5.0 mw	300 kw	212 watts/cm²

It can be readily seen that these values are extremely high and that for such systems the region between the feed and the reflector is dangerous.

In front of the reflector and behind the feed, the near field out to a distance of the diameter squared divided by the wavelength can be considered to have a field density equal to the total power divided by ¼ the area of the antenna. Thus, a 3000-Mc, 10-kw average power system 10 square using a meter-antenna reflector would have a field density of approximately 0.4 w/cm² out to a distance of 120 meters. Beyond this point the far field inverse square law with distance would hold.

Within the main beam, the minimum distance at which the 0.01 watt/cm² level is not exceeded can be obtained from the formula:

$$\text{Range in Meters} = 0.0886 \times \frac{\text{Ant Diam in Meters}}{\text{Wavelength in Meters}} \times \text{Square Root of Trans Power}$$

Figure 2 shows these values for existing radars, while Figure 3 shows the beam characteristics of the "hazard" region. Protective measures and standing-wave regions will be discussed.

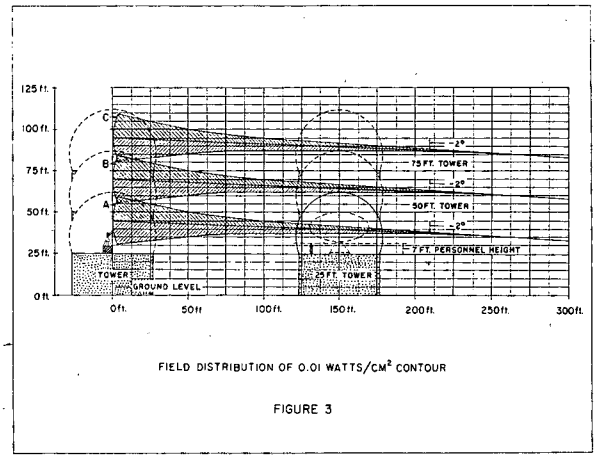

FIELD DISTRIBUTION OF 0.01 WATTS/CM² CONTOUR

FIGURE 3

SESSION V: Microwave Radiation I

5.4: Some Observations Regarding Temperature Sensations Due to Microwave Irradiation

E. Hendler, Air Crew Equipment Laboratory, Naval Air Material Center, Philadelphia, Pa., and J. D. Hardy, Physiology Dept., School of Medicine, University of Pennsylvania

MICROWAVE IRRADIATION is a useful tool in the study of temperature sensation mechanisms because the primary, volumetric heating of the tissues it produces is different from secondary heating due to conduction following heat application to the skin surface. However, it is usually more difficult to measure accurately the distribution and magnitude of microwave energy effective in heating the tissues, as compared, for example, to measuring these properties of infrared radiation. In some past experimental studies, microwave energy has been delivered to the tissues by direct application of the end of the waveguide over the region of the body to be heated. While this method provides for an efficient transfer of energy, there are several disadvantages inherent in its use. Among these are difficulties in accurately measuring skin temperature, in obtaining uniform distribution of energy over the irradiated surface and in avoiding undesirable tactile and thermal stimulation of the skin. To utilize a highly accurate radiometric method for measuring skin temperature, and to minimize the other difficulties mentioned above, a method for exposing human subjects to free-field microwaves was devised. It is the purpose of the present report to describe this method and to indicate the findings obtained from some initial experiments.

A radiometric apparatus was used consisting essentially of a sensitive radiometer to measure continuously skin temperature, a microwave generator to heat the skin and equipment to control the generator output and record skin temperature, temperature sensations and generator "off-on" periods. The principal components of this apparatus are described in greater detail and diagrammatically illustrated elsewhere in this Digest. A microwave pulse generator was used as the source of energy having a free-field wavelength of 3 cm.* A rectangular metal horn was positioned behind the peripheral portion of a revolving, metal chopper, which interrupted the radiation reaching the exposed forehead skin of seated subjects approximately 13 times per sec. The horn formed the terminal portion of a five-foot length of waveguide leading to the output section of the pulse generator. The generator was set to produce 2500 pulses per sec, each having a duration of 0.4 microsec. Sheets of microwave absorbing material were so arranged around components of the apparatus as to eliminate undesirable effects produced by reflected energy.

To control the duration of microwave irradiation, a switching arrangement was devised, whereby actuation of the pulse generator could be accomplished either manually or automatically. Automatic control was effected by a rotating cam activating a microswitch according to a fixed sequence of "off-on" intervals of various durations. Occurrence and duration of temperature sensations were recorded by means of signal pens activated by switches manipulated by the subjects.

To measure the intensity and distribution of energy at the location where the skin was exposed, a 5-mm thick water layer contained in plastic was used. Increase in water temperature was measured by one or more thermocouples positioned within the water, and absorbed energy was also determined calorimetrically by the method of mixtures. Both skin and water layer temperatures were found to increase linearly upon irradiation, the surface of the former at a rate about five times greater than the average of the latter. Both of these factors point to the primary nature of the microwave heating. In the case of skin, using an energy intensity of about 4 mcal/cm²/sec, the increase in temperature remained linear for approximately the initial 30 sec of heating.

The temporal relationship between temperature sensation and changes in skin temperature was characterized by its variability. A significant delay was usually found between cessation of stimulus (and accompanying rapid drop in skin temperature) and cessation of warmth sensation. This finding is in contrast to the usually immediate cessation of warmth sensation following cessation of stimulation with infrared radiation. The foregoing observation provides additional evidence against the hypothesis of the spatial intracutaneous gradient as the effective stimulus for temperature sensation.

---

* The microwave pulse generator (SG-58A/U) was made available for this study by the Aeronautical Electronic and Electrical Laboratory, Naval Air Development Center, Johnsville, Pennsylvania.

$\frac{10}{5/2} = \frac{10 \times 2}{5} = 4$

SESSION V: Microwave Radiation I

5.5: Characterization of the Thermal Response Among Animals Exposed to Microwaves or Increased Environmental Temperature

Sol M. Michaelson, Roderick A. E. Thomson and Joe W. Howland, Department of Radiation Biology, University of Rochester School of Medicine and Dentistry, Rochester, N. Y.

WITH THE EXPANDING USE of microwaves at military and industrial installations, the biological effects of this form of energy are receiving increased attention. Investigation of potential hazards to man has necessitated a biomedical approach to this problem.

To date definitive information for man can be obtained only by extrapolation from animals along with comparison to meager human data. Man is an extremely complex organism with numerous interacting parts and systems. The various functions and reactions of the body are regulated by feedback and homeostatic or control mechanisms.

Because of this complexity and the variability of mammalian biological responses, it is essential to investigate different species of animals under a variety of exposures before experimental results can be reliably extrapolated to man.

Numerous physiologic factors such as interspecies and interstrain variability; intraspecies age, sex, body-size differences, or previous medication, coupled with physical aspects of exposure, such as frequency or power density, result in marked alterations in the biologic response to microwave exposure. These factors must be considered before one can attempt to elucidate the effect of microwaves in the living, intact mammal.

For a first approximation of the biological effects of microwaves, characterization of the thermal response is essential. This has been done for three species of animals exposed to 200 and 2800-Mc microwaves and increased environmental temperature. In these three types of exposure, the inherent thermal regulatory capacity and the degree of microwave penetration and absorption would appear to be the determining factors in the animal's response to microwave exposure.

The thermal response in a dog exposed to 165 mw/cm²-2800-Mc pulsed microwaves has been characterized and found to consist of three distinct phases. Phase I consists of the *Initial Thermal Response* in which there is fairly rapid heating with a 2-3°F increase in body temperature within one-half to one hour after onset of exposure. After this initial period the animal equilibrates and enters Phase II—the *Period of Thermal Equilibrium.* This period may last one hour during which time the temperature will cycle between 105 and 106°F. Phase III—*Period of Thermal Breakdown* occurs when the temperature rises above 106°F, continues increasing rapidly until a critical temperature of 107°F or greater is reached, at which time the animal may collapse and if exposure is not stopped, death may ensue.

The rabbit and the rat are extremely sensitive to this frequency. A critical temperature is usually reached in 10 minutes in the rabbit and 20 minutes in the rat, with no equilibration taking place. Body size does not seem to be a factor in the thermal response at this frequency. The rat and rabbit respond fairly similarly.

At 200 Mc, 165 mw/cm², the dog equilibrates somewhat later than at 2800 Mc, remains in equilibrium for a longer period of time on the average of 5 hours, before thermal breakdown is evident. A four-kilogram dog responds the same as a larger dog. The rabbit equilibrates slightly and critical temperature occurs within 30 minutes, which is slower than at 2800 Mc. The rat shows some equilibration at ½ hour with thermal breakdown, absent at one hour.

Upon exposure to increased environmental temperature of 120°F, 50% humidity, none of the animals equilibrate and critical temperature is reached between 30 minutes and one hour for all animals. These results are summarized in Table I.

Anaesthetization with pentobarbital seems to delay the approach to a critical temperature in the rabbit and rat exposed to 2800 Mc, but not in the rat subjected to 200 Mc. The anaesthetized dog seems to reach a critical temperature much more rapidly than the normal dog when exposed to either 2800 or 200 Mc. Anaesthetization does not seem to influence the time required for reaching critical temperature for any of the animals exposed in the "hot room" (Table I).

Four dogs picked at random were exposed to 165 mw/cm²-10-cm microwaves in a latin square experimental design, while under medication with pentobarbital sodium, morphine sulfate, or chlorpromazine. At least one week elapsed between exposures. Continuous rectal temperature recordings were obtained on each dog.

The results are summarized in Table II. Thermal equilibrium is not reached with pentobarbital. Temperature increase is more rapid with morphine than in unmedicated dogs; thermal equilibrium is reached more rapidly and continues for a longer duration. Thermal breakdown under chlorpromazine occurred after approximately the same equilibration time as with unmedicated dogs. Since thermal equilibrium is not achieved while under pentobarbital medication, a critical temperature is reached much earlier in these dogs.

Evaluation of the differential white cell changes suggests a stress effect, which possibly is related to duration of exposure.

Although thermal effects have not been elucidated in the whole body exposed animal, head exposure of the rabbit would indicate that there may be a direct effect on the brain stem of such exposed animals.

	Microwaves — 165 mw/cm²				Hot Room	
	2800-Mc pulsed		200-Mc continuous		120°F 50% Humidity	
Animal	*Normal*	*Anesthetized*	*Normal*	*Anesthetized*	*Normal*	*Anesthetized*
Dog	*40/110	0/35	64/288	0/93	0/48	0/50
Rabbit	0/10	0/30	0/30	0/?	0/30	0/45
Rat	0/22	0/40	30/55+	0/20	0/35	0/38

* Minutes

Table I: Thermal response of animals exposed to microwaves or increased environmental temperature (Time for Thermal Equilibrium; Time for Thermal Breakdown)

Drug	Dose	Onset of Exposure After Administration of Drug (minutes)	Thermal Equilibrium (minutes after onset of exposure)	Thermal Breakdown (minutes after onset of exposure)	Initial 30-Minute Heating °F Increase Mean ± s.e.	Initial 30-Minute Cooling °F Decrease Mean ± s.e.
Control	.....	..	36-154	154	1.31 ± 0.47	3.75 ± 0.30
Pentobarbital Sodium	To Effect ca 30 mg/kg i.v.	0	0	36	4.44 ± 0.47	2.25 ± 0.40
Chlorpromazine	2 mgm/kg i.m.	40	43-173	173	2.50 ± 0.47	3.63 ± 0.29
Morphine Sulfate	4 mgm/kg s.c.	60	23-123	123	2.13 ± 0.47	2.63 ± 0.33

Table II: Thermal response of dogs exposed to microwaves after medication

Notes

1. Response of normal dogs to microwaves at 200 and 2800 MC/S.
   (CW) (Pulsed)
2. Response of dogs to microwave exposure at 100 MW and 160 MW.

SESSION V: Microwave Radiation I

5.6: Biological Effects of Pulsed Electromagnetic (2880 MC) Irradiation

Joe W. Howland and Sol M. Michaelson, Department of Radiation Biology, University of Rochester School of Medicine and Biology, Rochester, N. Y.

STUDIES ON DOGS exposed to 2880-Mc pulsed electromagnetic irradiation from an AN/MPS-14 search radar adapted for biologic experimentation will be reported in this paper.

Single and repeated exposures at energy levels of 100 and 165 mw/cm^2 for times up to 6 hours were carried out. Clinical reactions as observed in the animals will be noted and various physiological reactions described. Characterization of thermal response into periods of initial heating, thermal equilibrium, thermal breakdown and death of recovery will be made.

Changes in hemodynamics, as measured by blood assay, will be included with specific descriptions of behavior of cellular elements. Observations of eosinophil appearance and disappearance suggests a stress response at intermediate power (100 mw/cm^2); with high power level, an adrenal exhaustion phenomenon may occur.

Minor changes in fat absorption as measured by 1-131 labelled fat will be noted. Shortening of red cell life occurs in some animals at higher exposures. A response of injury in thyroid function will be commented upon.

Alteration of antibody production occurs. A prolongation of antibody life will be observed. Passively transferred antibodies may be metabolized more rapidly in exposed animals. Studies on repeated exposure indicate development of adaptation or accommodation responses suggestive of physiologic memory. This response is completely wiped out by chlorpromazine therapy. On short repeated exposures, a possible development of thermal and vascular fatigue gradually occurs. Studies on serial exposures to ionizing and microwave energies will be discussed. The gross and pathologic changes observed will be given in a future discussion.

Notes

SESSION V: Microwave Radiation I

5.7: Studies on the Behavior of Phantoms in Electromagnetic (Radar) Fields

H. Mermagen, University of Rochester Atomic Energy Project, Rochester, N.Y.

IT HAS BEEN repeatedly published that the determination of absorption characteristics from microwave energies are a prerequisite to biological experimental work with such radiations.

In order to investigate by physical means some of the experimental results, which will be presented in a paper on biological effects of microwave radiations, phantoms were designed by which this theory on penetration of microwaves could be tested.

The use of phantoms for the determination of radiation absorption is based on the experience gained in similar measurements in the field of ionizing radiations. With slight modifications of such phantoms, it is therefore possible to gain information of the quantitive transfer of energy from a microwave field, both in terms of depth of penetration of such microwave into the phantom, as well as temperature gradients which are indicative of the quantity of microwave energy absorbed in such a phantom.

Since the principle phenomenon studied on biological systems was that of temperature rise in animals under conditions of exposures to varying frequencies and varying field strengths and power densities, it seemed logical to correlate these phenomena with the physical phantom in both static and dynamic conditions.

The construction of these phantoms resolves itself primarily into a design of cylindrical shallow sections of between 1 cm - 2 cm in depth, to anywhere from 5 cm - 20 cm in diameter. Variations in these sizes were to indicate similarity between rats, guinea pigs, rabbits and dogs. The individual cells of these phantoms can be filled with aqueous solutions simulating the dielectric constants of tissue, primarily soft tissue. A thermocouple was introduced into each cell for the measurement of temperature during exposure of the phantom to microwaves. Stacked cylindrical cells were exposed to microwaves in the direction of the long axis of the cylinders. Cursory measurements of the transmission through the cylindrical array of cells were made to determine the approximate self-absorption within walls as well as the reflection from the front surface exposed to the microwave horn and the antenna. It was found that a 1/16-inch lucite separation between individual cells, amounting to a total of 3/4-inch of lucite for a stack of twelve cells, did not materially interfere with the transmission of microwaves as indicated by a power meter. The phantoms were placed behind an absorbing shield in such a way that the aperture within the absorbing shield was slightly smaller than the diameter of the phantom cell. Power meter measurements were then made with cells filled with water and measurements through various thicknesses of water barriers were obtained.

Simultaneous measurements of temperature rise of the liquid within the individual cells were recorded. From these temperature-time relationships, energy absorption calculations were made in terms of calories per gram. In view of the static nature of these measurements, no equilibration between input thermal energy and radiation losses from the phantoms was attained. Such equilibria conditions were not expected from the experiment.

The second type of experiment was that of introducing a flow-controlling pump which would circulate the liquids in the individual cells from the cell closest to the source of microwave radiation into the cells of the posterior portion of the phantom. This type of experiment was an attempt to simulate the vascular flow within an animal as the transport medium of thermal energy into the deeper sections of the animal tissues. The time-temperature relationships observed in the individual cells were such that equilibrium conditions could be reached simulating those found in animals when exposed to microwave radiation.

The purpose of these experiments was primarily to verify some of the calculated depth of penetration of microwaves of different frequencies into media with dielectric constants similar to that of water, under conditions of varying power densities of the incident microwave energy. Furthermore, the phantom exposures during dynamic operation were to demonstrate the need for considering the relation between power density and the exposure time, for purposes of establishing permissible exposure levels to personnel working in the vicinity of high power radar installations. At present, a level of 10 milliwatts-per-square centimeter is accepted as the provisional maximum permissible microwave exposure. However, it must be foreseen that under certain conditions individuals might be exposed to considerably higher power levels. Therefore, if an exposure time limit could be derived from physical and animal data, a more flexible concept of maximum permissible exposure with the added parameter of time might prove useful.

SESSION VI: Ultrasonic Radiation I

Chairman: William J. Fry,

Biophysical Research Laboratory, University of Illinois, Urbana, Illinois

6.1: The Absorption of Ultrasound in Biological Materials

Edwin L. Carstensen, U. S. Army Chemical Corps, Fort Detrick, Frederick, Md.

PHYSICIANS for several years have been making therapeutic application of the high coefficient of absorption of sound in tissue and biological materials. This discussion attempts to localize the site of action of ultrasound and investigate the mechanism of the absorption process.

This first clue comes from the observation that *solutions of macromolecules* have far greater absorption than the water in which they are dissolved. Perhaps the most thoroughly investigated protein is hemoglobin whose acoustic properties are summarized in Figures 1 and 2. Figure 2 demonstrates a dispersion in the velocity of sound. The observation of dispersion eliminates the classical heat conduction and viscous processes of absorption as well as hysteresis as defined by *Mason*[1]. It has been possible to demonstrate[2] from the relationship between the magnitudes of the absorption per wavelength and the dispersion in the velocity, that the absorption is caused by a relaxation process characterized by a broad spectrum of relaxation times.

Consider now a slightly more complex system: a *suspension* of cells, as exemplified by blood. Figure 3 gives the absorption from the cellular components of blood and plasma as well as for whole blood. Comparison of the absorption in packed red cells with that for hemoglobin at the same concentration forces us to conclude that all of this absorption is on a molecular level. The observed absorption in whole blood is somewhat higher at the lower frequencies than can be accounted for by protein absorption. It has been shown[3] that this additional absorption arises from relative motion between the dense red cells and the surrounding fluid.

To arrive at a similar understanding of the processes involved in the absorption of sound in *tissues* is a more difficult task for two reasons: *(1)* The structure is much more complex than suspensions of single homogeneous cells. *(2)* Acoustic measurements of an inhomogeneous, non-rigid solid are apt to be somewhat less precise than measurements of fluids. With the exception of certain kinds of fat, liver is probably the simplest of the tissues from the standpoint of homogeneity. Still, as indicated in Figure 4, the spread in data from various investigators is large. Some of this disagreement may arise from differences in technique. Part, of course, must come from true differences between liver tissues studied. Since a very large fraction of the total absorption in blood occurs on a molecular level, it is logical to look first for this process in tissues. *Schwan, Pauly* and *Smith*[4] have approached this problem by homogenizing liver tissue with grinders and blenders. The extent of break down—from intact tissue to almost complete cell destruction—had only slight effect on the specific absorption (absorption per gram dry weight) of the material. Furthermore it was found (Figure 5) that the specific absorption of one of the molecular components of liver was higher than that of liver tissue as a whole. It follows that for liver tissue as well as blood that a very large fraction of the total absorption occurs on a molecular level. Whether this statement could be broadened to include all soft tissue cannot be stated with knowledge presently available. Figure 5 illustrates that the specific absorption for different biological macromolecules varies over a large range.

Although the importance of molecular absorption in tissues cannot be questioned, the selective heating of the regions near macroscopic discontinuities is equally well established. In general, the reflection at a discontinuity will consist of a transverse wave as well as a longitudinal wave. The absorption coefficient for the transverse wave in tissue is so high that it is completely dissipated in the immediate neighborhood of the discontinuity. This effect is reduced as the discontinuities become smaller. In any given tissue, therefore, the absorption occurs primarily on a molecular level, but is modified to some extent by the presence of inhomogeneities.

---

[1]Mason, W. P. "Piezoelectric Crystals and Their Application to Ultrasonics", *D. Van Nostrand;* 1950.

[2]Carstensen, E. L. and Schwan, H. P., *J. Acoust. Soc. Am.* 31:305-311; 1959.

[3]Carstensen, E. L. and Schwan, H. P., *J. Acoust. Soc. Am.* 31:185-189; 1959.

[4]Schwan, H. P., Pauly, H., Smith, A., *unpublished data.*

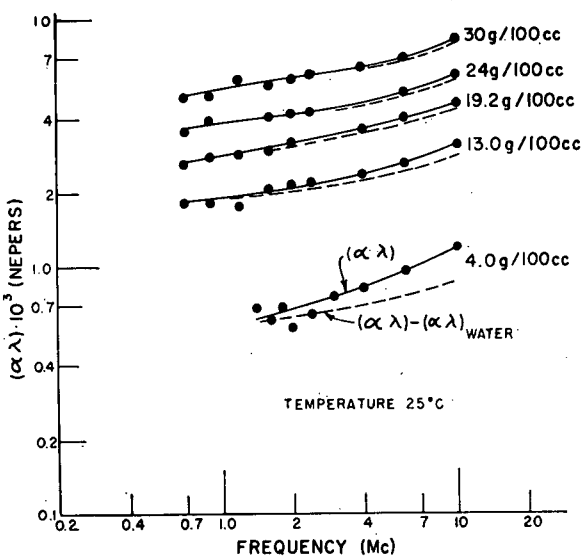

Figure 1—Absorption of sound in solutions of beef hemoglobin. The absorption is a linear function of concentration of hemoglobin up to approximately 15 gm/100 cc. At higher concentrations the absorption per gram Hb increases. Temperature 25°C.

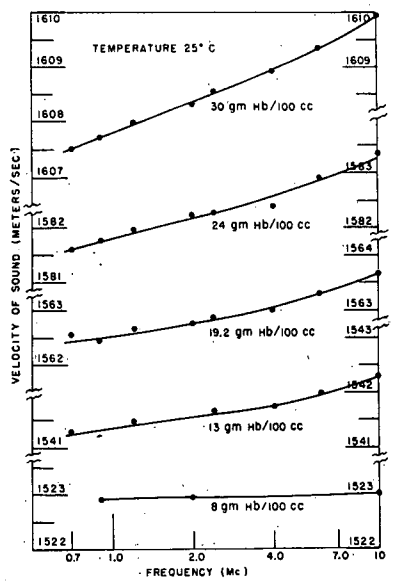

Figure 2—Dispersion of the velocity of sound in solution of beef hemoglobin. Temperature 25°C.

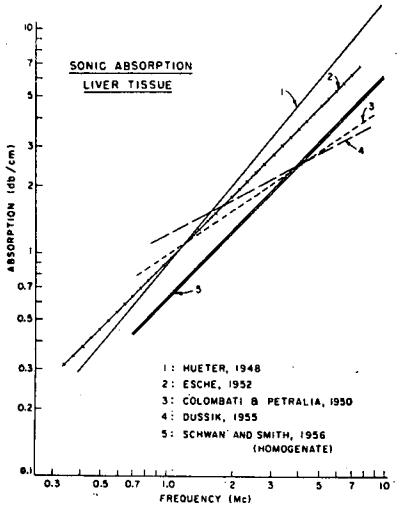

Figure 4—Absorption of sound in liver tissue. The data of several investigators are presented. The homogenate of *Schwan* and *Smith* is liver tissue which has been homogenized in a Waring blendor.

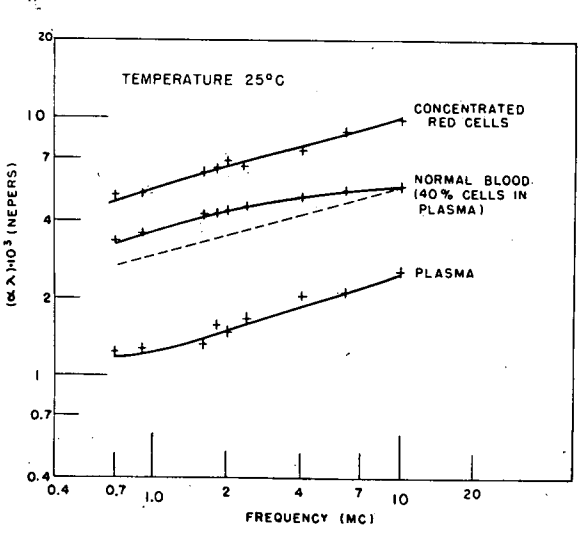

Figure 3—Absorption of sound in beef blood. Dashed curve is the absorption predicted for whole blood from the concentration of protein present. Temperature 25°C.

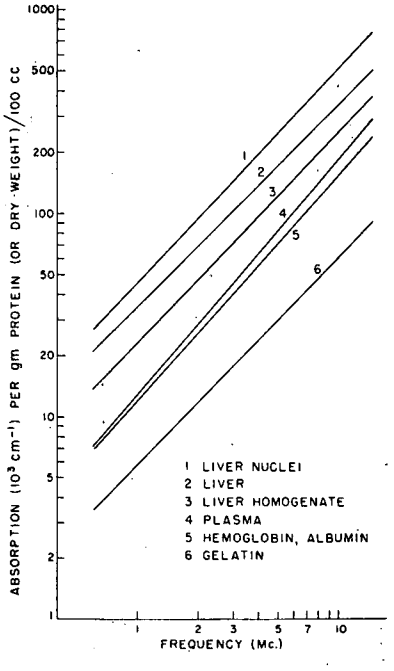

Figure 5—Absorption of sound in proteins. The absorption per gram for the blood proteins are similar in order of magnitude. Values for other proteins vary over a wide range.

SESSION VI: Ultrasonic Radiation I

6.2: Effects of Ultrasonic Irradiation on Hemoglobin

Alfred Weissler, Laboratory of Technical Development, National Heart Institute, Bethesda, Md.

LITTLE IS KNOWN about the chemical effects which may accompany the extensive use of ultrasonic waves in biology and medicine, for such purposes as disintegrating cells to isolate their enzymes, removal of the outer layer of cells from embryos, neurosurgery, visualization of internal structures, and clinically for deep heating to relieve pain.

The present work is a study of molecular changes in a biochemical material, caused by ultrasonic waves intense enough to produce cavitation in the solution. "Cavitation" means the formation and violent collapse of small bubbles or cavities in the liquid as a result of the rapid variations of pressure in the sound wave; it is accompanied by high local temperatures and pressures and probably also electric discharges. One result of cavitation is that some of the water molecules are broken down into highly reactive fragments (hydrogen and hydroxyl free radicals) which can cause chemical changes in other molecules present. If the solution contains dissolved air, nitrous and nitric acids as well as hydrogen peroxide are formed.

Hemoglobin in dilute aqueous solution was chosen as the test substance, because of general interest in the unusual properties of this molecule and also because its various derivatives have been well characterized by spectrophotometry and other methods. Oxyhemoglobin solutions were prepared fresh daily by diluting 0.1 ml of washed packed human red cells with 200 ml of cold distilled water, and centrifuging to remove the stroma. The solutions were kept cold in an ice bath, and the temperature was maintained below 40°C, even during the irradiation.

The ultrasonic generator operated at a frequency of 400 kc and delivered about 50 watts of acoustic power into the test solution of 25 ml volume (Figure 1). At the focal point of the convergent ultrasonic beam, the intensity is estimated at several hundred watts per cm^2, which is about one hundred times greater than in ultrasonic therapy machines.

Spectrophotometry was the principal technique used for measuring the chemical changes produced. It was found that oxyhemoglobin in solution, when irradiated with ultrasound, undergoes a rapid change in absorption spectrum, with the peak shifting from 4150 Å to 4050 Å and also becoming somewhat greater (Figure 2). This latter spectrum is characteristic of methemoglobin, in which the ferrous iron of oxyhemoglobin has undergone oxidation to the ferric state and the molecule has lost its ability to transport oxygen reversibly.

Continued ultrasonic irradiation of the solution caused gradual destruction of the methemoglobin, as shown by the progressive decline in the absorption at 4050 Å; after thirty minutes treatment, this peak disappeared completely.

Although sonochemical oxidation effects are reported to be suppressed by the addition of a little ether or acetone to the solution[1] it was found that, in the presence of ether, oxyhemoglobin does not remain unchanged by ultrasound, nor is it converted into methemoglobin. Instead, the absorption peak shifts to 4200 Å, which is characteristic of carboxyhemoglobin (Figure 3). The carbon monoxide is formed presumably by cavitational disruption of the ether molecule. Upon prolonged irradiation the carboxyhemoglobin suffers some destruction, but it is more resistant than methemoglobin.

Inasmuch as heme (the color-absorbing portion of the molecule) is an iron-porphyrin complex, the effect of ultrasound on a dilute solution of hematoporphyrin hydrochloride was investigated. Spectrophotometry showed that the porphyrin suffered partial breakdown in a manner similar to that of the hemoglobins. This destruction was confirmed by measurement of the porphyrin's characteristic red fluorescence on an Aminco-Bowman spectrophotofluorometer (Figure 4).

Ultracentrifuge studies showed that lengthy irradiation of oxyhemoglobin in more concentrated solution causes also some splitting off of the heme from the protein component (globin).

To explore the detailed sonochemistry of the production and disintegration of methemoglobin, a set of oxyhemoglobin irradiations was performed in different chemical environments (Figure 5). The results obtained suggest that sonochemically produced nitrous and nitric acids, rather than hydroxyl radicals or hydrogen peroxide, are the agents mainly responsible for the formation and destruction of methemoglobin by ultrasound.

[1] R. O. Proudhomme and P. Grabar, *Ann. Inst. Pasteur* 76, 460; 1949.

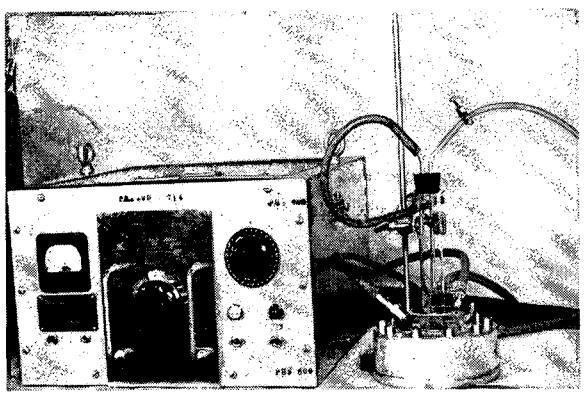

Figure 1—Ultrasonic generator with reaction vessel in place.

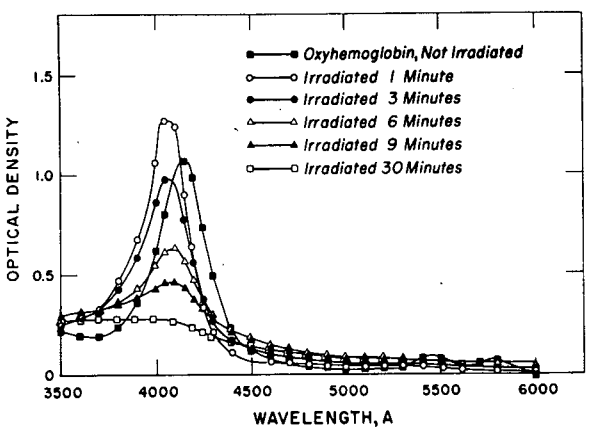

Figure 2—Ultrasonic production and destruction of methemoglobin from oxyhemoglobin.

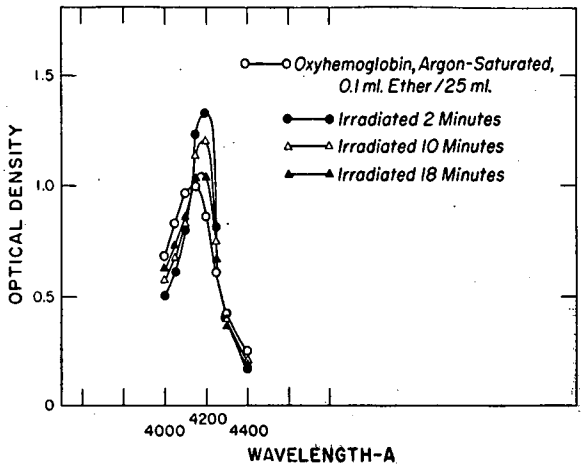

Figure 3—Formation and destruction of carboxyhemoglobin in oxyhemoglobin solution containing ether.

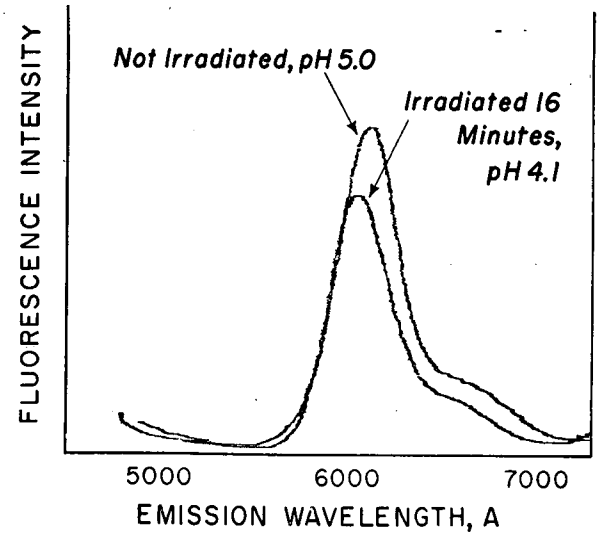

Figure 4—Ultrasonic destruction of hematoporphyrin fluoresence.

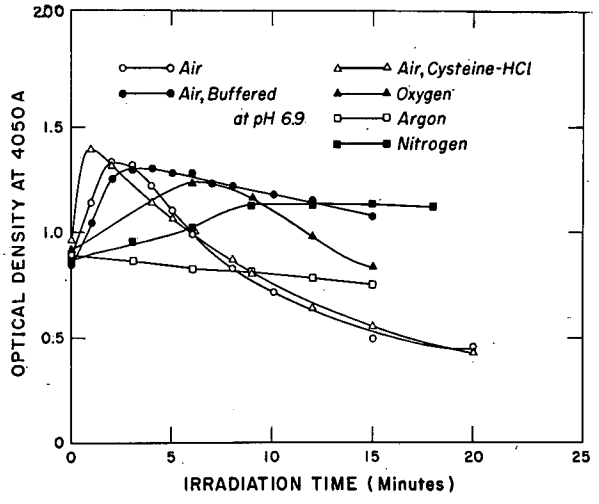

Figure 5—Ultrasonic treatment of oxyhemoglobin under various conditions.

SESSION VI: Ultrasonic Radiation I

6.3: Ultrasonically-Induced Movements in Cells and Cell Models*

Hubert J. Dyer (Botany Dept.) and Wesley L. Nyborg (Physics Dept.), Brown University, Providence, R.I.

EVENTS OCCURRING in plant cells and in models as a result of localized wall vibrations will be discussed and illustrated in a motion picture. The latter may be produced either by contacting the wall with the tip of a vibrating needle or by ultrasonic excitation of a small gas bubble resting on the wall. Our experiments were carried out at a frequency of about 25 kc using a Cavitron magnetostrictive transducer.

Observations on sonically-excited plant cells, made by use of conventional microscopy, reveal a complex pattern of intracellular movement which stops and starts promptly as the sound is turned on and off. These movements assume different forms, depending on the circumstances; possibilities include (*1*) orderly motion such as might occur in simple fluids, (*2*) displacement of intracellular particulates from equilibrium positions, to which they slowly return when the sound ceases, and (*3*) violent and chaotic churning with destructive effects on the cell[1].

Studies using models were carried out for the purpose of reproducing phenomena observed in the plant cells under controlled conditions. The construction of a typical model is shown in Figures 1 and 2. Representing the cell interior is a trough about 3-mm wide, 3-mm deep and 2-cm long milled in a ¼-inch thick piece of clear plastic. The "cell" is closed at one end by a plastic membrane (M) held firmly in position by means of clamping between pieces (A) and (B). This "cell model" is filled with the desired fluid, and enclosed above by a microscope cover slip. An entry port in piece (B) permits the point of an exciting needle (N) to be brought into contact with the membrane at a point near the upper surface of the cell. An alternative to use of a vibrating needle is to place a small air bubble on the membrane, the bubble being set into oscillation by acoustic excitation of the surrounding fluid. With the cell mounted on the stage of a conventional research microscope, observations can be made in the fluid adjacent to the membrane in the vicinity of the small vibrating area, using magnifications up to 400 x. Motions of the fluid are detected by viewing the paths of suspended particles, e.g., *Lycopodium* spores.

When the model contains a *Newtonian* fluid steady flow results, the nature of which depends on the fluid viscosity, and the membrane thickness. For a highly viscous fluid (Figure 3) particles approach the membrane along the projected axis of the vibrating needle (or an analogous axis when the bubble is used). As a particle nears the membrane its speed increases suddenly, and it is projected outward along the membrane surface, away from the vibrating area. Regions of especially high speed and acceleration are indicated on the figure.

Interesting and illuminating results involving visco-elastic behavior have been obtained by filling the cell with a suitable dilute suspension which in time develops a weak gel structure. Observations are made at various stages in the gel formation; Figure 4. In very weak gels one finds that immediately after vibration commences, particles suspended in the gel "flow" for a short distance, following streamlines of a viscous fluid, as in Figure 3. The flow velocity quickly decreases to zero, however, the particles coming to rest at positions such that the displacement vectors are distributed like the velocity vectors in acoustic streaming. The particles remain displaced as long as the sound continues, but return slowly to their original positions when the vibration source is turned off. When sound is applied in an on-off cycle, the particle displacement follows a time course similar to that indicated in the lower part of Figure 4. As rigidity of the gel develops, the displacements occurring in such a cycle become smaller and finally may be too small to observe.

*Research supported in part by the U.S. National Institutes of Health and in part by the U.S. Air Force of Scientific Research.

[1] W. L. Nyborg and H. J. Dyer, "Ultrasonically Induced Motions in Single Plant Cells," *Second International Conference on Medical Electronics;* June 24-27 1959, Paris, France (*Iliffe & Sons, Ltd.*, London; publication probably 1960).

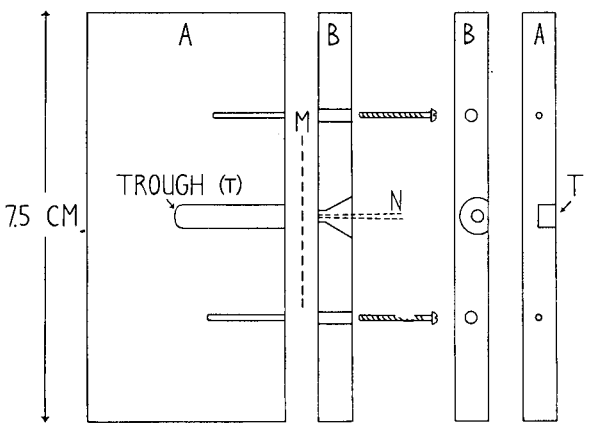

Figure 1—Construction of plastic "cell" model. A membrane (*M*) of polyethylene or similiar material is clamped between pieces *A* and *B*. The trough *T* is filled with fluid. A vibrating needle *N* contacts the membrane.

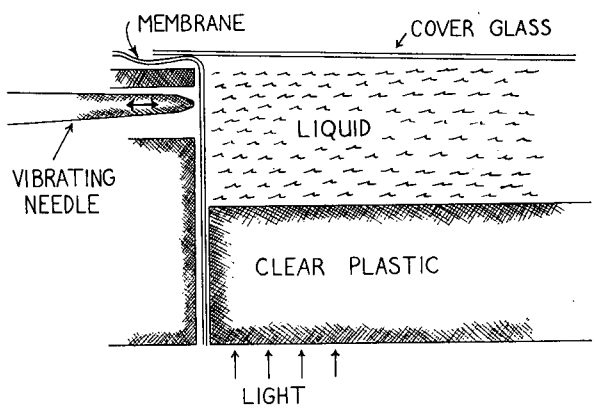

Figure 2—Vertical section along plane of symmetry of cell model. Vibrating needle contacts membrane at area only a short distance below coverglass; motions near this area may therefore be observed with high magnification.

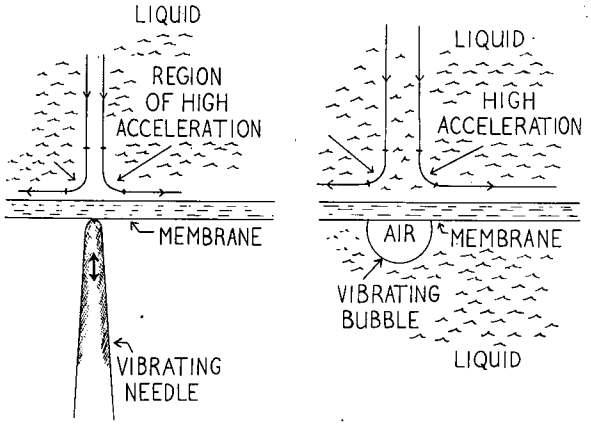

Figure 3—Acoustic streaming in cell model containing liquid of high viscosity (0.1 poise or more). Most rapid motion may be localized in area no more than 0.1 mm in extent.

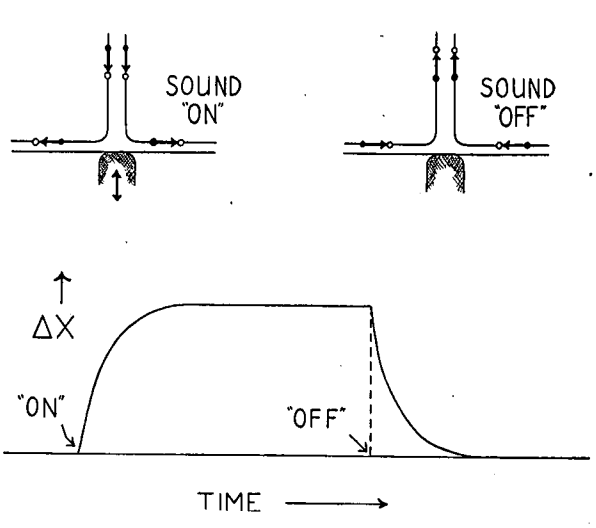

Figure 4—Sonically-induced displacements in a weak gel. Displacement *directions* similar to those of particles in ordinary fluid (*Cf*, Figure 3). Magnitude Δx of displacement follows time course indicated.

Notes

SESSION VI: Ultrasonic Radiation I

6.4: Method to Study Biological Cell Suspensions—An Application of Colloidal Vibration Potentials

Karl Sittel, Franklin Institute, Laboratories for Research and Development, Philadelphia, Pa.*

PERIODICALLY-VARYING electrical potentials have been measured in colloidal suspensions by *Yaeger*[1] and other workers. They submerged a sound transparent test cell in a water tank sending ultrasonic wave pulses through it. By these pulses potential differences were set up within the suspension which varied with the same frequency as the ultrasonic wave. These electrical potentials were detected by two platinum wires dipping into the liquid and connected to an amplifying system. The signal is maximized when the wires are half the acoustical wavelength apart.

The objectives of this investigation, to be reported, are *first*, to establish this effect in aqueous suspensions of biological cells, and *second*, to determine the order of magnitude.

The experimental setup, except for some modifications, is essentially like the one used by *Yaeger*, et al. A simple rubber bath tub has proved to be adequate for a water tank. A 3″ diameter barium titanate transducer and the test cell are supported from an optical bench. The electrical signal from a double probe is differentially amplified and fed through a tuned amplifier before being displayed on an oscilloscope screen. The test cell is a 6″ diameter plexiglas cylinder with ρv windows on both sides. The test liquid can be circulated through the cell by means of a special nozzle. This prevents the biological suspensions from sedimentation. The double probe, a cathode follower directly attached to it, is inserted through a plexiglas tube. Outlets are provided for the differential output and for applying a calibrating voltage. A calibrated ⅛″ x ⅛″ barium titanate cylinder probe, exchangable with the electrical probe, measures the acoustical energy.

The average sound pressure in the test cell was 2.49 x 10^5 dynes/cm^2. The test frequency was 300 kc, pulse duration 150 μs, pulse repetition rate 1 kc.

The double probe minimized direct electromagnetic pick-up which was also separated timewise by proper delay in the tank. The internal impedance of the vibration potential source was calculated from two impedance measurements. *First*, one probe grounded and the other measured against ground; *second*, both probes paralleled and measured the same way.

For a reference a silica suspension (*Ludox HS*) was measured. The suspension was pretreated as described by *J. S. Dereska*[2]. As a biological sample, a suspension of pure yeast in distilled water was prepared with a pH of 7.6. As a second biological sample we used an approximate 1.5% erythrocyte suspension of ox blood in a 5% glucose solution.

The results are shown in *table one*. The silica effects are roughly proportional to the concentration/conductance predicted by the theory of *Enderby*[3]. The yeast measurements show disagreeing results which so far lack explanation. The necessity for more well controlled measurements is indicated. Interesting is the time study of a yeast suspension with and without sedimentation taking place. In contrast to the other measurements these seem to indicate a decrease of the effect with decreasing concentration caused by sedimentation. The erythrocyte effect is in the same magnitude as the lower yeast values. While the experimental results are still too few to draw any definite conclusion, valuable experience has been acquired for the future development of a proper biological test cell.

The cause of this effect is intimately connected with phenomena occurring on the solid-liquid interface. Consequently metabolic processes, as well as physical changes of the cell surface, may be found to modify the vibration potentials. Furthermore, the ultrasonic probing does not interfere with the biological processes and permits time studies.

*Now with RCA, Moorestown, N. J.

[1] E. Yaeger, et al., *JASA*, 25, 443; 1953.
[2] J. S. Dereska, *Doctoral Thesis*, Western Reserve University; 1957.
[3] J. Enderby, *Proc. Roy. Soc.* 207A 329; 1951.

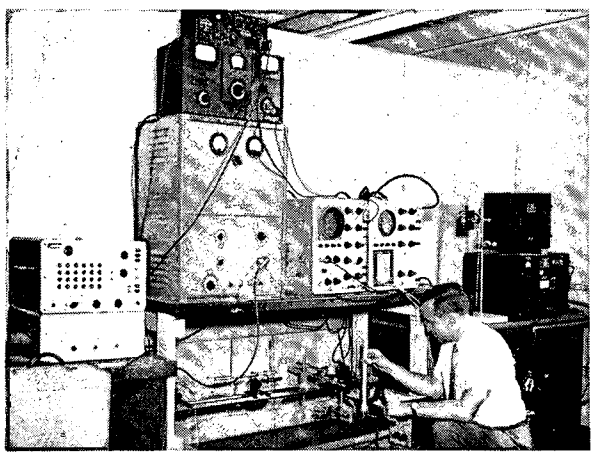

Figure 1—Test setup. Operator holds small sample test cell. Sound transducer (not visible in photograph) is on the left side of rubber water tank. Ultrasonic pulse equipment and display scopes are arranged above tank.

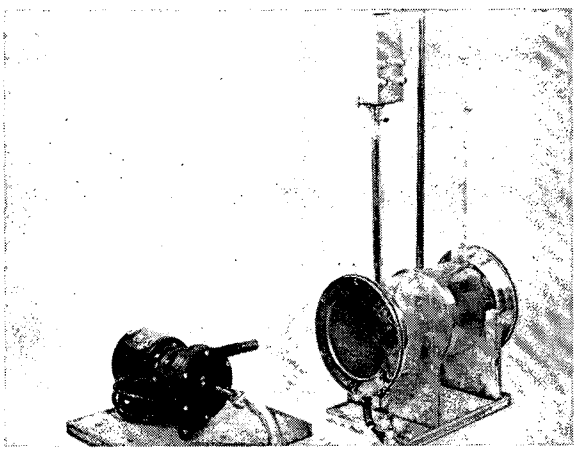

Figure 2—Large sample test cell. Pump circulates test suspension through cell. Dual probe is inserted through front tube. Cell is immersed in water tank.

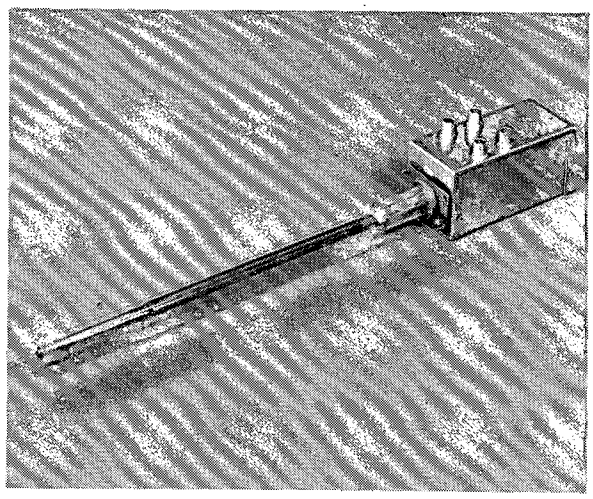

Figure 3—Vibration potential probe. The two platinum wires extending from the end of the probe and the double-shielded connection with the dual-cathode follower on top are embedded in a plastic tube.

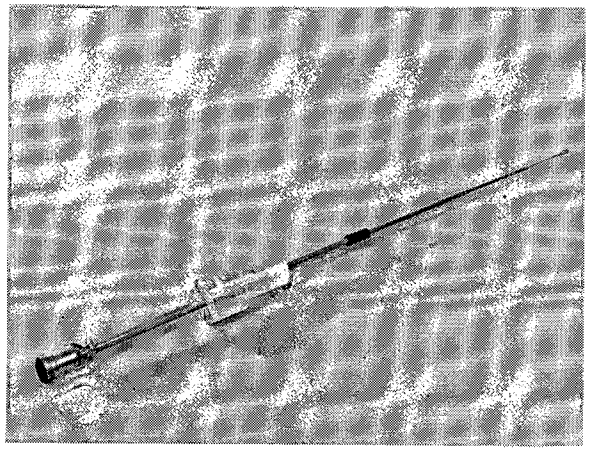

Figure 4—Hydrophone: A 1/8" x 1/8" barium-titanate cylinder connected to the tip of the probe used to determine sound pressure.

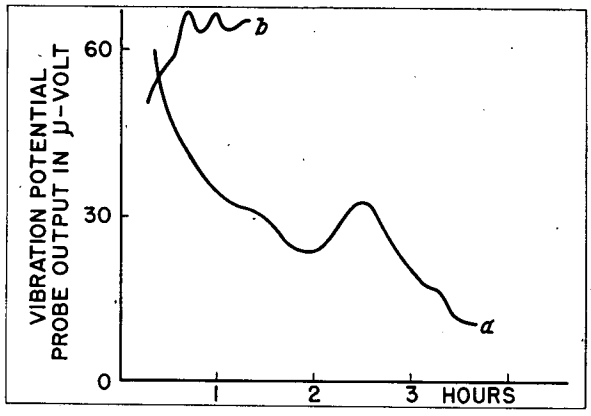

Figure 5—Time study of yeast suspensions in small test cell: (a)—Sedimentation of yeast cells uninhibited; (b)—sedimentation minimized by air bubbles.

	SILICA		YEAST			BLOOD
	1	2	1	2	3	1
CONCENTRATION WEIGHT PERC.	.8	3.6	.2	1.0	.2	1.5
SPEC. COND. μ-MHO/CM	78	160	150	620	–	1000
VIBRATION POT. μ-VOLT/CM/SEC	270	460	5.3	3.3	32	4.4-7.5
YEAST SUSPENSION 1 AND 2 CIRCULATED " " 3 AERATED						

Table I: Results on aqueous suspensions*

* Silica 1, 2 = Commercial Ludox-HS. Yeast 1, 2, 3 = In distilled water pH 7.6. Blood 1 = Ox-blood in 5% glucose solution.

SESSION VI: Ultrasonic Radiation I

6.5: Ultrasonic Resonances of Simple Biological Cells*

Eugene Ackerman, Biophysics Laboratories, Pennsylvania State University, University Park, Pa.

During The Last Decade, a variety of investigations were undertaken to ascertain if single biological cells exhibited characteristic, surface-type resonances. Experiments, particularly with dilute suspensions of mammalian erythrocytes in the frequency range from 0.1 to 1.0 Mc, support the existence of surface modes of resonance. The simplest experiment might be to expose the cells to plane waves in the absence of cavitation and determine the scattering and absorption. Such experiments have never indicated any type of surface modes of resonance. Theoretical studies show that the cellular cross-section for the excitation of surface modes by plane waves is so small that it should be impossible to detect such resonances by the scattering or absorption of plane ultrasonic waves. Likewise, model experiments using bubbles confirm that surface modes are difficult to excite in a plane wave field.

On the other hand, it is easy to excite surface modes of bubbles if the acoustic pressure is not uniform over the bubble surface. By analogy, one might suspect that similar resonances could be excited in biological cells, provided the acoustic pressure varied sufficiently over the cellular surface. Such resonances would be important if the cell is subjected to large ultrasonic pressures diverging from small cavitation nuclei close to the cell. All experimental methods which indicate that mammalian erythrocytes exhibit surface resonances, involve cavitating ultrasonic fields.

Theoretical analyses have shown that surface modes of resonance are to be expected either for a cell whose shape is maintained by an interfacial tension or for a cell whose outer layer (cortex) is a protein gel. These surface resonances vary only slightly with the exact cell shape and have a very low Q for mechanical resonances. However, the computed values, both of the interfacial tension and of the shear modulus of the cell cortex, (depending on which model is used) are of the same order of magnitude as found by more conventional methods.

The original observations supporting ultrasonic resonances of biological cells involved the rate of destruction of cells in a given ultrasonic field. This rate was compared to the rate of destruction of other types of cells in the same field. The intensity of the ultrasonic field is somewhat critical. At low levels cavitation does not occur, whereas at high levels non-resonant destruction masks all resonant effects. Nonetheless, there exists a range in which the resonant-cell destruction is several fold larger than the non-resonant effects.

Bubble experiments indicated that resonances with ten or more nodal lines are easier to excite that lower order resonances. The data for mammalian erythrocytes similarly supports the existence of resonances with many nodal lines. In the case of the bubbles, the mode could be determined by microscopic observation and by photographic technique. In attempts to determine the modes of the surface resonances of mammalian erythrocytes several types of experiments were undertaken. These included direct recording of the optical density of the erythrocyte suspensions in the sound field, the determination of the relative thresholds for destruction of erythrocytes from four different species, and the photographic observation of erythrocytes in the ultrasonic field.

In the latter it was impossible to distinguish those cells which were permanently altered from those reversibly altered presumably due to cell resonances. Although unsuccessful in determining which modes were excited, all those experiments supported the existence of ultrasonic resonances of biological cells.

*This report includes the data of several co-workers, especially *L. Binstock, D. B. Lombard, T. F. Proctor,* and *F. Oda.* The work was aided by a grant from the National Heart Institute of the National Institutes of Health.

Notes

SESSION VII: Microwave Radiation II

Chairman: Herman P. Schwan,

Electromedical Division, The Moore School of Electrical Engineering, University of Pennsylvania, Philadelphia, Pa.

7.1: Opacities in the Lens of the Eye Experimentally Induced by Exposure to Microwave Radiation

Russel L. Carpenter, Department of Biology, Tufts University, Medford, Mass.

THE LENS of the eye is known to be particularly affected by radiated energy, whether ionizing, infrared or radio-frequency, all of which cause the development of opacities (cataracts) in this normally transparent optical body. Induction of lens opacities by microwave radiation was reported in experimental animals by *Richardson, Duane* and *Hines* in 1948, and has since been confirmed by *Daily, Wakim, Herrick, Parkhill* and *Benedict*, also by *Ely* and *Goldman, Williams, Monahan, Nicholson* and *Aldrich*, and by *Carpenter, Biddle* and *Van Ummersen*. It has also been reported by *Belova* and *Gordon* in Russia. Frequencies employed have been 2450, 3000 and 10,000 Mc. Although early reports of work in this field lacked information as to field intensity, *Williams*, et al, reported opacities in the rabbit eye after a 70-minute exposure at 290 mw/cm², and we have observed opacities resulting from a single 35-minute exposure to continuous wave radiation at 120 mw/cm².

Conversely, *Osborne* and *Addington* have found in guinea pigs no adverse ocular effects from radiation at 200 Mc, when the field intensity was 480 mw/cm² and the period of exposure 60 minutes, even though exposures were repeated five times a week for a period of five weeks. Employing 400-Mc radiation, *Cogan, Fricker, Lubin* and *Donaldson* found no effect on the lens of the rabbit, even though duration of single whole body exposures was just short of being lethal.

The minimal duration of a single exposure to continuous wave radiation which will cause a lens opacity to form has been determined for a series of different field intensities at the 2450-Mc frequency. The lower the intensity, the longer the duration of a single exposure required to cause a cataract.

It has been demonstrated for this frequency that lens opacities may develop as the result of repeated exposures of the eye to microwave radiation, even though any one such exposure period is not sufficient to cause apparent damage. In the rabbit eye, cataracts have been caused by: Three three-minute exposures spaced four days apart at power density of 280 mw/cm²; three 30-minute exposures spaced two days apart at power density of 120 mw/cm²; and 19 one-hour exposures made daily at power density of 80 mw/cm².

It has been assumed generally that the effect of microwave radiation on living tissue is entirely a thermal one, an effect of the heat resulting from absorption of *rf* energy by the tissue. The peculiar susceptibility of the lens to damage by microwave energy has been ascribed to its location near the body surface and to its relative inefficiency in dissipating heat. It has been shown that the temperature within the eye during microwave irradiation bears a direct relation to the field intensity. As intensity is increased, the more rapidly does the ocular temperature rise and the higher is the level it reaches before tending to flatten out. Nevertheless, it is not possible to designate a temperature critical for cataract formation; opacities have developed after exposure to microwave radiation when the accompanying ocular temperature was elevated only 4°C above body temperature. It is significant that an unanesthetized rabbit gives no evidence of discomfort during an irradiation when the ocular temperature may rise as much as 7°C. A damaging exposure is thus not necessarily accompanied by a pain warning.

When the eye is subjected to pulsed radiation with high peak intensity, lens opacities result from exposures which are significantly shorter than those required for induction of opacities by continuous wave radiation of identical average power. Inasmuch as ocular temperature is related to average field intensity and not to peak intensity, it seems apparent that in analyzing the biological effects of microwave radiation, attention must be given to the influence of peak power as a factor.

SESSION VII: Microwave Radiation II

7.2: Analytical and Experimental Investigation of Unicellular Organisms Under Microwave Irradiation

C. Susskind and P. O. Vogelhut, University of California, Berkeley, Calif.

Polonsky has attacked the age-old riddle of life, the functioning of a single cell, by the modern method of information theory. He arrives at the following conclusions: The cell is a quantum-cybernetic system, with generators, amplifiers, and effectors of information, shielded from disrupting influences by its membrance. Deoxyribonucleic acid, the seat of the hereditary material is considered to act as a generator; ribonucleic acid is the amplifying element of the system; enzymes or proteins act as the effectors, which obey the signals from the *DNA* and *RNA*. These signals are coded pulses in various regions of the electromagnetic spectrum, with a high degree of redundancy to insure undisturbed information transfer between the components of the system. The energy of the signals depends on the action which it is to elicit.

A theory of functioning of a single cell can only be appraised in its value by the predictive power it offers in resolving hitherto unexplained phenomena by the use of its invented general principle. *Polonsky* leaves the task of proving or disproving of his hypothesis to the biophysicist.

Numerous investigators have shown nonthermal effects of short waves, ultrahigh frequencies, and microwaves upon living organisms, but have failed to give an integrated explanation of *(1)* changes in reaction speeds of enzymes under the influence of short waves, *(2)* changes in the denaturation process of serum proteins in ultrahigh-frequency fields, and *(3)* changes in the plane of polarization of macromolecules under the influence of microwaves.

The constituents of a single cell are influenced in their actions by electromagnetic waves and as a result the whole cell function has to undergo appropriate changes. This fact is also substantiated by experiments on unicellular organisms, which change their survival characteristics in electromagnetic fields.

Polonsky's hypothesis gives a starting point for investigations that study the functioning of single cells in such adverse environments by postulating an information-transfer system inside the single cell that can be disrupted or modified by injection of noise—as it may seem to the cell.

The shield against external influences, the cell membrane, is being investigated in an effort to correlate its properties with those predicted by *Polonsky*'s hypothesis, and to see what kind of signal and in what manner it would penetrate such a filter.

By this approach it may be possible to gain a better understanding of the intricate processes that occur in the single cell.

SESSION VII: Microwave Radiation II

7.3: Dielectric Constant and Conductivity of the Interior Erythrocytes and Pearl Chain Formation in Blood*

Herman P. Schwan and H. Pauly, Electromedical Division, The Moore School of Electrical Engineering, University of Pennsylvania, Philadelphia, Pa.

PEARL CHAIN FORMATION establishes a significant nonthermal mechanism of electromagnetic fields which can affect biological matter on a cellular and subcellular level. Pertinent theoretical concepts, as originally formulated by *Krasny-Ergen*, have been extended by us and treat pearl chain formation phenomena as one special case of the movement of dielectrically-differentiated particles in nonhomogeneous fields. Our experimental findings substantiate this interpretation by successfully relating experiment and theoretical prediction. Thus the detailed understanding of pearl chain formation and other effects of nonhomogeneous fields is shown to demand, as a prerequisite, the knowledge of the composite dielectric data of the particular biological unit under study and subject to movement due to electric forces.

Hence detailed investigations of the dielectric parameters of a variety of cellular and subcellular organism have been conducted by us. A particularly detailed analysis of the electrical properties of erythrocytes has been performed. It includes the following: *(A)*—The impedance characteristics of erythrocytes of man, beef, sheep, dog, cat, rabbit and chicken have been investigated from 0.5 to 250 Mc; *(B)*—The electrical conductivity of the interior of the red cells was investigated with particular care between 70 and 100 Mc. Values differ from species to species within the rather limited range from 4.4 to 5.3 mMho/cm; *(C)*—Theoretical values, calculated on the basis of the salt content of the cell, its ion mobility and the hemoglobin concentration, are about twice as large as measured values. While there is as yet no quantitative detailed understanding of this phenomena available, it is certain to reflect the interaction of macromolecular systems with their ionic environment; *(D)*—The aforementioned discrepancy is not only typical of red blood cells. After changeover of the cell interior into a highly concentrated hemoglobin solution, the conductivity remains practically unchanged. This means, that the cell interior behaves like a highly concentrated hemoglobin solution without any indication of organizational features, which may be considered typical for cells. Figures 1 and 2 demonstrate this by the independence of the high-frequency dielectric data above 100 Mc from the degree of lysis achieved by the addition of saponin. The frequency dependance at lower frequencies simply reflects the strong destructive effects of the lytic agent on the membrane. The latter's impedance has been shown in previous investigations by others and us to contribute increasingly to the total cellular impedance as the frequency is lowered substantially below 100 Mc.

For spherical cells it is readily possible to relate composite "effective" cellular impedance data ("equivalent homogeneous sphere admittance K") with the data characteristic of cell interior and membrane. This may be achieved by use of the relation:

$$\frac{K-K_s}{K+2K_s} = \left(\frac{R}{R+d}\right)^3 \frac{K_i-K_s}{K_i+2K_s}$$

where $K = K+j\omega\varepsilon$ is the complex conductivity, p the relative volume fraction taken by the cells in solution and the subscripts i and s pertain to interior and membrane, respectively. An important extension of this theorem to ellipsoidal shape is considered in the paper by *Shen* and *Schwan* which follows. The effective cellular admittance data are lower than those of the surrounding medium at frequencies above 100 Mc. Their dielectric constants are, however, higher at frequencies below 100 Mc. This and the strong frequency dependance of the ratio of capacitive and resistive current leads to a complicated frequency dependance of the onset of pearl chain formation, since the latter can be shown to be a direct function of the ratio

$$\frac{\varepsilon_1^* - \varepsilon_2^*}{\varepsilon_1^* + 2\varepsilon_2^*}$$

where the complex dielectric constants ε_1^* and ε_2^* relate to internal and external cellular medium. It also can be shown to cause pearl chain formation to be mainly a high-frequency phenomena at least as long as cells and subcellular components are concerned.

Above summarized studies explain the often observed complexity of the frequency dependance of pearl chain formation effects quantitatively. Pertinent experimental data will be shown by us later.

*We gratefully acknowledge support by a research contract between the Office of Naval Research and the University of Pennsylvania Nonr 551 (05).

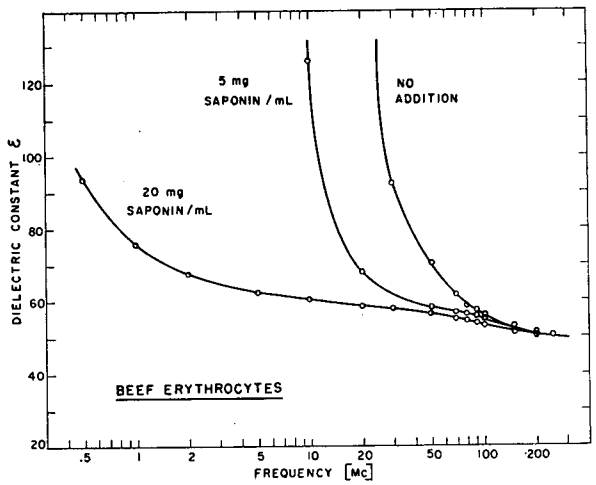

Figure 1—Dielectric constant of beef erythrocytes lysed with saponin as function of frequency.

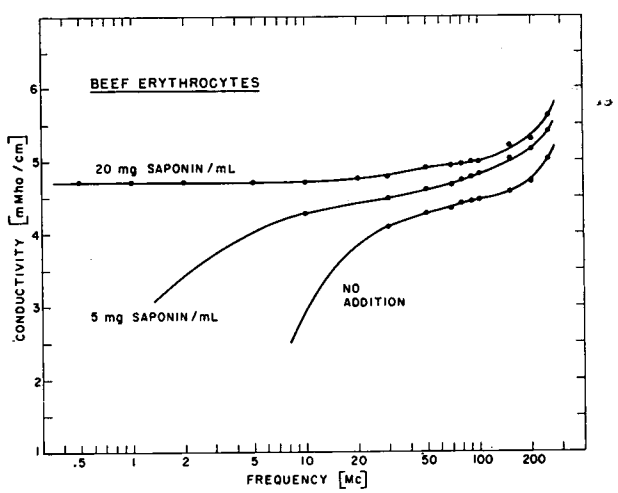

Figure 2—Conductivity of beef erythrocytes lysed with saponin as function of frequency.

SESSION VII: Microwave Radiation II

7.4: Relaxation Parameters of a Suspension of Membrane-Covered Ellipsoids

D. W. C. Shen and H. P. Schwan, Electromedical Division, Moore School of Electrical Engineering, University of Pennsylvania, Philadelphia, Pa.

THE APPLICATION of *Maxwell-Wagner's* theory of inhomogenous dielectrics to the biological medium has resulted in a number of contributions dealing with the analysis of the dielectric behavior of biological cell suspensions and tissues. Recently *Pauly* and *Schwan* published a detailed mathematical analysis of a suspension of spherical particles, surrounded by a shell, as a model for the dielectric behavior of cell and protein suspensions. Their formulas permit a wider variability of all parameters than previously published results. However, from the viewpoint of mathematical generality and considering the structure of some biological materials the spherical model of dielectric structural relaxation effects appears insufficient. A model that is more flexible and of particular interest for cases such as mammalian erythrocytes or bacteria, is given by a suspension of membrane-covered ellipsoids.

This paper attempts to give a theoretical treatment of the ellipsoidal model without any restriction imposed on the electrical parameters of the various phases involved in and outside membrane. The membrane-covered ellipsoid is taken as an ellipsoid confocal with its inner core. Figure *1* shows such a single membrane-covered ellipsoid suspended in a medium. The electrical properties are described by $\varkappa$ and ε, where $\varkappa$ is the conductivity and ε the permittivity. The subscripts *1*, *2* and *3* denote the quantities pertaining to the inner core, the membrane and the medium, respectively.

The problem can be dealt with in a simple manner by first considering the electrical behavior of a corresponding heterogeneous system composed of pure conductors. Solving the *Laplace* field equation in ellipsoidal coordinates with relevant boundary conditions, it is found that a heterogeneous confocal ellipsoid, which is suspended in a medium and subjected to an external field parallel to one of its principal axes, is replaceable by an equivalent homogeneous ellipsoid that has the same geometrical configuration. The present investigation includes *Maxwell's* result for a stratified sphere as a special case.

Next, a suspension of pure conducting ellipsoids is considered under the assumption that their effects in disturbing the field may be taken independent of each other. For parallel ellipsoids, the formula derived agree with *Fricke's* formula both for low and high concentration. With random orientation of axis, our formula is identical with *Fricke's* formula for low concentration only, but differs slightly for higher concentration. By combining the concept of the equivalent homogeneous ellipsoid with the conductivity equation of a suspension of homogeneous ellipsoids and by using complex variable, a complex conductivity equation for the same geometrical system of conducting dielectrics is obtained. The dispersion equations for conductivity and permittivity are thereby obtained by separating real and imaginary parts.

The analysis shows that for random orientation of axis, the relaxation phenomena are characterized by six time constants, two associated with each axis. Usually the thickness of the cell membrane is very much smaller than the ellipsoidal axis. Then the two time constants associated with each axis are distinguished in a manner that one characterizes the dispersion of the "full" ellipsoid given by the core in the medium, while the other essentially describes the dielectric property of the membrane. These results prove that the electrical behavior of a suspension of membrane-covered ellipsoids may be presented by the equivalent circuit shown in Figure 2, where the time constants of the six series *R-C* combinations $T=RC$ are to be identified with the time constants which characterize the frequency dependence of the dielectric properties of the suspension. Figure 3 displays a typical case, where the 3 high-frequency dispersions due to the core are well separated from the three lower frequency ones due to the membrane. Figure 4 presents the equations which describe the electrical behavior as discussed above.

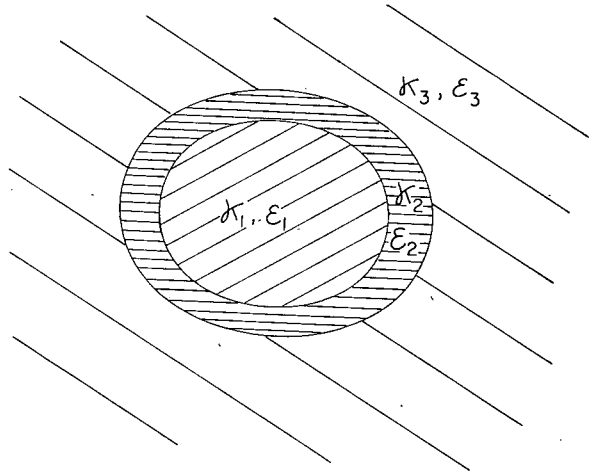

Figure 1—Membrane-covered ellipsoid. Core properties are indicated by subscript *1*, those of the membrane by subscript *2*, and those of the internal medium by subscript *3*.

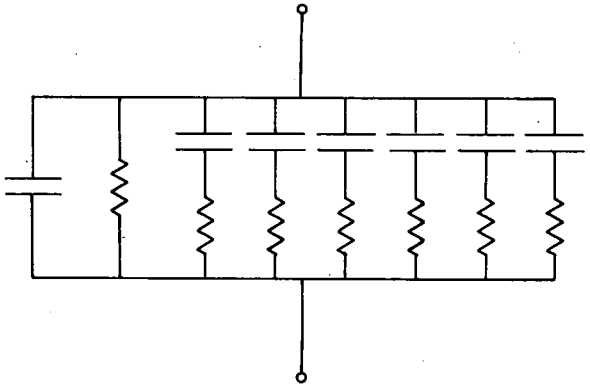

Figure 2—Equivalent circuit of frequency-independent components which describe the electrical behavior of a suspension of membrane-covered ellipsoids.

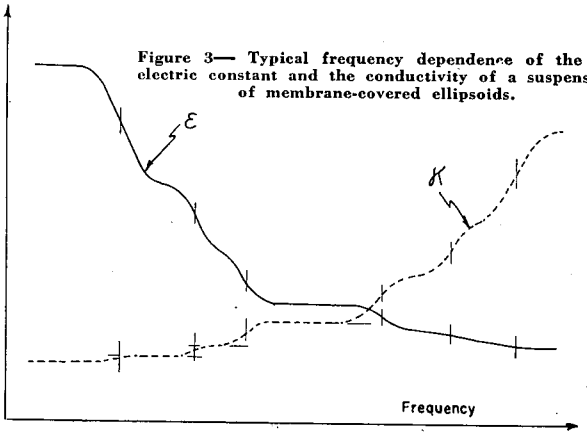

Figure 3— Typical frequency dependence of the dielectric constant and the conductivity of a suspension of membrane-covered ellipsoids.

$$\varepsilon = \varepsilon_\infty + \sum \frac{\Delta\varepsilon_\nu}{1+(\omega T_\nu)^2}$$

$$\kappa = \kappa_0 + \sum \Delta\kappa_\nu \frac{(\omega T_\nu)^2}{1+(\omega T_\nu)^2}$$

$$\Delta\kappa_\nu = \frac{\Delta\varepsilon_\nu}{T}$$

Figure 4—Mathematical relationship characterizing the frequency dependence of dielectric constant and conductivity of membrance-covered ellipsoids. The subscript *O* and ∞ pertain to extremely low and high frequencies.

SESSION VII: Microwave Radiation II

7.5: The Effect of Electromagnetic Fields on Unicellular Organisms

John H. Heller, New England Institute for Medical Research, Ridgefield, Conn.

THE BASIC INSTRUMENTATION consists of a variable frequency oscillator (1 to 100 megacycles). The voltage is continuously variable from 0 to 20 kilovolts. The field is pulsed with pulses ranging from 1 microsecond to 20 milliseconds with a repetition rate varying from 30 to 10,000 per second. The energy from the radio-frequency source is coupled either directly or through a link from the tank circuit of the oscillator and brought into two electrodes which can be placed in a variety of configurations. The most common is to have the two electrodes made with silver circuit paint on a glass microscope slide with a several-millimeter air gap between them. Particulate matter, bacteria, or protozoa are placed between two cover slips sealed with a silicone gasket. These two cover slips are laid across the painted silver electrodes. At lower frequencies, motile protozoa will migrate along the lines of force. At higher frequencies, they will migrate across the lines of force. The frequencies at which these phenomena occur are quite specific for each different type of organism. Hence, it is possible to have three species in the field at the same time where one will migrate along the lines of force, the other across the lines of force, while the third is apparently oblivious to the field. Exposure of living cells to these fields results in a variety of chromosomal aberrations which appear to be frequency specific, and these aberrations result in subsequent mutations.

Figure 1—Squash preparation of garlic root tips 24 hours after 5 minutes of exposure in the electromagnetic field. At top, resting stage of an irradiated cell showing two nuclei linked by a chromatic bridge and no cytodieresis; center, metaphase with linear shortening of chromosomes; bottom, bridging.

SESSION VII: Microwave Radiation II

7.6: Bionegative Actions of Microwaves

Victor T. Tomberg, Biophysical Research Laboratory, Elmhurst, N. Y.

SHORTWAVES were introduced in 1926 for biological research and medical treatment, based on observations by *Schereshevsky* and *Whitney* in the U.S.[1], *Esau* and *Pätzold* in Germany[2, 3] and *Stieböck* and *Tomberg* in Austria[2, 11, 9, 13]. Subsequently, microwaves were introduced for research and treatment.

It was found that the *Joule* effect—the thermal action—of a high-frequency capacitive field is more evenly distributed throughout an exposed body, due to the dielectric losses, than in the case of an ordinary diathermy treatment, where the body forms part of the current circuit. Because of the stimulating action of heating biological objects or ailing parts, this improved method of shortwave heating is still in use by the medical profession. The frequency of the field is responsible for the rate of heat developed. Therefore, in objects composed of different layers or structures with differing dielectric constant and electric conductivity, the rate of the developed heat is uneven and inequally distributed. The heat-conduction effect tends to equalize the unevenly distributed temperatures, but going slower than the *Joule* effect, temperature differences in a heterogenous object are inevitable. They depend mainly upon the field intensity, the electrical characteristics and the structural composition of the irradiated object.

It was found that the biological effect or the curing action of a high-frequency capacitive field depends on the applied energy multipled by the time of action; a product called dose. When the dose is small, one can expect a biologically stimulating or curing effect. When the dose is high, relative to a certain threshold depending on the nature of the object, a harmful or destructive effect can result. The former action of the field is often called *bio-positive*, the latter *bio-negative*[3].

A number of investigators pretended that besides the thermal positive bio-action, there must be an *electrical* biological action of the capacitive field, because certain cures and biological effects happen at low field intensities and without apparent temperature rise. In most of the investigated cases, cooling was also applied from the outside to eliminate, as they thought, any temperature rise within the object. The idea that some wavelengths—similar to light waves—behave biopositive and others bionegative was also advanced.[3]

However, up to now, no proof exists that short and microwaves at low energies produce any *biopositive* action which could not be traced to the action of the thermal *Joule* effect, when certain aspects of thermal action are—as research work has revealed—examined and taken in account[4, 11, 12, 20, 23].

What was found, in short, is the following:

Besides the thermal effect of high-frequency fields, there is an effect which looks like a non-thermal electrical effect, yet it is an effect based on a thermal action of particular behavior which can not be imitated by other means of heating, like in control tests. This particular effect was called the selective or *specific-thermal* effect. It is based on the foregoing temperature gradients arising from structural differences of a heterogenous biological object when two conditions are present: *(1)*—Marked differences of electrical conductivity and dielectric constant throughout the structure elements, for example, between liquid and solid phase, and *(2)* poor thermal-conductivity behavior, macroscopically, as well as structurally through the interboundaries of particles, layers, etc. When these conditions exist, then brisk temperature gradients with elevated temperature points in discrete areas are possible, which in most instances are very hard to detect or to measure. Cooling from outside cannot eliminate them, because the cooling action in poor thermal conductors is much slower than the temperature producing action of the high-frequency field. Measurements with thermometers or electrical devices show only the averaging temperature rise.[10, 12]

To show the existence of those phenomena, artificially composed objects (phantoms) of heterogenous structure have been used and the rate of temperature rise measured with tiny thermoelectric needles. We used also microscopical objects and emulsions, the microscope featuring a dielectric lens tubing, insulating the observer from the radiation field of the microscopic field-capacitive-electrodes, and thermosensitive dyes introduced in the object to change their color at a predetermined temperature. We could so observe that the highest temperature gradients arise in interboundary space and layers.

To measure the relationship of the biological effect with the dose *(intensity x time)* we use transmitters with pulsed energy output. The pulses are of square or rectangular form, and the ratio between pulse width and off-time is adjustable. The coupling between object electrodes and the transmitter output circuit is by means of a Lecher wire system, or by dipole radiation field. The intensity is adjustable from low values, about 0.1-watt per cm² up to 50-watt per cm², at wavelengths from 6 meters down to the centimeter region.

Actually, the increased use of microwave transmitters at very high energies, i.e., for radar, poses an interesting health hazard problem due to the destructive[23, 14] or bionegative action of microwave fields. Because of the high dose range—for medical purposes one uses only the low dose range—three kinds of actions and effects should be considered:

(1) Ordinary thermal effects *(Joule)* in more homogenous areas

(2) Specific-thermal effects in heterogenous material or areas due to:
- (a) Irregular absorption which can be inherent to the heterogenous structure of the exposed object, or to irregular field intensity distribution with peaks near metallic objects or dielectrics having resonating qualities, which build up induced fields with enough high-voltage gradients[9, 15].
- (b) Temperature gradients with peaks in some discrete areas of the structure of the exposed object when differences in electric conductivity and dielectric constant in the adjacent areas are present[12, 14, 17, 18, 19]. Low thermo-conductivity helps to build up these phenomena especially in interboundary areas.

(3) Electrical effects:
- (a) Orientation effects, like the pearl-chain effect[5, 6, 7, 8, 23, 16], which occur in emulsions, when the two components, which may be solid in liquid or liquid in liquid, show different electrical characteristics. One of the components, particles or liquid droplets, when free to move and not hindered by *Brownian* motion aligns in a pearl-chain-like formation.
- (b) Frequency dependent voltage and dielectric phenomena, which are connected to the known physical effects of *Wien* and *Debye*, involving molecular resonance anomalous dispersion and relaxation[2, 4, 16, 17, 23]. Generally, they occur at wavelengths below 300 Mc and to be biologically important, higher voltage gradients at pulsed energies are required.

Energetically, the pearl-chain effect occurs only at very low energies. because the *Joule* effect hinders the free motion of the aligning particles or droplets. This effect has been

observed actually only in experiments under the microscope, and recently rediscovered by *Heller* and by *Herrick* (Mayo Clinic). It is a frequency-independent effect and may be observed also at alternating frequencies[6]. We observed it in polymeric emulsions where it can be used to influence the polymerization process under appropriated conditions[23].

Our investigations also disclosed that low-intensity fields yield specific-thermal effects when the field has tendency to concentrate on some areas or when the exposed object possesses areas of high absorption. In the human body, for example, these are the eyes and the testicles. Here, locally-caused high-temperature peaks may be induced without any feeling of general heat.

The exposure to high-frequency fields is naturally not limited to capacitive fields. Coil fields, especially flat coil fields, and then dipoles with concentrating reflectors can produce harmful, destructive effects. To avoid them one has to avoid exposure to fields whose average dose exceeds certain safety values. These safety values should not be generalized, as the actual tendency shows, but adapted to any of the field patterns in use.

[1] McLennan, R., "The Heating Effect of Short Radio Waves," *Arch. Phys. Ther.* 143; 1931.
[2] Kowarschik, J., "Kurzwellentherapie," *Wien, Springer;* 1950.
[3] Liebesny, P., "Kurz-und Ultrakurzwellen," *Wien, Urban and Schwarzenberg;* 1935.
[4] Saidman-Meyer, J., "Les Ondes Courtes en Therapeutique," *Paris, Doin;* 1951.
[5] Krasny-Ergen, W., "Mechanische Wirkungen der Kurzwellen," Acta of I, *Internat. Congress of Shortwaves in Vienna,* pp. 180-184; 1937.
[6] Blüh, O., "Einige Bei der Untersuchung von Kolloiden im Wechselfeld Auftretende Erscheinungen," Koll.-Z.37,267; 1925.
[7] Muth, E., "Ueber die Erscheinung der Perschnurkettenbildung von Emulsions-Partikelchen unter Einwirkung eines Wechselfeldes," *Koll.*-Z.41,97; 1927.
[8] Denier, A., "Archives d'Electricite Medicale."; Mars-April 1935.
[9] Stieböck, P., Report in *Wr. Kl.Woch,* 27; 1930.
[10] Haase-Schliephake, E., "Versuche uber den Einfluss Kurzer Elektrischer Wellen auf das Wachstum von Bakterien", *Strahlentherapie* 40,133; 1931.
[11] Groag, P.-Tomberg, V., "Zur Kurzwellentherapie," *Wr.Kl.-Woch,* 30,31; 1933.
[12] Groag, P.-Tomberg, V., "Zur Biolog.Wirkung Kurzer Elektr. Wellen," *Wr.Klin.*Wo.9; 1934.
[13] Groag, P., "Kurzwellentherapie, eine spezif Warmetherapie." Acta of I, *Internat. Congress of Shortwaves,* Wien; 1937.
[14] Heller, R., Lokalisierte Durchwarmung mittels Ultra-Kurzwellen," Z.F.Exp.Med., 83; 1932.
[15] Tomberg, V., "Punktwärme-effekte im Kurzwellen Feld," Report in *Wr.-Balneol.Ges.;* 1930.
[16] Tomberg, V., "Spezifische Wirkungen Kurzer Elektr.Wellen," Report in Acta, *Ges.f.Kurzwellenforsch,* 21; Nov. 1934.
[17] Tomberg, V., "Die Spezif.Biolog.Wirkungen kurzer elektr.Wellen," Report in Acta of *I.Internat.Congress of Radio-Biology,* Venice; 1934.
[18] Schweinburg, F., "Uber die Beeinflussung des Wuterregers im Kurzwellenfeld," Acta of *I.Internat.Congress of Shortwaves,* pp. 217, Vienna; 1937.
[19] Tomberg, V. "Verteilung,Absorption und Messung der Energie im Kurzwellenfeld," Acta of *I.Internat. Congr. of Shortwaves,* (2 reports), Vienna; 1937.
[20] Tomberg, V., "Bases Scientif. et Conceptions Nouvelles de L'utilisation des Ondes Courtes," Acta *Physioth.Rheumat.Belg.,* 4, 109-15; 1947.
[21] Tomberg, V., "A Propos des Modalites D'Application de la Therapeutique Par Ondes Courtes," *J. Radiolog.et Electrolog.,* Paris,30,138-40; 1949.
[22] De Loz, A., "Influence des Ondes a Haute Frequence sur L'Hypercholesterinemie" *Scalpel;* May, 1951.
[23] Tomberg, V., "L'effet Destructif des Micro-ondes en Biologie," Acta of *I. Internat.Congress of Medical Electronics,* Brussels; 1947-Act. *Physioth.Rheum.Belg.,* 6,295-309; 1948.

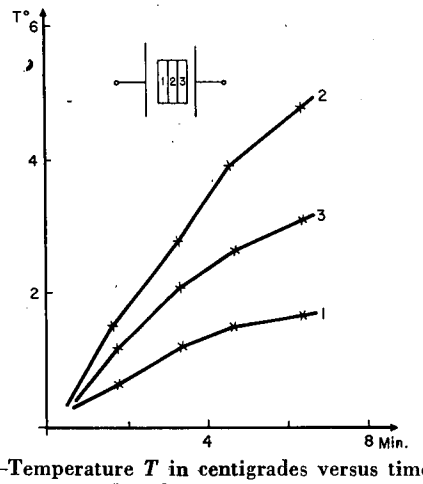

Figure 1—Temperature *T* in centigrades versus time in min of irradiation at a wavelength of 76 cm. The object is a phantom body consisting of soft bread and wetted with saline. The absorption in center (*2*) is higher than in (*1*) and (*3*).

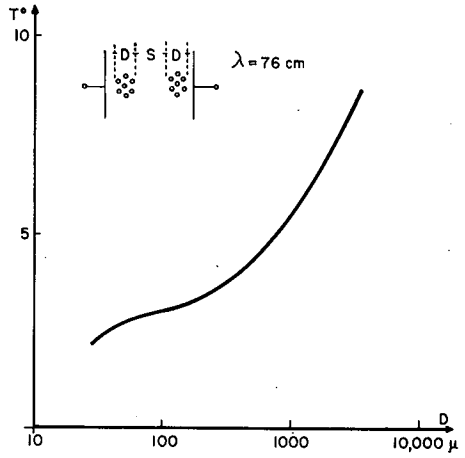

Figure 2—Temperature rise *T* in centigrades versus diameter *D* in microns μ in a particle suspension. The particles are plastic spheres (*PVC*) and agglomerated in grapes of *D* microns diameter. The space between the grapes *S* is about 5.D microns. The particle size is about 5 microns. Irradiation time is 2 minutes; wavelength is 76 cm; observation under the microscope.

SESSION VII: Microwave Radiation II

7.7: Pearl Chain Formation

J. F. Herrick, Rochester, Minn.

DIATHERMY is prescribed clinically for only one reason: To heat. Clinical investigators of outstanding competence have concluded, after extensive and ingenious researches, that all effects of diathermy can be explained by the production of heat within bodily tissues.

Despite this well-established and generally accepted fact, there has been a persistent search for nonthermal effects of high-frequency alternating currents. This unceasing search has resulted in establishment *in vitro* of one definite nonthermal effect which has been observed experimentally, namely, the tendency of microscopic particles, in the presence of alternating electromagnetic fields of low intensity, to become rearranged from a random distribution to an orderly chain formation. This chain formation is strikingly similar to the more familiar alignment of iron filings in a magnetic field. Such chain formations, which are popularly called "pearl chain formations"[1] were reported in the literature more than 30 years ago. Pearl chain formations may be convincingly illustrated microscopically in fat emulsions, in yeast emulsions and in diluted blood on a slide in an electromagnetic field of high frequency. Recently this phenomenon has been studied more extensively. Pearl chain formations have been demonstrated in vitro in other biologic fluids. Illustrations of pearl chain formation in undiluted lymph will be shown.

As yet, no objective clinical investigation of this phenomenon has been attempted, so far as we know.

[1] In the German literature the term is *Perlschnurkettenbildungen.*

Notes

SESSION VIII: Ultrasonic Radiation II

Chairman: Edwin L. Carstensen,
U. S. Army Chemical Corps., Fort Detrick, Frederick, Md.

8.1: Instrumentation, Techniques and Mechanism of Action of High-Intensity Ultrasound in Fundamental Neurological Investigations and in Human Neurosurgery*

F. J. Fry, Biophysical Research Laboratory, Department of Electrical Engineering, University of Illinois, Urbana, Ill.

BEFORE DISCUSSING the instrumentation and techniques utilized in human neurosurgical procedures, accomplished by means of high-intensity ultrasound, it is well to review our investigations on the physical mechanism by which high level ultrasound selectively affects tissue structures in the central nervous system. Cavitation phenomena is not important in the physical mechanism of action. The role of temperature change during irradiation has been investigated and found not to be the fundamental physical factor of importance in the production of irreversible changes in the tissue. In order to separate the effects of the various sound field variables (frequency, pressure, particle velocity, particle acceleration amplitudes, etc.) and to determine the pressure and temperature coefficients of the primary mechanism, a large amount of data has been taken in a precision dosage study involving the production of hind-leg paralysis in the day-old mouse. The test animal, placed under rigidly controlled environmental conditions, is exposed in the third lumbar region of the spinal cord to a sound field which is precisely controlled.

Human neurosurgery utilizing focused high-energy ultrasonic beams and precise localization of the brain structures to be irradiated, which was introduced by this laboratory in 1957, has reached the point where a fairly standard pattern of procedural steps has been established for the overall programming of a patient. The steps are essentially the same for a large number of disorders which are being treated by this technique. There has also been a considerable evolution of the mechanical and electronic instrumentation and the data processing and analysis. The steps listed below do not refer to the various medical and psychiatric examinations which all patients must undergo. The procedural steps are: (1) The removal of a bone flap and the sewing back of the overlying tissue. The position and size of the bone flap is determined relative to the structure or structures to be irradiated such that the entrance of the ultrasonic beam will not be impeded by bone. (2) Precise localization of the internal brain structures to be irradiated. This requires extremely rigid clamping of the patient's head while X-rays are being taken and while the patient is being irradiated. The head holder ultilizes four stainless steel pins which are inserted in cup-shaped indentations drilled into the patient's skull. Accurate repositioning of the patient in the head holder is readily accomplished with this instrument. X-ray ventriculography utilizing a radio-opaque dye is used to determine the position of the anterior and posterior commissure, the midline of the third ventricle and the width and tilt of the third ventricle. This requres three X-ray tubes and three cassettes for rapid successive exposures from the lateral position, the anterior posterior position and a position approximately 45° off the vertical axis of the skull in the midline plane. (3) The repositioning of the patient in the head holder and the irradiation through the intact skin; steps (1) and (2) may precede step (3) by at least one week. Irradiations may involve one or more individual doses of the sound; the patient may be observed for several hours in the head holder on any given irradiation procedure. Step (3) may be repeated a number of times depending upon the patient's progress. (4) The replacement of the bone flap with either bone or a suitable replacement material. This step would be eliminated when an appropriate solid material, acoustically transparent and having a low rate of acoustic absorption, becomes available.

For the irradiation of structures requiring lesions of prescribed shapes, small individual lesions (of the order of a few cubic millimeters) can be produced by an instrument comprising an electronic driver capable of delivering several kilowatts of electrical power at a frequency of 1 Mc driving a sound transducer of the multiple source type. The problem of greater precision in the localization of neural structures continues and ultrasound appears to offer at least two approaches. Ultrasonic reflection techniques, locating landmark structures, may offer one type of solution since it can be applied an indefinite number of times without producing harm to the patient and without introducing instruments or other foreign materials into the brain. The previously observed reversible effects of ultrasonic irradiation, without the production of histologically observable lesions, may offer a solution in the accurate localization of almost any type of brain structure.

A film strip illustrating the pre-operative and post-operative condition of a patient with a non-patterned hyperkinetic disorder will be shown.

*This work was partially supported by (1) The Physiology Branch of the Office of Naval Research, (2) The Institute of Neurological Diseases and Blindness of the National Institutes of Health, U S. Public Health Service, (3) The Easter Seal Foundation and (4) The Parkinson's Disease Foundation.

SESSION VIII: Ultrasonic Radiation II

8.2: Techniques Used in the Ultrasonic Visualization of Soft Tissue Structures*

Douglass H. Howry and Joseph H. Holmes, Departments of Radiology and Clinical Medicine, University of Colorado Medical Center, Denver, Colo.

PULSE-ECHO ULTRASOUND, in the megacycle-frequency range, can be used to produce accurate pictures of the interior structures of the living body, when certain special physical requirements are met.

Ultrasonic, cross-sectional pictures of both the interior of solid metal objects and of living tissue structures have been produced for some time. Such pictures were first made independently by two groups of investigators working in different fields in 1950[1]. These pictures were similar to the familiar radar B scan type of presentation; Figure 1. A high-voltage pulse generator produces a pulse which is a fraction of a microsecond in duration. The pulse is applied across a piezoelectric crystal such as quartz or lithium sulfate. Under the influence of the voltage pulse, the crystal develops a short train of ultrasonic, mechanical waves which travel out through a focusing lens into a tank of water. When these waves strike any object which presents a mechanical impedance different from the water, an echo is produced which is reflected back to the transducer. Under the influence of these mechanical waves, the crystal produces a small electrical signal which is amplified and presented as a bright spot on a cathode-ray tube. The electrical sweep on the cathode-ray tube is adjusted so that the time distance separation of the echo signals is in a 1:1 relationship with the structures producing the echoes. The transducer, or sound generator head, is caused to scan back and forth, so that consecutive lines of echoes are sequentially formed on the tube face adjacent to each other, thus resulting in a cross-sectional picture of the structure sonically studied in the water bath.

Early pictures[2] produced of living anatomic and pathological structures were very disappointing since many structures were either seen incompletely or not at all. Thus, the *somagrams* or sound pictures did not have the degree of reliability necessary to make the instrument useful clinically.

A lengthy investigation of this problem showed that the majority of normal tissue structures, such as muscle surfaces, bones, etc., were all specular or mirror-like reflectors. Thus, only those segments of anatomic structures were seen which presented a surface normal or perpendicular to the beam. Other surfaces reflected their echo signals away from the receiving transducer and were not detected. Attempts to produce the correct picture by "brute force" methods of increasing the sensitivity by 60 db were not successful.

For this reason, a system of compound circular scanning was developed which allows the transducer to look at all structures from all directions within a 360° plane. This scanning is achieved by moving the transducer in a circle around the object while it is making simple B scans every 5°.

This type of complex picture registration produces the improvements desired; Figure 3. The test object seen in the upper left of the figure is composed of a lead brick which contains a *V* and point. Over two of the brick's surfaces, pieces of plastic film are applied, and a small wire is placed in the *V*. The resultant sequential ultrasonic pictures are seen in Figure 3, parts 2-5. These are simple B scans made by looking in the directions shown by the arrows. The summation of all the pictures produced (every 5° around the brick) does produce a faithful representation of the outlines of the test object for reasons which will be described. Five improvements are produced in ultrasonic pictures produced in this way:

(1)—The curved or angular surfaces are seen in their entirety.

(2)—Nonspecular reflectors are seen as well as specular reflectors.

(3)—There is a marked improvement in the azimuth resolving power.

(4)—False indications (spooks) in the pictures, which were due to multiple path reflections, are largely eliminated.

(5)—Little trouble is had from structures being in the *sonic shadow* of other structures.

Figures 4, 5, 6 show the application of this method of image formation to an anatomic section of the leg and to the neck of one of the investigators. Note that all major arteries, veins, muscles, vocal cords, thyroid gland, etc., can be accurately seen.

---

* The financial sponsorship of the United States Public Health Service is gratefully acknowledged.

[1] Donald C. Erdman, Electrocircuits, Inc., Pasadena, Calif., and Douglass H. Howry and W. Roderick Bliss, Denver, Colo.

[2] Howry, D. H. and Bliss, W. R., *Ultrasonic Visualization of Soft Tissue Structures of the Body*, J. Lab. and Clin. Med., 40:579-592; 1952.

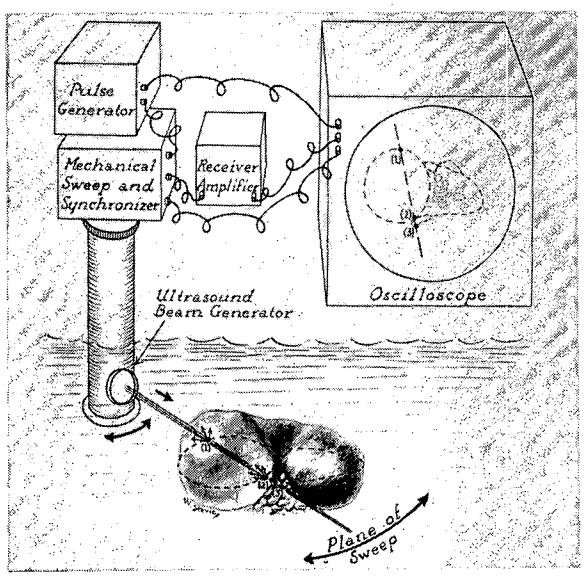

Figure 1—Diagram of Somascope scanning tissue specimen.

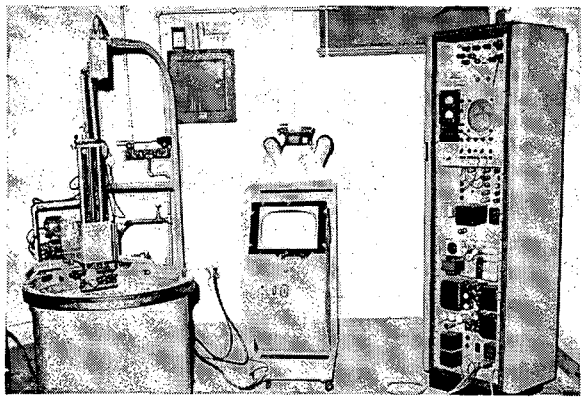

Figure 2—The Somascope: The ultrasonic diagnostic apparatus used at the University of Colorado School of Medicine.

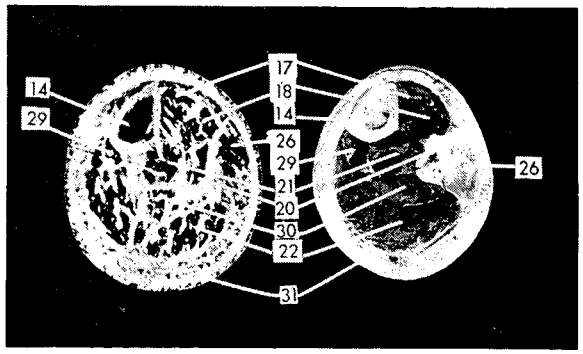

Figure 4—Comparative ultrasonic and photographic studies of anatomic section of lower leg: *14*—tibia, *21*—fibula, *22*—gastrocnemius muscle, *31*—junction between fat layer and muscle.

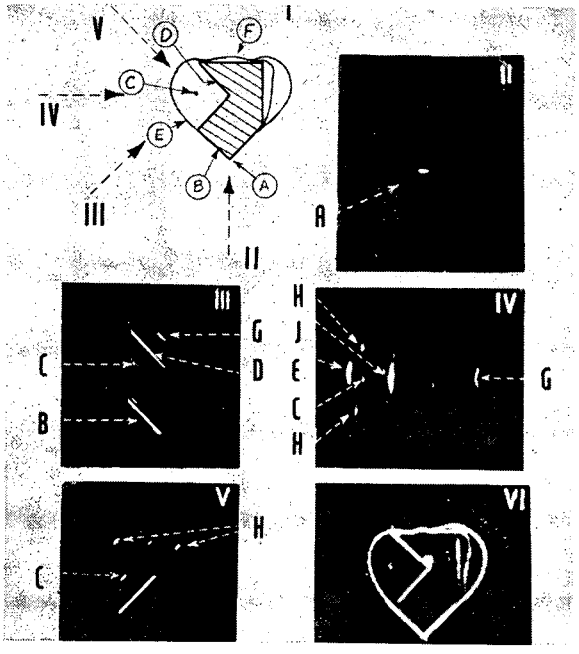

Figure 3—Somascope studies of a complex test object: *I*, Diagram of lead brick; *E*, sheets of plastic; *C*, fine wire. *II* through *V*—simple *B*-scan ultrasonic pictures produced in direction of arrows; *VI*, compound circular scanning.

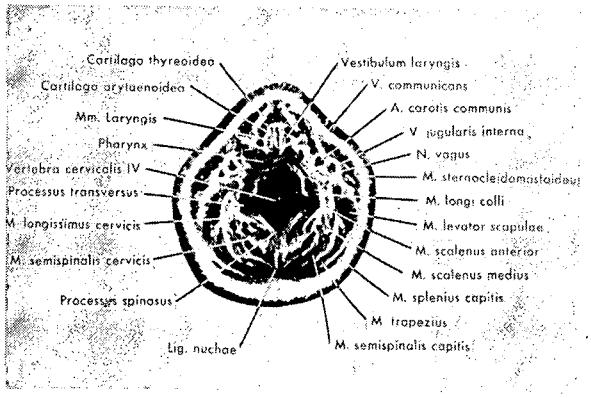

Figure 5—Cross-section Somagram through mid-neck. Note: *Adam's Apple*, Cartilage Thyroidea; vocal cords, M.M. Laryngis; large neck artery, A. Carotis Communis; neck vein, V. Jugularis interna.

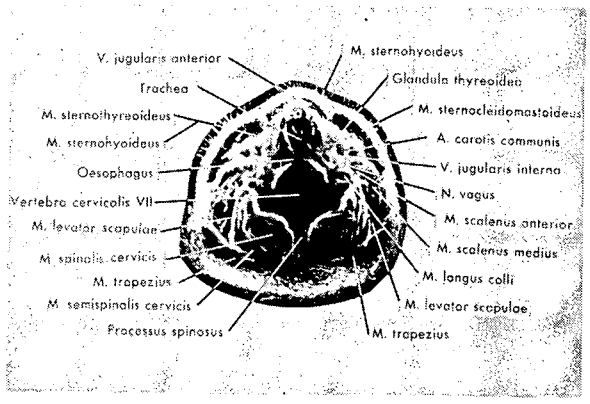

Figure 6—Cross-section Somagram of lower neck. Note: *Wind pipe*, Trachea; thyroid gland, Glandula Thyreoidea; and Jugular and Carotid vessels.

SESSION VIII: Ultrasonic Radiation II

8.3: Ultrasonic Visualization of the Eye*

Gilbert Baum, Department of Ophthalmology, New York University Post-Graduate Medical School, New York City, N.Y., and Ivan Greenwood, New York University and General Precision Laboratories, Pleasantville, N.Y.

ULTRASONOGRAPHY has proven to be an invaluable tool in clinical ophthalmology, because it can reveal information which cannot be obtained by any existing ophthalmic instruments or other techniques.

For the first time it is possible to make accurate diagnoses in eyes opaque to light and in the orbit. Existing ophthalmic instruments are dependent upon light and transparent refractive media for their successful use. Their scope of usefulness is limited to the surface of the retina; hence, it is impossible to obtain cross-sectional views of the eye, short of removing the eye and sectioning it.

The eye is an ideal structure for the application of ultrasonic visualization techniques, since most of its interior is sonically homogeneous and transparent, and its basic geometry is simple. Because of the clinical significance of small size abnormalities, very high resolution is needed. With our present equipment, soft tissue detail in the sub-millimeter size range can be resolved.

Equipment design objectives for this application include the following:

(1) Very high resolution and accurate mapping
(2) Sufficient penetration to reach all structures of interest
(3) Safe ultrasonic power levels
(4) Ability to illuminate sonically eye structures from many directions
(5) Visual presentation of results
(6) Permanent recording of results
(7) Quantitative localization
(8) Quantitative echo amplitude measurement

Description of Equipment

Our research equipment uses pulsed ultrasound from a scanning transducer. A map-like display representing a cross section of the eye is produced by an intensity-modulated radar cathode-ray tube having deflection circuits suitably coordinated with the scanning motions of the transducer. The basic scanning motion is a fast sector scan, and the display is a sector-scanned *PPI* (plan-position indicator). The indicator is part of an AN/APS-23 airborne radar system. Permanent records are made by photographing the indicator tube on 35-mm film.

Detailed measurements of the acoustic absorption and the acoustic impedance of occular tissues have indicated that 15 Mc is an appropriate frequency for this application. A higher frequency would not yield the required penetration, while a lower frequency would compromise resolution. High angular resolution is obtained by means of an acoustically focussed transducer, using an acoustic lens cemented to the front surface of an X-cut quartz crystal. The lens is made from an epoxy resin compound; because of its absorption at 15 Mc and its concave shape, it serves also to control the sound intensity distribution across the face of the transducer in such a way as to suppress side lobes. Good range (depth) resolution is achieved by mechanical damping of the transducer with a metal-loaded-epoxy backing block and by wideband amplifier circuits. The transducer is shock excited.

Compound scanning is currently under development. In this technique, the transducer is slowly and continuously moved in a major arc of 90° about the eye while the fast sector scan is in operation. The resulting super-imposed images on the *crt* are photographically integrated. Compound scan photographs offer better mapping of the eye at the possible expense of some loss of resolution.

Echo intensity measurement as an aid to clinical interpretation is currently being studied. Each film strip is internally calibrated by means of echos from a standard test object with various inserted electrical attenuations. Tissue echos may then be compared with the internal standard by means of photographic densitometry.

Clinical Significance

X-ray is of little value for soft tissue examination about the eye. Contrast media are irritating when used about the eye, and have not materially improved the soft tissue visualization properties of X-ray. Ultrasonography can demonstrate both radiolucent and radio-opaque foreign bodies. Localization is much more precise because the soft tissue can be visualized and the relationship of a foreign body to the soft tissue can be seen and accurately measured. Location measurements to a fraction of a millimeter and less than one degree may readily be made.

Radioisotope evaluation of eye lesions has been unsatisfactory because it is limited to anteriorly located tumors and to those tumors which can take up and retain the radioactive tracer. Surgery is required for examination of lesions in the posterior half of the eye. Orbital lesions cannot be evaluated by this technique. Such lesions are readily demonstrated by ultrasonography. In addition to demonstrating the size, shape, and location of such lesions within the light opaque eye and orbit, one may also determine if these lesions are cystic or solid. A purely cystic lesion would rule out a tumor.

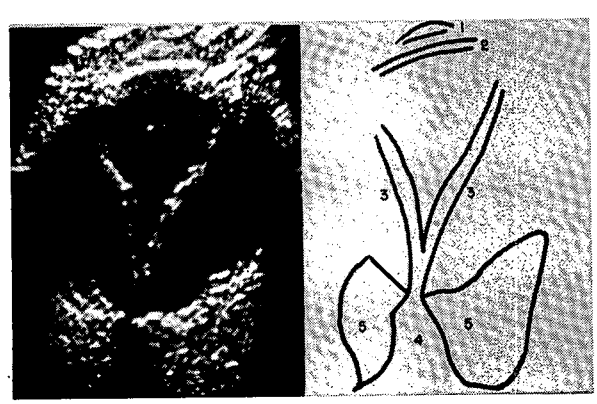

Figure 1—Ultrasonogram of an eye which was mis-diagnosed. The diagnosis was blindness due to glaucoma. Ultrasonography demonstrated a total retinal detachment in this eye. *1*=cornea; *2*=iris; *3*=detached retina; *4*=optic nerve, and *5*=orbital fat.

*We gratefully acknowledge support of this activity by the U.S. Public Health Service, Grant B-993-C1.

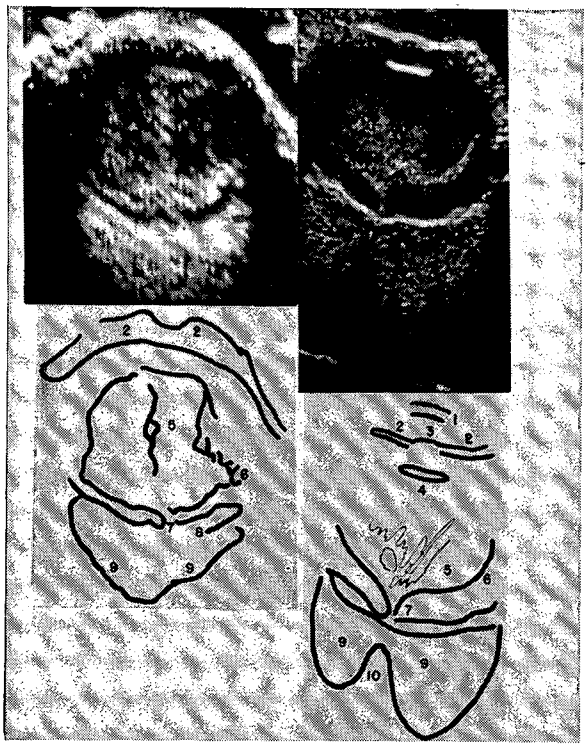

Figures 2 (left) and 3 (right)—Figure 2 shows a massive vitreous hemorrhage and early retinal detachment in patient with sickle-cell anemia. Figure 3 illustrates condition six months later; progression of the detachment despite the absorption of blood. This could now be confirmed ophthalmoscopically. These changes can only be followed by ultrasonography. *1*=cornea; *2*=iris; *3*=anterior lens; *4*=posterior lens; *5*=vitreous hemorrhage; *6*=detached retina; *7*=detached retina attached to optic nerve; *8*=sclera; *9*=orbital fat, and *10*=optic nerve.

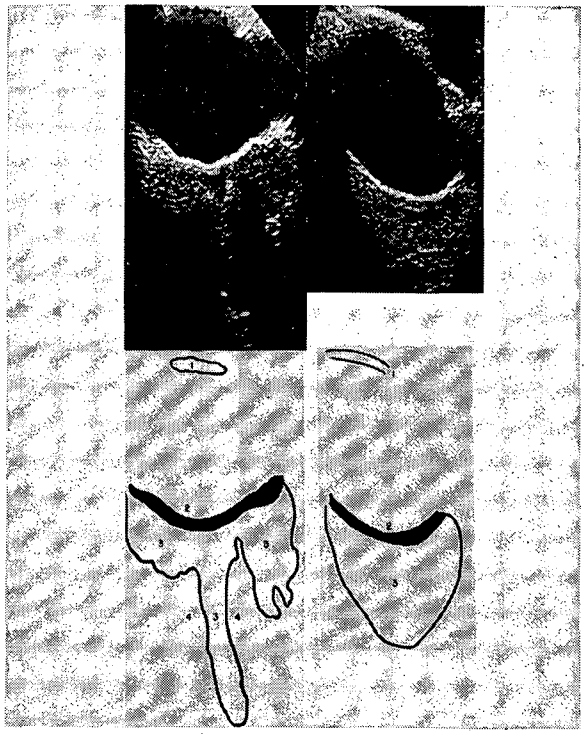

Figure 4 (left)—Angioma of the orbit—confirmed at operation. Figure 4 (right)—Normal eye of this patient does not show any distortion of the fat pattern with the orbit. *1*=cornea; *2*=sclera; *3*=normal orbital fat, and *4*=absence of fat pattern due to tumor.

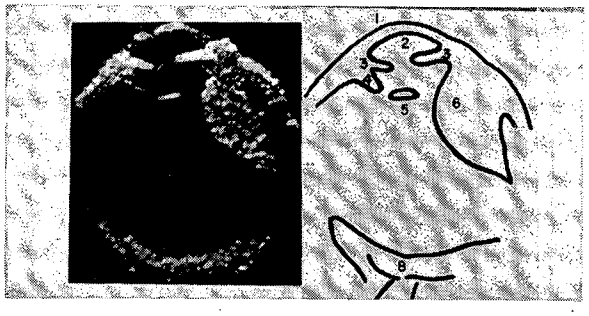

Figure 5—Melonoma of the ciliary body, confirmed by pathological examination. *1*=cornea; *2*=anterior chamber; *3*=iris; *4*=ciliary body and zonular fibers; *5*=posterior lens, and *6*=sclera.

SESSION VIII: Ultrasonic Radiation II

8.4: Gas Chromatograph Detector Based on Measurement of Sound Velocity

Frank W. Noble, Laboratory of Technical Development, National Heart Institute, Bethesda, Md.

THE DEPENDENCE of the velocity of sound upon well-known properties of gases and gas mixtures and the consequent physical significance of measurements of this quantity suggest such measurements as the method of choice for the analysis of effluents from a gas chromatograph column. A prototype having a sample volume of 1/30 cc and sensitivity vastly exceeding that of the thermal conductivity detector has been constructed. It can be shown that the sound detector is sensitive to the molecular weight of the effluent gas, that the cell volume can be made exceedingly small, and that the sensitivity can be increased without limit. The device does not affect any of the physical or chemical properties of the effluent and can be used with any carrier and sample gases over wide ranges of temperature and pressure. Finally, the speed of response is inherently quite fast, being typically of the order of several microseconds.

The velocity of sound in a mixture of two ideal gases is

$$v^2 = \frac{RT}{M_1 + a(M_2 - M_1)} \quad \frac{C_{p1} + a(C_{p2} - C_{p1})}{C_{v1} + a(C_{v2} - C_{v1})} \qquad (1)$$

where; v = sound velocity
R = universal gas constant
T = absolute temperature
a = mole fraction of gas *2*
C_{pn} = specific heat at constant pressure for gas n
C_{vn} = specific heat at constant volume for gas n
M_n = molecular weight of gas n

Consider a plane sound wave of frequency f travelling down a tube of length s. If pure carrier (gas *1*) is contained in the tube, the phase difference between the sound at the transmitting end and the sound at the receiving end is Φ_1, whereas if the tube contains a mixture of two gases, the velocity will be different except in very unusual cases and the phase angle will change to a new value, Φ_2. The phase change produced by the addition of the second gas is

$$\Delta\Phi \equiv \Phi_2 - \Phi_1 = 360\ s\ f \left[\frac{1}{v_2} - \frac{1}{v_1}\right] \text{ degrees} \qquad (2)$$

If a minute amount of a foreign substance having a molecular weight much larger than that of the carrier gas appears in the effluent, $M_2 >> M_1 >> aM_2$ and $\gamma \cong \gamma_1 = \frac{C_{p1}}{C_{v1}}$.

Then $$\Delta\Phi = \frac{180\ f\ s\ a\ M_2}{\sqrt{R\ T\ \gamma_1\ M_1}} \text{ degrees} \qquad (3)$$

from which it is evident that the phase change produced by the presence of the second gas is approximately proportional to the product of its amount and its molecular weight.

The design of the sound tube is arrived at from the following considerations: In order that the wave be essentially plane, the transmitter and tube must have a diameter at least of the order of ten wavelengths of frequency f in the gas. In order for the transmission to be essentially unidirectional, the length of the tube must be chosen such as to provide sufficient attenuation to render the reflected wave of no consequence. Lengthening the tube beyond this point produces increased sensitivity and cell volume and decreased signal-to-noise ratio.

The block diagram of a system for measuring the phase delay of sound travelling through a tube is shown in Figure 1. Oscillator 1, quartz controlled at 4.00 Mc, drives a sound transmitter located at one end of a tube through which the column gas flows. The sound transmitter is a quarter-inch round x-cut quartz crystal resonant with the driving frequency. At the receiving end of the tube is located a second identical crystal used as a sound receiver. A phase-stable wide-band tuned amplifier is used to raise the level of the received signal. The phase difference between the voltage driving the transmitting crystal and the voltage produced by the receiving crystal is to be measured. Since the frequency is inconvenient for phase measurement with commercially available equipment, a conversion system is used to change the frequency without altering the phase difference. This is accomplished by beating the transmitted and received signals against quartz controlled oscillator *2*, which has a frequency differing from that of oscillator 1 by 10 kc. The outputs of converters *1* and *2* are 10-kc signals which have the same relative phase as the transmitted and received signals. The delay line is used to set the baseline phase to any convenient value. An important feature of the conversion process is that the signal-to-noise ratio is improved by reducing the bandwidth of the receiver without materially impairing the phase stability.

When the switch is in position "Φ" the converter outputs are connected directly to a commercial phasemeter which has been arranged to record on a strip chart. If greater sensitivity is desired, the switch is set to position "9Φ". The frequencies of the outputs of converters *1* and *2* are then multiplied by *8* and *9*, respectively, and these signals beat in converter *3* to produce a third 10-kc signal. For each degree of phase difference between the outputs of converters *1* and *2* there will be 9° phase difference between the outputs of converters *1* and *3*, and the sensitivity of the detection system will be increased by a factor of *9*. Clearly this process of sensitivity multiplication can be repeated indefinitely.

In Figure 2 are shown simultaneous tracings taken from the sound detector and from the *Burrell* thermal conductivity detector. The sample is a commercial methyl pelargonate and the carrier gas is helium. The column is of 6 mm (*i.d.*) glass tubing eight-feet long packed with acid washed Chromosorb 'W'[1] which has been coated with polyvinyl acetate[2] 15 per cent by weight. The thermal conductivity detector is operated at its maximum sensitivity; the sensitivity of the sound detector can be increased by a factor of 70 above that shown, using the present model.

This device is subject to the disadvantage that the baseline and sensitivity both shift with temperature and to some extent with pressure. The baseline drift can be compensated by employing two sound paths of identical length operated at the same temperature and pressure, one containing pure carrier gas, the other containing the effluent from the column. It must be pointed out that this does not correct for the sensitivity drift, which can be reduced only by reducing temperature changes.

[1]Johns-Manville
[2]Union Carbide *AYAC*

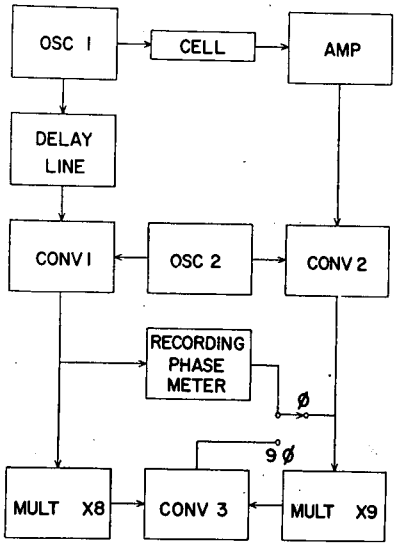

Figure 1—Block diagram of a system for measuring the phase delay of sound travelling through a tube.

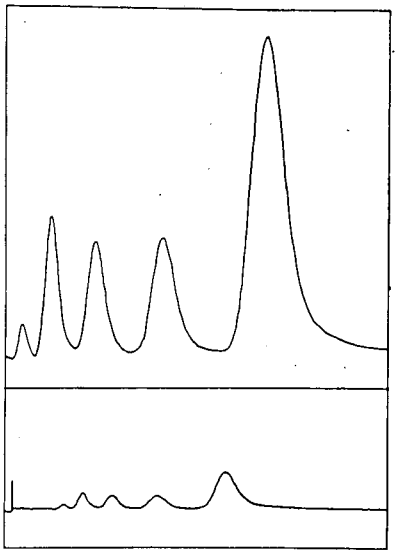

Figure 2—Simultaneous chromatograms taken by the sound detector (*top*) and the *Burrell* thermal conductivity detector (*bottom*).

Notes

SESSION IX: Infrared Radiation I

Chairman, E. Hendler,

Air Crew Equipment Laboratory, Naval Air Materiel Center, Philadelphia, Pa.

9.1: The U. S. Army Quartermaster Solar Furnace

Eugene S. Cotton, Radiation Physics Laboratory, U.S. Army Quartermaster Research and Engineering Center, Natick, Mass.

DURING ITS FIRST YEAR of operation the *Quartermaster* solar furnace has been used primarily for basic-performance measurements and studies of its thermal effects in biological exposures. The fundamental purpose of this device is to simulate the thermal radiation emitted during nuclear-weapon detonations and thus aid in developing methods of protection for soldiers who might be exposed to such radiation.

An overall view of the instrument is shown in Figure 1. On the right is the heliostat, a movable array of flat glass mirrors 36-feet high and 40-feet wide. Mounted on this framework are 356 square mirror segments, which are 1/4-inch thick and 2-feet on a side. These segments are made of water-white plate glass, silvered and copper-plated on the back surface, with a protective enamel coating over the copper. Each mirror is mounted on three studs through loosely-fitting holes in the glass; a locking nut with washer presses the mirror firmly against a compressed spring, thus permitting mirror adjustment from the front.

The attenuator is the large open framework shown in the center of Figure 1. This "venetian blind" assembly is placed so that the reflected solar radiation from the heliostat passes through its openings and thus regulates the amount of light on the concentrating surface. The attenuator is placed so that the concentrated radiation passes unhindered through its center opening and it does not cast a shadow on the heliostat. The attenuator blades cut off radiation from the heliostat when they are at 45° from the horizontal, thus providing wind relief for the structure. They can be closed by gravity in about 1/3 second under emergency conditions; this is used as the primary safety interlock point.

The structure on the left of Figure 1 is the concentrator, which holds the concave mirror segments. This framework has a spherical surface, designed to place each mirror in the position where its optical performance is optimized. The radius of curvature of this surface is 35 feet, while the radius of curvature of the individual glass-mirror segments is about 70 feet. On the framework are mounted 180 concave, spherical mirrors, made of ¼-inch plate glass which has been slumped to have the correct curvature. The mirrors are approximately square, 2 feet on a side, and utilize a vacuum-deposited aluminum reflective layer on the front surface, overcoated with silicon monoxide. Each mirror is fastened to an aluminum ring which can be adjusted to hold the mirror at the proper angle. The effective concentrating area of the composite mirror surface is about 750 square feet.

The images from all of these mirrors are superposed at the focal point, 35 feet from the center of each segment. The composite image has a diameter of about 4½ inches with a maximum flux density exceeding 100-gram calories cm^{-2} sec^{-1}. This image is formed about 3 feet inside the test chamber, where shutters are available to produce timed exposures of samples for periods of 0.1 second or longer. The image measured at maximum flux is shown in Figure 2, as compared with the measured image produced by the *Quartermaster* carbon-arc source.

Detailed measurements on the optical performance of all mirror segments were necessary before mounting was accomplished. The maintenance of reflecting surfaces and optical alignment has proved to be a continuous task. A two-channel *dc* servomechanism drive provides automatic tracking for the heliostat to keep the reflected beam incident upon the concentrator at all times when solar radiation is available.

The effectiveness of this solar image on unprotected pig skin has been compared with that of the unfiltered carbon arc in rectangular exposures of ½-second duration. It was found that the concentrated solar radiation is much less effective in producing 2+ burns (Rochester scale) than radiation from the carbon arc operating at about 5800°K, as shown in Figure 3. This difference is largely due to the excess ultraviolet radiation available from the carbon arc; it is also felt that the solar furnace is a better simulant of nuclear weapon thermal radiation than the unfiltered arc. A comparison of burns on pig skin protected by an absorptive fabric shows that the sources are equally effective when spectral differences are taken into consideration.

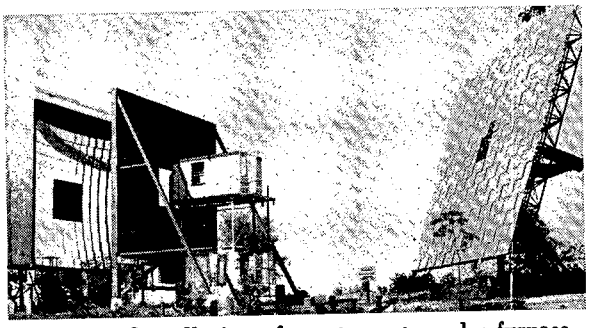

Figure 1—Overall view of quartermaster solar furnace.

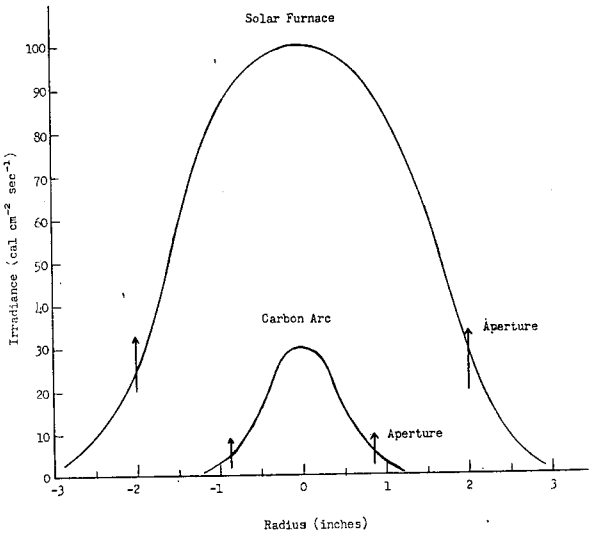

Figure 2—QM thermal-source flux-density distributions and aperture sizes used.

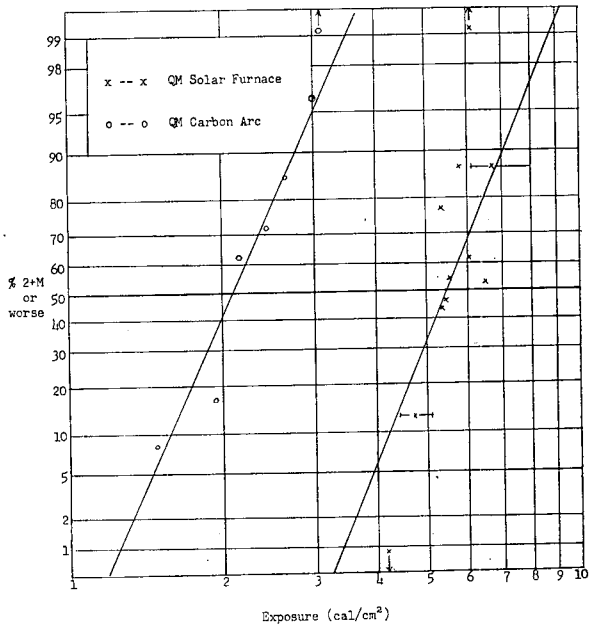

Figure 3—Regression curves for ½-second exposures of unprotected pig skin.

SESSION IX: Infrared Radiation I

9.2: Radiant Heat Sources Employed in Thermal Burn Studies

J. A. Carter, W. L. Derksen and T. I. Monahan, Naval Material Laboratory, N. Y.. Naval Shipyard, Brooklyn, N. Y.

THE DETONATION of the atomic bombs at Hiroshima and Nagasaki opened a new field of research on the effects of intense thermal radiation on materials. The Naval Material Laboratory was the first to utilize and develop the carbon-arc imaging furnace as a suitable instrument for investigating these effects in the laboratory.

The first *NML* arc-imaging furnace consisted of dual 24-inch Navy signalling searchlights with paraboloidal reflectors, which were placed facing each other. In the "transmitter" the standard searchlight lamp was mounted; the "receiver" collected the emitted flux and refocussed it to a spot effectively 5 mm in diameter. The maximum irradiance was 85 cal/cm²sec, and the spatial distribution of the flux at the target was approximately gaussian. The incident beam at the collector's focus was highly convergent, making a solid angle of 130°. For "dynamic" exposures the specimen was moved through the focus at constant acceleration. For "static" exposures the specimen was fixed in position in the focal spot, the duration of the exposure being set by a knife blade shutter. The pulse shape is essentially square wave. To meet the need for higher irradiances a similar unit was constructed with 36-inch paraboloidal reflectors; the effective spot was increased to 9 mm and the irradiance to 100 cal/cm²sec.

The need for larger exposure areas and less beam convergence resulted in the fabrication of a source employing a 24-inch ellipsoidal reflector, as shown in Figure 1. The positive carbon was placed at the primary focus of the reflector, the carbon's crater making a solid angle of approximately 120° with the reflector; the flux was reimaged at the secondary focus with a magnification of somewhat greater than 5. The acceptance angle is 30°; the maximum irradiance obtained is 17.5 cal/cm²sec.

The Laboratory designed a mechanism which monitors the irradiance to give a rapid rise to a maximum value followed by a slow exponential decay, as shown in Figure 2. The pulse simulator consists of a radial-vane shutter rigidly coupled to a precision cut cam and driven by a variable speed electric motor. The pulses obtainable represent nuclear detonations of from 15 to more than 100,000 kilotons.

A pulsing mechanism, Figure 4, was designed for the 36-inch paraboloidal source, giving a peak irradiance of 55 cal/cm²sec. In the 24-inch ellipsoidal unit the use of higher density carbons and the addition of a phototube device to position the positive carbon more accurately increased the irradiance in the plane of the secondary focus to 16.5 cal/cm²sec.

A tungsten source was assembled, consisting of six 500-watt quartz envelope infrared tubular lamps arranged to make a radiator 5½ inches square, and operated at twice the rated wattage. The maximum irradiance 3 cm from the filaments is 6 cal/cm²sec.

A dual 24-inch ellipsoidal source has been assembled, in which a second ellipsoidal reflector is positioned with its secondary focus coincident with that of the first reflector, resulting in an imaging of the positive carbon's crater at the primary focus of the receiver, with a maximum irradiance of 155 cal/cm²sec. A commercial unit is being procured having the same basic design with a higher current density. A maximum irradiance in excess of 300 cal/cm²sec over a 9.5 mm diameter image will be obtained

A source is being designed for the use of other laboratories in studying retinal burns. The luminous objective of a high radiance source of fairly uniform brightness will be reimaged by a simple lens system. An aperture stop in the image plane will adjust the size and shape of the irradiated spot on the retina. Possible sources under consideration are the carbon arc, compact mercury or xenon arc, and, for higher retinal irradiances, the sun.

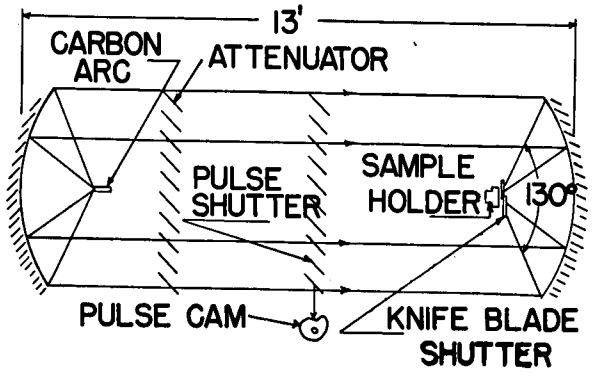

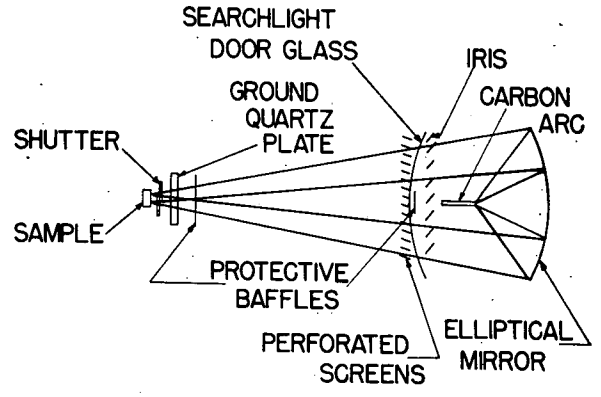

Figure 1—Carbon-arc furnace which burns 11-mm positive carbons at 80 amperes and 78 volts and delivers an irradiance of 17.5 cal/cm²sec across the secondary focus that has essentially a gaussian distribution.

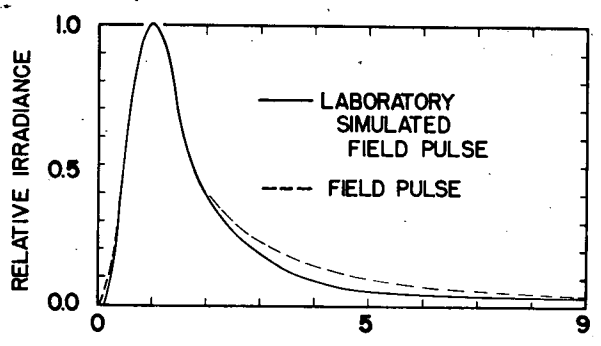

Figure 2—The Laboratory-simulated pulse which decays to 3.5% of the maximum irradiance at 10 times the time to maximum irradiance and delivers in this time interval 6% more radiant energy than the generalized field pulse. Relative time indicated on abscissa.

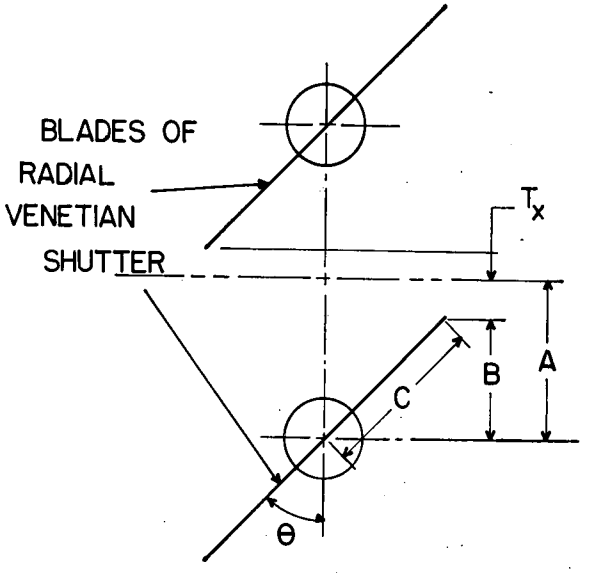

Figure 3—The transmittance of the pulse shutter is:

$$T_x = \frac{A-B}{A} = \frac{A-C\,(\cos\Theta)}{A}$$

$$\text{then } \cos\Theta = \frac{A\,(1-T_x)}{C}$$

$$\text{and } \Delta\gamma = \left(\frac{\pi D}{4}\right)\left(\frac{\pi/2-\Theta}{\pi/2}\right) = \frac{D\,(\pi/2-\Theta)}{2}$$

where $\Delta\gamma$ = *change in pulse cam radius*
and D = pitch diameter of transfer gear

Figure 4 (Left)—Dual 36-inch paraboloidal arc-imaging pulse source. Laboratory-simulated field pulses from 20 to more than 100,000 kilotons can be generated.

SESSION IX: Infrared Radiation I

9.3: Measurement of Temperatures in Thermal Burn Studies

T. I. Monahan, W. L. Derksen and G. P. deLhery, Naval Material Laboratory, N. Y. Naval Shipyard, Brooklyn, N. Y.

LIVE TISSUE DAMAGE is associated with the temperature of the subject and the time interval during which this temperature is maintained. *Moritz* and *Henriques* showed that, in the case of hot water burns, threshold irreversible tissue damage takes place at a skin temperature between 44° and 45°C. For radiant energy *Buettner* demonstrated that pain occurs between 42° and 45°C. *Hardy* and co-workers have shown that pain and tissue damage are not sustained at skin temperature below 45°C and increase with increasing temperature over 45°C.

The Naval Material Laboratory's interest in temperature measurements arose in the development of its skin simulant. With proper correlation it should be sufficient to predict the severity of burns in humans from the temperature histories of the skin simulant in similar exposures. A direct approach to the problem would be to introduce temperature-sensing elements into the tissue of the animal. Since there are several difficulties to this approach, it was necessary to employ an indirect method, that of measuring surface temperatures of animals and humans in burn and sub-critical situations and of the skin simulant on the surface and in depth.

Fine-wire thermocouples were made by electroplating part of 0.0033-cm constrantan wire with copper to a diameter of 0.0065 cm. The copper's low electrical resistance, compared with that of constantan, effectively forms a thermocouple at the plating terminus. The thermocouple is pushed into firm contact with the subject. Careful checks were made to ascertain the range of conditions under which the thermocouple would accurately measure the surface temperature.

In the development of the skin simulant as an instrument for measuring equivalent burn severity, since only meager burn data are available for humans, it is necessary to use the corresponding animal data on the assumption that human and animal skin degrade thermally similarly. The heat flow theory for opaque and diathermous media is employed and the thermal conductivity, diathermancy and optical characteristics of human and animal skin are measured.

The surface temperatures of blackened human skin were measured for various times of exposure to the thermal source. Representative data, shown in Figure 1, yield an average *kpc* value of 8.6 x 10^{-4} cgs units, which appears to be constant for irradiating pulses of 0.2 to 10 seconds. The temperature rise of unblackened skin, Figure 2, is unlike that of the painted (opaque) skin, due partly to the diathermancy of skin. To reconcile the experimental temperatures for the various exposure times it is necessary to postulate a time-variant extinction coefficient, which varies from 75 to 280 cm^{-1}. The variation with time is due in part to the wavelength-selective penetration of radiant energy within skin.

We now wish to cross over from animal burns to the corresponding situation in the human. The *kpc* effective extinction coefficients and radiant absorptances of human and animal skin have been measured. The temperature rises of human and rat skin have been determined for given radiant energy pulses. The critical radiant exposure for a second degree burn in human skin was computed as the product of the ratio of these rises and measured critical radiant exposure for the same burn severity in rat skin, uncovered and behind a uniform system with which it was in contact and separated. The skin simulant with an embedded thermocouple 0.05 cm below the surface was irradiated in situations duplicating these three conditions; thus a family of temperature histories corresponding to the same thermal damage was obtained. Since 45°C represents the temperature for threshold thermal damage, it would appear that the burn severity index would be some function of the amount by which the skin temperature exceeds this value and of the time interval during which the temperature exceeds 45°C. The temperature history data are presented in Figure 3, in which each history is given in terms of these parameters. The data fall reasonably close to the curve shown. It would appear that this curve represents a good working tool for interpreting skin simulant temperatures in terms of corresponding burn severities.

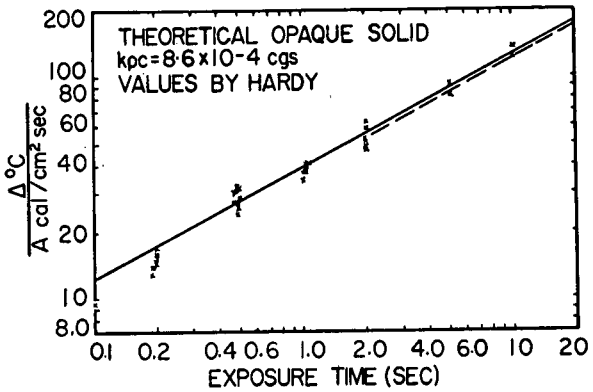

Figure 1—Temperature rise of the surface of blackened human skin. The experimental data fit the opaque solid theoretical curve reasonably well.

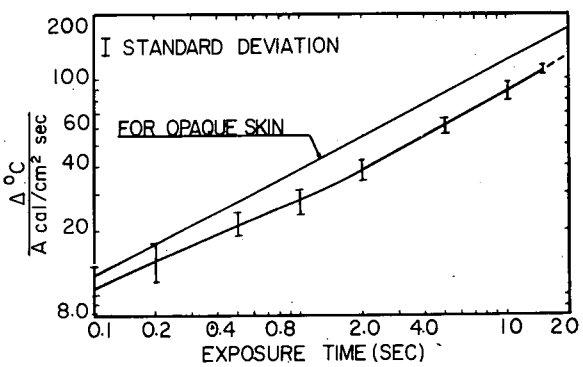

Figure 2—Temperature rise of the surface of human skin for carbon-arc radiation. The effect of human skin's diathermancy is demonstrated, as well as the variation of diathermancy with exposure time, due in large part to skin's wavelength-selective absorptance.

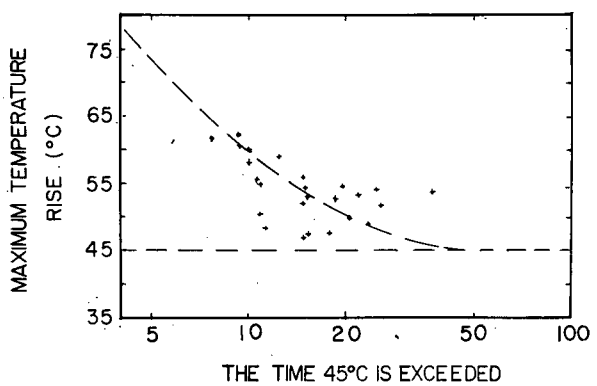

Figure 3—Human skin burns: Relationship between maximum temperature of skin simulant and the time for which the threshold temperature of 45°C is exceeded.

SESSION IX: Infrared Radiation I

9.4: Radiometric Technique in Skin Temperature Measurement

E. Hendler, Air Crew Equipment Laboratory, Naval Air Materiel Center, Philadelphia, Pa., and J. D. Hardy, Physiology Dept., School of Medicine, University of Pennsylvania

RADIOMETERS enjoy certain advantages in accuracy, response time and convenience for measuring skin surface temperatures as compared to those devices, such as thermocouples and thermistors, which must make physical contact with the skin surface. The radiometric technique to be described is applicable to those cases where a relatively flat area of skin can be exposed and remain stationary during the experimental period. Temperature measurements made with this technique have been used to study the mechanisms involved in temperature sensation, as well as to determine the thermal properties of cutaneous tissues.

The components of the apparatus and their disposition are shown diagrammatically in Figure 1. A subject is seated so that a central circular area of forehead skin (37 cm^2) is exposed through an aperture in a face shield. Various kinds of energy sources can be used to change the exposed skin temperature in a controlled manner. Near and far infrared sources have been employed for this purpose, as well as microwaves. Control of the infrared sources is exercised by the use of either manual or motor-driven rotating shutters. The microwave source and its control is described elsewhere in this Digest. A thermocouple detector located at the focal point of a parabolic mirror is activated by emitted radiation from the skin surface, and provides an electrical signal which eventually drives the pen of a stripchart recorder. Amplification and rectification of the electrical signal is produced by standard commercial components*, and a potentiometer is used to balance out most of the rectified signal. Recorder pen deflection is adjusted under most circumstances to provide a deflection of ten inches for approximately 2°C. Much higher and lower temperature spans can be obtained for the same extent of pen deflection, depending upon the experimental conditions. For purposes of calibrating the radiometer, a black-body radiator consisting of the blackened cone of a *Leslie* cube, maintained at various known temperatures, is placed in the face shield aperture. Radiation measurements made at five locations within the face shield aperture, using a calibrated, portable radiometer, determine the optimum position of the heat source to provide a uniform energy flux over the exposed area.

Application of the radiometric technique as described depends upon the sheet aluminum chopper shown in Figure 2. The motor-driven chopper, rotating approximately 13 times-per-second, mechanically interrupts the radiation exchange between the skin and thermocouple detector on the one hand, and between the heat source and the skin on the other. Examination of Figure 2 indicates the manner in which heat source and detector are alternately exposed to the skin. Interruption of the radiant energy reaching the detector results in an alternating electrical signal which is amplified by a conventional *ac* amplifier tuned to the chopping frequency. Alternate interruption of heat source and detector eliminates the undesirable effects of reflected radiation, which otherwise can obscure and confuse the skin temperature records obtained. Figure 3 illustrates this important point.

One of the important uses to which the radiometric apparatus has been put concerns the determination of the thermal inertia for surface heating, or $k\rho c$, of the skin (where k=thermal conductivity, ρ=density and c=thermal capacity). Changes in skin temperature with time were recorded for a group of subjects on repeated occasions. An average value for $k\rho c$ of $108 \pm 8 \times 10^{-5}$ $cal^2/cm^4/°C^2/sec$ was determined for the forehead skin of resting, non-sweating subjects, who were in thermal equilibrium with comfortable surroundings. Because of the relatively low levels of infrared radiation used to change the skin temperature (approximately 2.5 $mcal/cm^2/sec$), values of $k\rho c$ remained almost constant for heating periods of 140 sec.

*Manufactured by the Perkin-Elmer Corporation, Norwalk, Connecticut.

Reports of temperature sensations accompanying measured skin temperature changes indicated that rate of change of skin temperature was adequate to explain the mechanism of temperature sensation only under certian conditions. Consideration of recent electrophysiological findings, together with observations on continuous and pulsatile heating of the skin, has given rise to the hypothesis that a change of temperature occurring within the dermis produces phasic nervous discharges in undifferentiated nerve endings which give rise to temperature sensations.

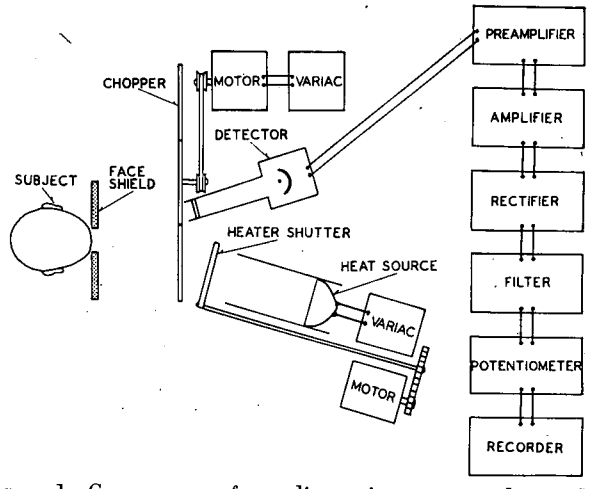

Figure 1—Components of a radiometric apparatus designed to simultaneously change and measure skin temperature.

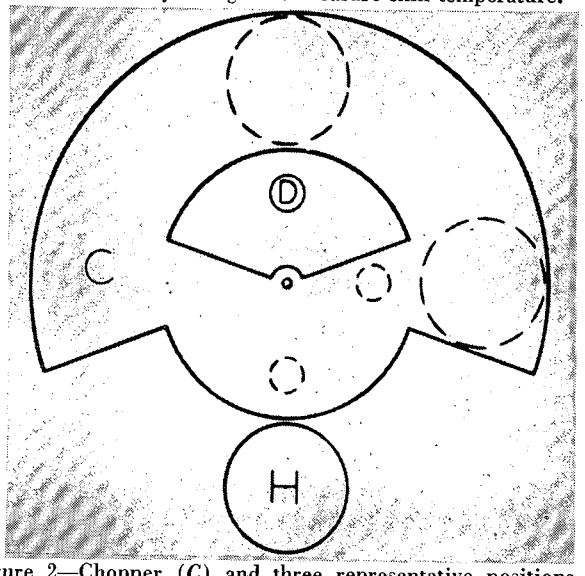

Figure 2—Chopper (*C*) and three representative positions of detector (*D*) and heat source (*H*) during one chopper revolution (solid circles exposed, dashed circles occluded).

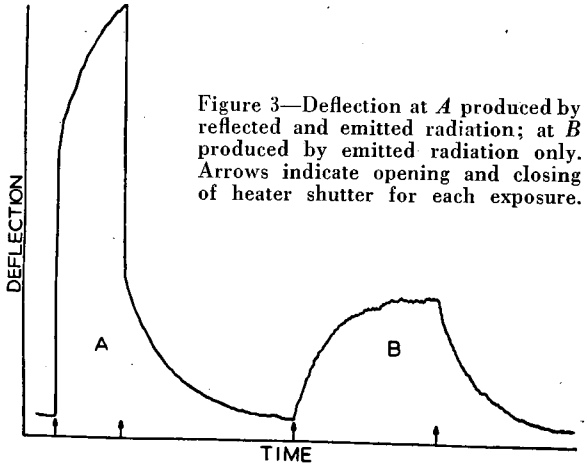

Figure 3—Deflection at *A* produced by reflected and emitted radiation; at *B* produced by emitted radiation only. Arrows indicate opening and closing of heater shutter for each exposure.

SESSION IX: Infrared Radiation I

9.5: Penetration of Corneal Opacities by Infrared Electronics*

Joel Friedman, Brooklyn, N. Y.

TISSUE PENETRATION by infrared waves as an aid to medical diagnosis has been applied with varying success to peripheral vascular disease, collateral circulatory studies, dermatology and ophthalmology. Yet, despite the apparent capacity of the infrared photographic and electronic image to elicit data significant in differential diagnosis, there has not taken place the logical sequel of acceptance and routine use of infrared diagnostic techniques in medical practice.

W. A. Mann[1] demonstrated the usefulness of infrared photography in opacities of the cornea, contrasting panchromatic films with infrared sensitive plates, and quotes *Dekking's*[2, 3] observation that the pigment in the iris reflects infrared rays strongly, thereby acting as a protective barrier against its absorption by the eye.

Ogg[4] adapted a British World War II tube to one ocular of a slit lamp, and was able to see through all type of opacities except calcareous degeneration. He noted that the greater the vascularity of the opacity, the more complete the penetration of infrared radiation.

The penetrative phenomenon of the .8 to .9-millimicron range appears particularly effective for examination of the anterior chamber of the eye in the presence of corneal opacification. The information acquired by this means is useful in evaluation of status of the iris, transparency of the lens, and turbidity of the aqueous humor. In the presence of a dense opacity of the cornea, the ophthalmic examining instruments in use frequently do not provide a subcorneal view.

Improved resolution of image-converter tubes reflects the measure of progress in ophthalmic research. Previous studies were limited to the 1P25A American type used in World War II sniperscopes, or its British (CV-147) and German (Vampire) counterparts. These formed images only in the near infrared, using cesium photocathodes. Resolution was in the range of 12± 2 line-pairs per mm. They were fitted with optics obscured by target-centering reticles, and with relatively coarse-grained cesium silver-oxide phosphor screens.

Theory of Operation

The studies in this paper were made with a U. S. Navy infrared receiver utilizing a type 6032 image converter tube[5]. It has a resolution of 18 line-pairs per mm at the center of the semi-transparent photocathode, with highest sensitivity in the near infrared. The electrons activated in the cathode are directed electromagnetically to the phosphor screen anode (P20) with the aid of a 19,000-volt power pack. The erect visible image on the 5/8" diameter screen is viewed through an enlarging lens. The curvature of the face of the photocathode produces a curved field, which is partly compensated by a correcting lens in front of the cathode.

Since image-converter tubes are all highly sensitive to infrared radiation, tungsten lamps provide an adequate source of light. Many infrared diagnostic applications in ophthalmology entail the elimination of visible light; (*1*) to permit full dilatation of the pupil, and (2) to afford the observer an opportunity to watch spontaneous eye movements in the absence of any distracting lights in the patient's field of vision. A deep infrared filter is fitted over the light sources for this purpose. The infrared light passes from the tungsten source to the subject's eye, then to the ophthalmic instrument, and finally through the infrared receiver to the observer's eye.

There are instances requiring the interposition of the infrared tube earlier in the sequence, for example, when an infrared instrument is used in conjunction with another electronic tube such as a vidicon insensitive in the infrared zone. The infrared tube would then come before the vidicon, to provide the penetrative effect.

Discussion

As utilized in these studies, the instrument has definite technical shortcomings and biologic limitations. The grain structure of the phosphor screen interferes with good photographic rendition of the observations made through the viewer. Pincushion field distortion is marked, even with the correcting lens built into the optics, and peripheral blurring is apparent.

Limitations to the penetration of opaque corneas have been noted in six patients out of twenty-one studied thus far. These were chiefly in long-standing, thick opacities with marked formation of new scar tissue and well organized circulatory elements.

Applications

The direct visualization of subcorneal structures in blind patients with opacified corneas is facilitated by the use of the infrared-sensitive electronic tube in conjunction with ophthalmic diagnostic instruments. Preoperative appraisal of the likelihood of success in corneal transplantation is more definitive. Studies of iris and pupil under dense opacities, observations on pupillary reactions and eye movements in darkness, and differentiation between solid and cystic retinal detachment may be made.

Conclusions

Some areas of usefulness of the infrared image converter tube to diagnostic procedures in cases of opacification of the cornea will be presented. Further technical progress will be paced by advances in infrared optics, quality of screen image, and simplification of design to facilitate the adaptation of the tube as an auxiliary for direct ophthalmic examination.

---

*This research was aided by loan of equipment by the Office of Naval Research. The clinical studies were made at the Brooklyn Eye and Ear Hospital Corneal Clinic, Dr. A. B. Rizzuti, Physician-in-Charge.

[1]Mann, W. A. "Infrared Photography of the Eye", *Arch. Ophthal.* v. 13, pp. 985; June, 1935.

[2]Dekking, H. M., "Infrarotphographie des Auges", *Arch. f Ophthal.* v. 130, pp. 373; Aug., 1933.

[3]Dekking, H. M., "Infrarotphotographie des Auges", *Arch. f Ophthal.*, v. 133, pp. 20; Nov. 1934.

[4]Ogg, A. J., "Examination of the Eye with Infra-red Radiation", *Brit. J. Ophthal.*, v. 42, pp. 306; May, 1958.

[5]RCA

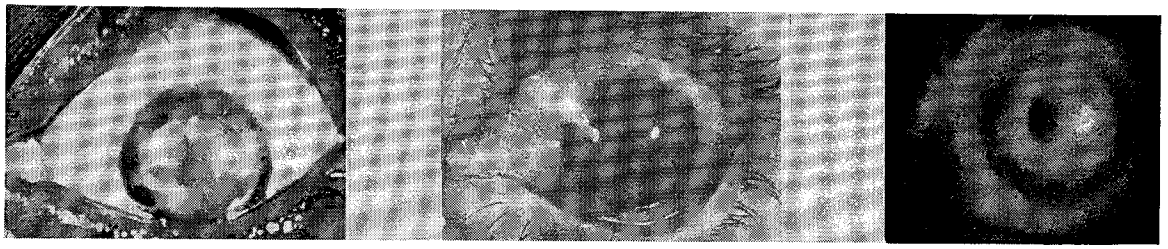

Figure 1—E. B.: Reproduction of films detailing corneal graft which developed a cloudy result. Left film shows clinical condition of the graft. Center film shows iris and pupil via infrared photography. Right film records the still photograph taken on Ilford HP3 film through an infrared image converter. The grain of the phosphor screen, on which the eyepiece optics are set in fixed focus, is markedly apparent. In use, the observer is no more aware of this than of the scan lines of a television screen. The single tungsten light source is reflected from the patient's lens. This reflex can be moved about by changing the viewing angle. The opacity appears to be more in evidence over the iris than in the infrared photograph, where it is only faintly seen.

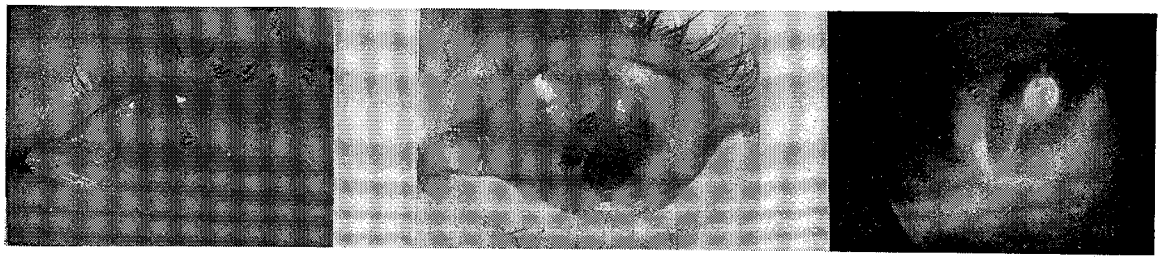

Figure 2—E. E.: Diffuse corneal scar after graft and partial iridectomy. Left film presents the corneal opacity with cloudy view of pupil and iridectomy. Center film shows the eye via infrared photography, giving a distinct image of the extent of the iridectomy and clarity of the lens. Right film, through the electronic receiver, manifests a comparable view to the right film of case *1*.

SESSION IX: Infrared Radiation I

9.6: Temperature Control in a Bio-Satellite

K. L. Cappel, The Franklin Institute, Laboratories for Research and Development, Philadelphia, Pa.

SINCE SMALL laboratory mammals (such as rats) cannot tolerate large extremes of temperature without deterioration of performance of learned behavior, the temperature of the life cell of an orbiting satellite carrying such animals must be actively controlled, if absence of gravity is to be the only condition whose effect on behavior is to be investigated. The *Bio-Satellite* prototype, now being built for the Aero-Medical Acceleration Laboratory (NADC, Johnsville), is designed to achieve such active control without internal heat sources or sinks by automatic regulation of the rate of rejection of internally generated and absorption of incident heat from both the sun and the earth. Sources of heat generation are the metabolism of the two rats, the exothermic reaction of water and carbon dioxide with the lithium hydroxide used to absorb both, and the electronic equipment, air circulation pump, etc. Calculated rates of heat production range between 21 and 80 BTU/hr.

While the configuration of the proposed satellite was not primarily determined by the temperature control problem, it was possible to adapt the structural components to serve as appropriate conductors, heat reservoirs and radiators. The roughly cylindrical life cell is shielded by a pair of frustated conical shields which are supported by thermal insulators on four pairs of ribs radiating from the center of the cylinder. An inner layer of reflective foil in each conical shield provides additional thermal insulation and permits neglect of heat transfer between the life cell and space in a preliminary analysis.

Between the cones, and supported by the ribs, is a cylindrical shield with alternating stripes of high and low ratios of solar absorptivity to emissivity. This cylindrical shield is

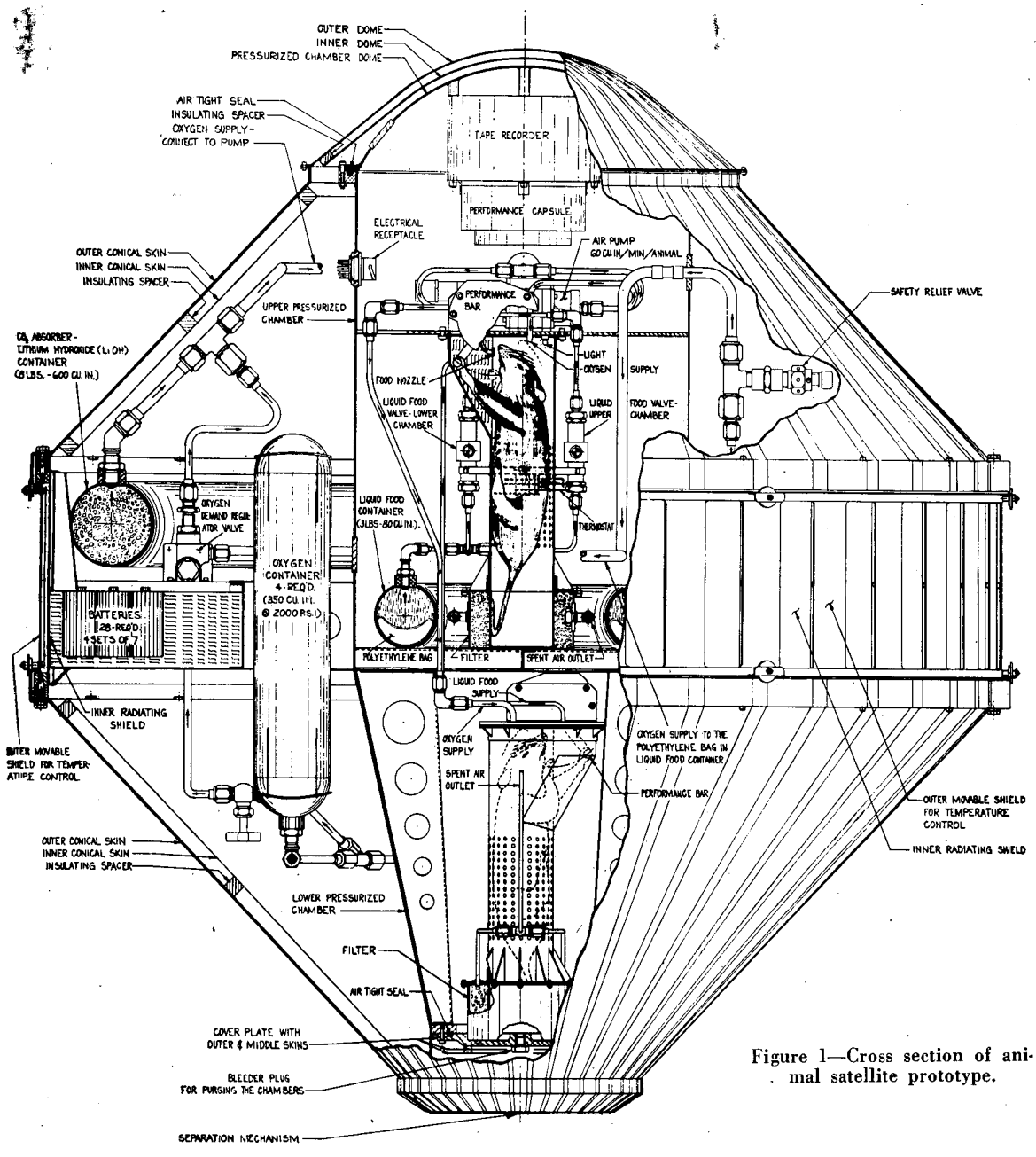

Figure 1—Cross section of animal satellite prototype.

covered by an outer shield having windows which may be aligned with either set of stripes, as determined by the temperature inside the life cell.

One advantage of the proposed configuration is that equipment which must be protected from temperature extremes such as the batteries, the oxygen, tanks, and the lithium hydroxide (where freezing of water would cause blocking of the air supply) may be located within the outer shell, but need not be pressurized, which results in a saving in weight and elimination of large airtight joints. Also the outer cones may serve as meteor shields, thus reducing the chances of puncture of the life cell. Finally, location of heavy equipment close to the "equatorial" plane of the satellite makes for a large moment of inertia about the body axis of the animals, thus increasing the stability of spin which is considered essential for maintaining the rats as closely as possible in a zero-g condition.

Since battery power is required to change the position of the outer shield, it was important to determine how frequently such shifting would be required under the expected conditions of internal heat generation, and external heat input.

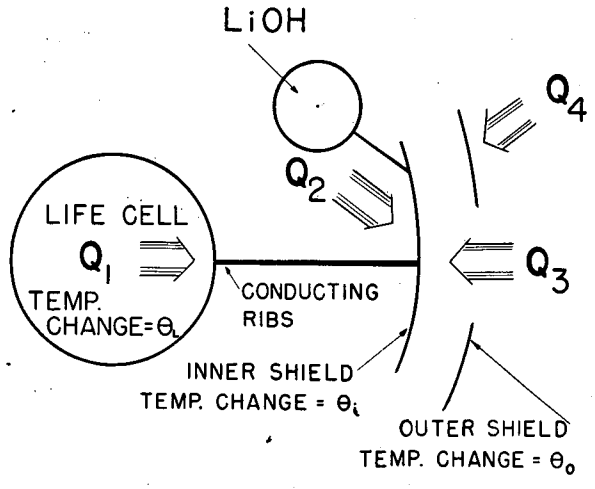

Figure 2—The Bio-Satellite represented as an idealized thermal system, with main sources of heat gain: C_1—from animals; C_2—exothermic reactions in LiOH; C_3 *and* C_4—heat absorbed by inner and outer shields.

$$\dot{\Theta}_L = \frac{Q_1}{C_L} - \frac{KA'}{C_L L}(\Theta_L - \Theta_i) - \frac{KA'}{C_L L}(T_L - T_i) \qquad (1)$$

$$\dot{\Theta}_i = \frac{Q_2 + Q_3}{C_i} + \frac{KA'}{C_i L}(T_L - T_i) + \frac{KA'}{C_i L}(\Theta_L - \Theta_i) - \frac{\sigma A \epsilon_i}{C_i} T_i^4$$

$$- \frac{4\sigma}{C_i}(A\epsilon_i + A_c\epsilon_c) T_i^3 \Theta_i + \frac{4\sigma A_c \epsilon_c T_o^3}{C_i}\Theta_o - \frac{\sigma A_c \epsilon_c}{C_i}(T_i^4 - T_o^4) \qquad (2)$$

$$\dot{\Theta}_o = \frac{Q_4}{C_o} + \frac{4\sigma A_c \epsilon_c T_i^3}{C_o}\Theta_i - \frac{4\sigma A_c(\epsilon_c + \epsilon_o) T_o^3}{C_o}\Theta_o$$

$$+ \frac{\sigma A_c \epsilon_c T_i^4}{C_o} - \frac{\sigma A_c(\epsilon_o + \epsilon_c) T_o^4}{C_o} \qquad (3)$$

Figure 3—Equations expressing change in temperature (Θ) from assumed base temperature (T) in life cell, inner and outer shields. Emissivity of inner shields (ϵ_i) is changed by displacement of outer shield.

The two extreme conditions explored were: *I*—Satellite between sun and earth, with maximum area of the adjustable shield exposed to radiation and *II*—zero heat input (i.e., Satellite completely surrounded by a perfect heat sink at absolute zero). For each of these conditions three different rates of heat generation were assumed constant per one hour, (*A*—maximum *B*—average, *C*—minimum) and the temperature change of the life cell was computed for the two settings of the shield.

The assumption of a residual rate of spin eliminates the necessity for calculating lateral temperature gradients in the skin.

Three simultaneous, linearized, first-order, non-homogeneous differential equations of the idealized thermal system were solved by the *Laplace transform* method, using a desk calculator. Results indicate that, for the assumed conditions, and surface properties of the radiators, fairly close control of life cell temperature can be achieved with only occasional shifting of the outer movable shield. However, before the proposed scheme may be considered acceptable, step-by-step calculations for a variety of possible conditions must be carried out.

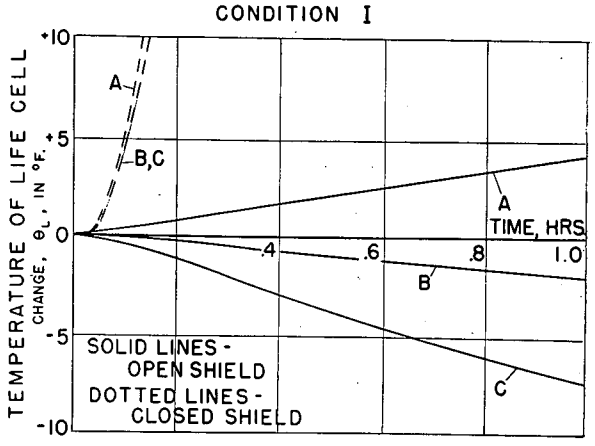

Figure 4—Temperature changes in life cell of Bio-Satellite, with thermal control shield of satellite receiving maximum amounts of radiation from sun and earth, and maximum (*A*), average (*B*) and minimum (*C*) internal heat generation.

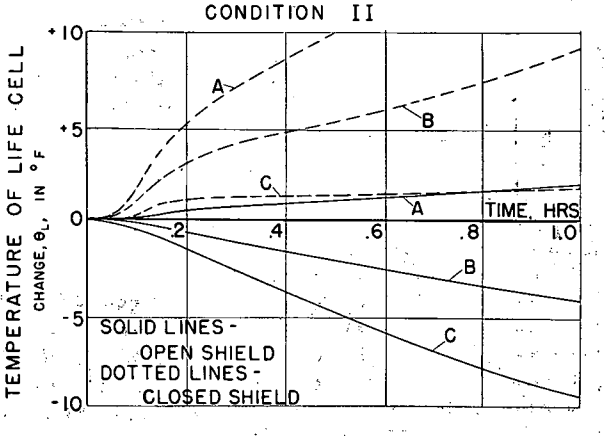

Figure 5—Temperature changes in life cell of Bio-Satellite, without external heat inputs, and with same rates of internal heat generation as in Figure 4.

SESSION X: General II

Chairman, L. E. Flory,

RCA Laboratories, Princeton, N. J.

10.1: Lighting Regimen and Experimental Method: Light-Synchronized Periodicity Analysis

Franz Halberg, University of Minnesota Medical School, Minneapolis, Minn., and Cambridge State School and Hospital, Cambridge, Minn.

MANY PHYSIOLOGIC functions show changes with periods of roughly 24 hours: circadian rhythms (*L.* circa-about and *L.* dies-day). When periodic environmental stimuli are eliminated as far as feasible, circadian rhythms may "free-run" from a 24-*h* clock and from each other, with periods that are of *about* 24-*h* length, but not necessarily of *exactly* that length. A schedule of light and dark alternating at 12-*h* intervals can serve most simply for equalizing the periods of different rhythms as well as for frequency synchronization of the animals' rhythms with the environmental schedule.

If observations are made in the absence of unusual stimulation, with standardized lighting, one does *direct* light-synchronized periodicity analysis. Maps in time for circadian rhythms at different levels of physiologic organization thus can be obtained; Figure 1. Such resolution of phase relations among periodic changes in health yields a refined standard of comparison for functional alterations in disease.

Indirect light-synchronized periodicity analysis involves application of an unusual agent under study in different phases of circadian rhythm: Separate groups of inbred mice with comparable past history are exposed, e.g., to noise or to a poison every 4 hours for 24 hours. Convulsions or death will or will not occur as a function of predictable circadian changes in the organism's physiologic state. Hours of diminished resistance to noxious agents, which may vary from one agent to the next, thus are disclosed; Figure 2.

Phase of rhythms *in relation to the 24-h clock hour* may be reset by shift of light-dark schedule, provided that one allows for the appropriate synchronization-time and for several other precautions (Halberg, F., Z. f. Vit., Horm. u. Fermf., in press).

During the synchronization time, rate of shift may change, being slow at first and faster thereafter (4-*h* shift in liver glycogen peak of mice during first 4 days after lighting inversion, 8-*h* shift during next 4 days) (Figure 3). During the second 4-day period following lighting inversion, corticosterone in mouse serum is released on the new schedule, while the glandular corticosterone rhythm, as yet, has not fully shifted.

Phase relations among some of the physiologic *rhythms themselves* change during the shift since synchronization times of different functions in the inbred mouse may differ from variable to variable (blood eosinophils versus pinnal mitoses) and from tissue to tissue (mitoses in pinnal epithelium versus liver parenchyma).

Change in period involving desynchronization from light-dark schedule after blinding (Figure 4) and alteration of certain rhythms after adrenalectomy also are revealed by light-synchronized periodicity analysis (Postgrad, Med., 24: 349; 1958). Direct light-synchronized periodicity analysis was applied to study of milk-agent induced breast cancer of C_3H mice (Figure 5): The mitotic rhythm in ear pinna was found altered before tumors became palpable. It cannot be decided whether this precancerous alteration of rhythm is an unspecific sign of agent activity or whether it underlies carcinogenesis.

Circadian periods characterize the rhythms in body temperature and blood eosinophils of human beings on "unacceptable" schedules. Desynchronization of temperature rhythm came to the fore in > 3% of a sample of N170 institutionalized patients, each studied for at least 100 days. Problems of frequency desynchronization of rhythm in man have been analyzed with electronic computer techniques which will be demonstrated.

Direct or indirect analysis of light-dark synchronized circadian changes (Figures 1 and 2) might contribute to *temporal resolution* of functional inter-relations, of the mechanisms involved in such time relations (Figure 6) and of their alterations in disease.

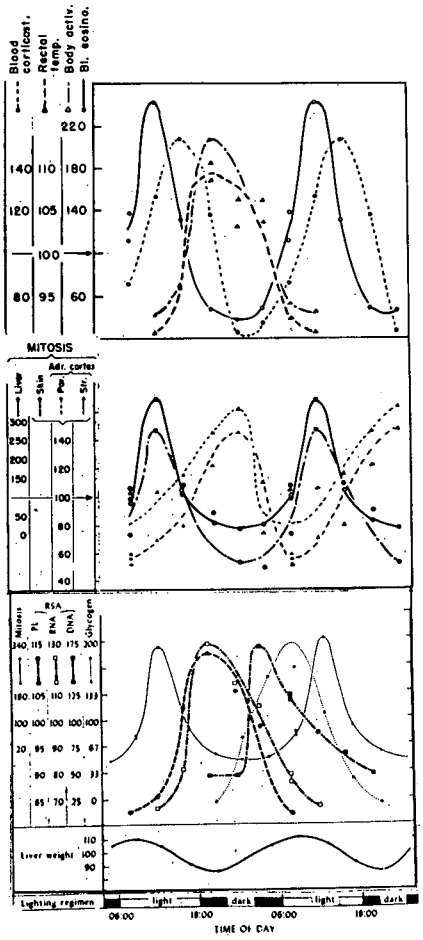

Body as a whole (activity), its core (temperature) and blood (eosinophils, corticosterone).

Different organs and tissues, (skin epidermis, liver parenchyma, adrenal cortical parenchyma and stroma).

Organ, different functions, (liver) ("formation" of phospholipid, of RNA, of DNA; glycogen content, mitoses, organ weight).

Figure 1—Functional frequency synchronization and phase relations of circadian rhythms at different organization levels.

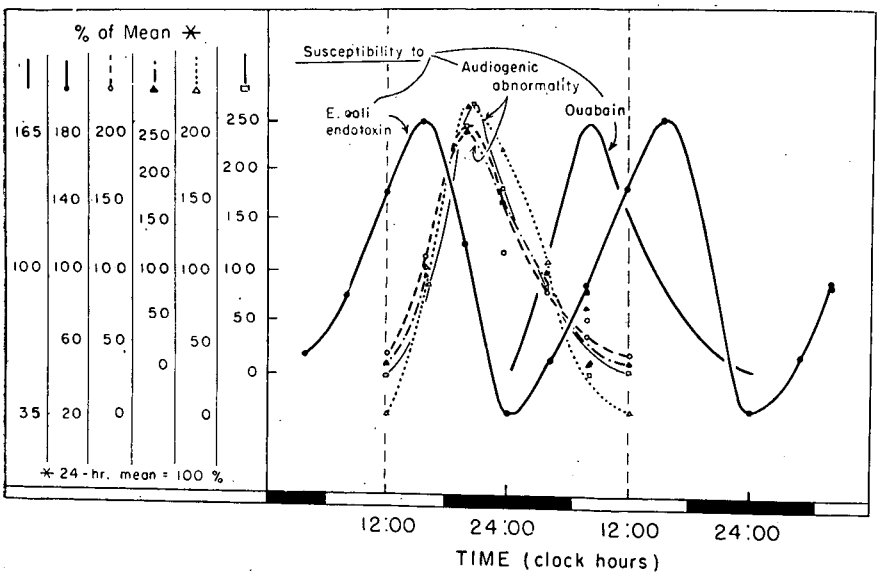

Figure 2 (Above)—Hours of diminished resistance.

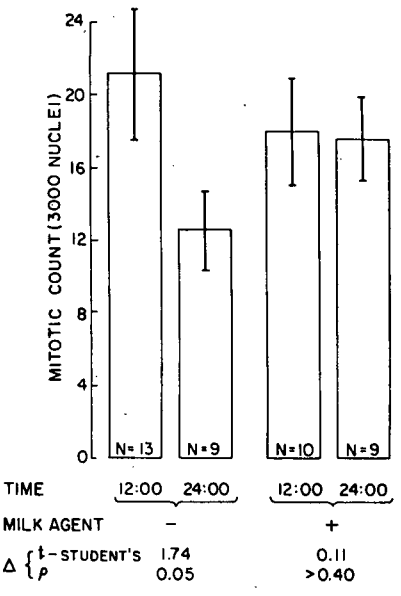

Figure 5 (Right)—Effect of milk agent upon mitotic rhythm in ear epidermis of female C3H mice, one year of age (*before* breast cancers are noted).

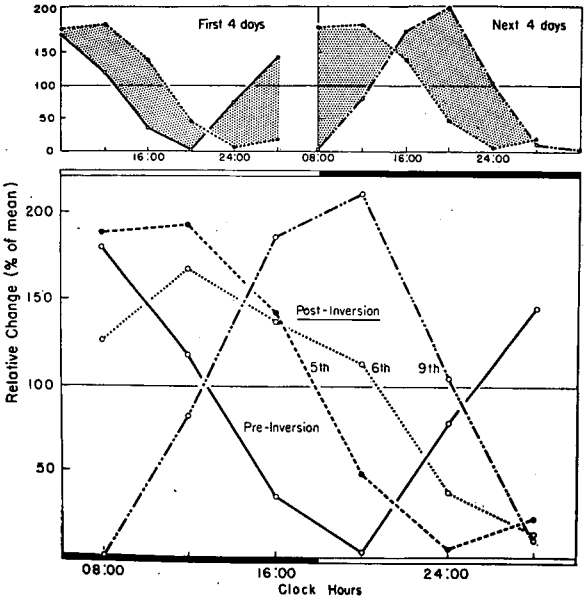

Figure 3 (Above)—Shift of rhythm in glycogen of mouse liver following inversion of lighting. Preinversion schedule with light from 06:00-18:00 (top).

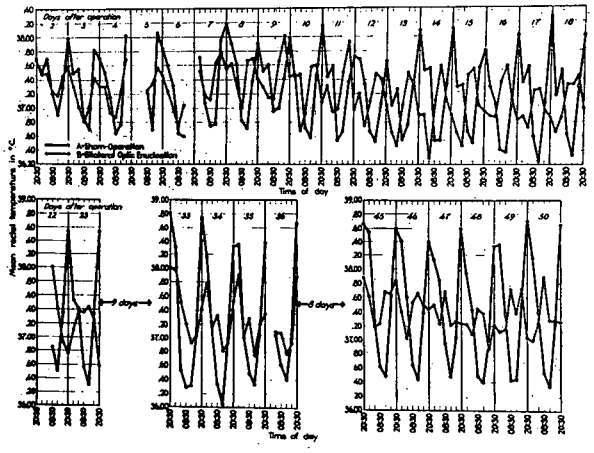

Figure 4 (Above)—The effect of bilateral optic enucleation upon the 24-hour rhythm in rectal temperature of male CBC mice.

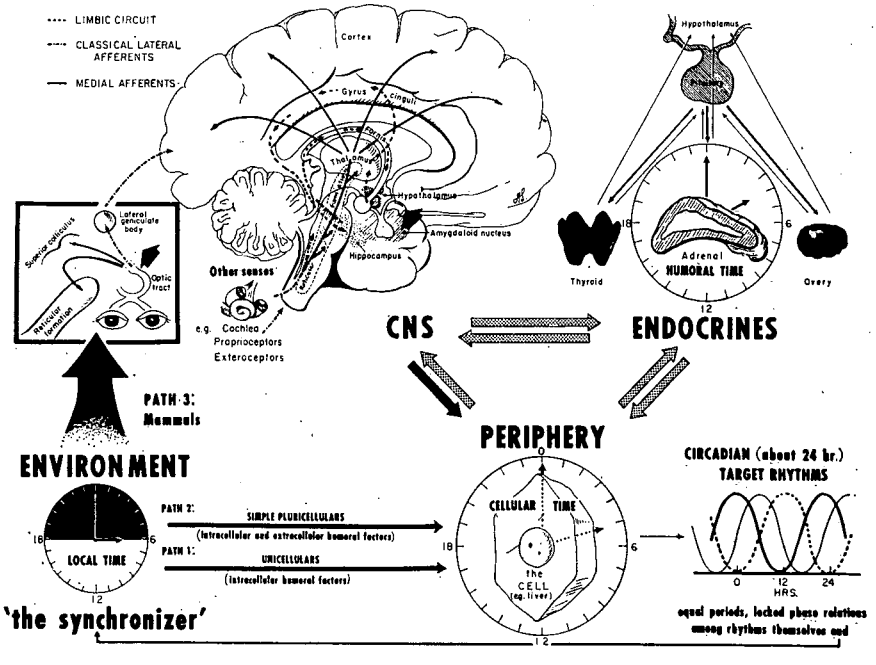

Figure 6 (Right)—Sketch of factors and pathways known or hypothesized to participate in frequency synchronization *among* circadian rhythms themselves, as well as in synchronization *between* rhythm(s) and environmental synchronizer(s).

SESSION X: General II

10.2: Control of Information Input by the Television Eye Marker

E. Llewellyn-Thomas and N. H. Mackworth, Defense Research Medical Laboratories, Toronto, Canada

THE TELEVISION EYE MARKER utilizes the corneal reflection of a light from the surface of the eye. This reflection appears as a bright spot, and its movements follow the subject's gaze. If it is viewed by a television camera, while the scene is viewed by a second television camera, and the outputs of the two cameras are combined, then the resultant picture on the monitor cathode-ray tube shows the scene with a bright spot superimposed, indicating the position of gaze[1].

If a matrix of photocells is mounted on the face of the monitor tube, then, besides being an indicator of eye movements and fixations, the eye spot can be used as a control mechanism. As each position on the tube face is correlated with a position of fixation in the subject's field, when he looks at that fixation point the equivalent photocell in the matrix is energized. The resultant photocell output can be used to operate circuits which vary the sensory input, in effect a feedback loop.

Thus, for example, in a meter display reproduced on a cathode-ray tube, or in a radar display, areas can be blacked out after they have been examined or, conversely, it can be arranged that only the area which is under visual inspection is illuminated. By the same method visual field defects such as hemianopsia or scotoma can be simulated.

In the clinical investigation of visual field defects, continuous and adequate fixation can be ensured by arranging for the photocell at the point of fixation to control the stimulus, so that it can only appear while the patient is correctly fixated. In this way we can make quantitative assessment of fixation as a factor in various types of amblyopia, and particularly in amblyopia exanopsia. Here, it would be especially useful in assessing the efficacy of treatment, particularly interesting because of the recent advances in the field of pleoptics. It should also enable us to measure and perhaps classify the types of pathological nystagmus.

A similar type of circuit is being used to investigate vision during saccadic eye movements. Here, the photocell is wired so that the stimulus cannot appear until the movement has actually started; that is, until the eye spot has moved away from the position of fixation and the photocell, no longer energized, has released the stimulus.

In this type of investigation a fairly short response time is required, for in short movements the eye rotates through one degree in about fifteen milliseconds. We are using at present a self generating selenium cell[2] with a single-stage CK 722 transistor amplifier.

Apart from using the eye movements to control the immediate information input, they can also be automatically recorded and used as a factor in deciding the future input. For this purpose the successive eye fixations can be recorded on punched tape, suitable for feeding directly into a programmed computer. Thus, they can be analyzed either for an investigation of what movements have taken place, or the analysis used for the automatic control of future stimuli.

The apparatus used for this type of recording is shown in Figure 3. The photocell output fires the first of six twenty-two millisecond one-shot square-wave multivibrators connected in series, so that the falling phase of each square wave triggers the next multivibrators in the chain. The outputs of the multivibrators are connected in parallel, and each photocell at the same time as it triggers the cascade also operates coded-gating circuits, so that the final output signal is in the teletype seven-element code. These signals are then recorded on a teletype printer-perforator so that each eye fixation is represented by a symbol by looking at it. At present, we are using a matrix of twelve photocells only, but the number can be increased. As the information rate is comparatively low we are able to use photocells of a higher wattage[3].

---

[1]Mackworth, J. F., and Mackworth, N. H., "Eye Fixations Recording on Changing Visual Scenes by the Television Eye-Marker", *J. Opt. Soc. Am.*, 48, 439; 1958.

[2]International Rectifier type B2M.

[3]Hupp CDS-10.

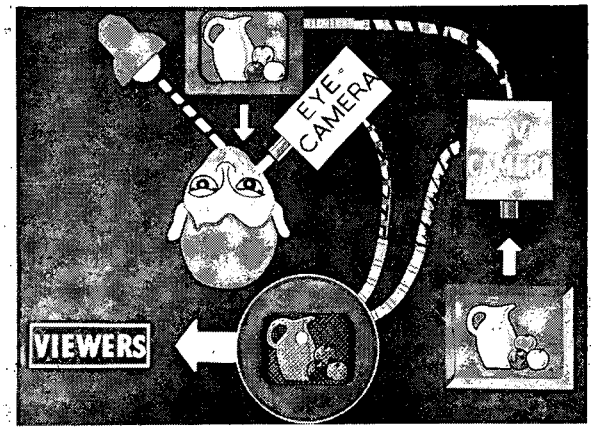

Figure 1—The television eye marker. Light reflected from the cornea is viewed by one camera and the scene by another. The two cameras outputs are mixed to give a composite picture.

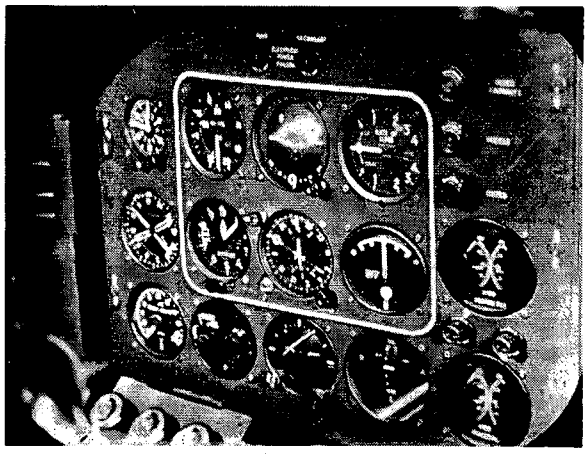

Figure 2—Eye-marker in use. The position of visual fixation shows as a bright spot of light in the composite picture.

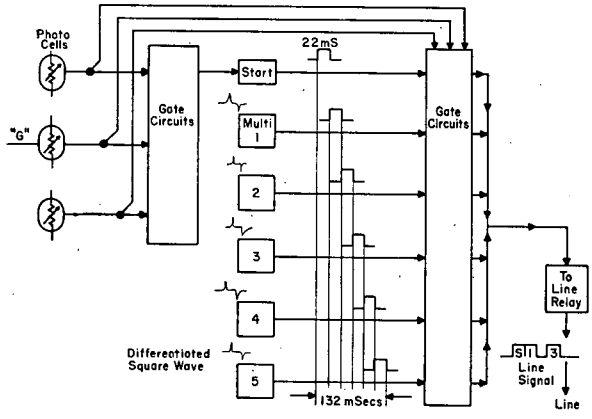

Figure 3—Coding circuit. When a photocell is illuminated by the eye-marker a signal in teletype code is applied to the line.

SESSION X: General II

10.3: A Fully Automatic Primate Test Apparatus with Response-Contingent Stimuli[1]

D. G. McConnell, D. R. Meyer and J. E. Alt, Laboratory of Comparative and Physiological Psychology, Ohio State University, Columbus, Ohio

A PRIMATE TEST UNIT, which uses stimuli projected by a television projector[2] and IBM cards for selection of stimuli, interpretation of responses and recording of data, has been developed. The unique departure of the present unit from the previous one[3] is its use of the projector — a random-access, 50-slide rotary drum machine—rather than film strip. This projector has been modified by adding a reverse-mounted stereo lens-pair and twin high-speed shutters across the lenses[4]. This permits simultaneous projection of figures from both halves of a 35mm slide-frame, and precise control of exposure time for each figure.

A particular slide is selected for projection by pre-punching its numerical index on an IBM card, which subsequently initiates rotation of the projector drum to the address of that slide.

When an animal inserts its head into a fixed-position mask, it sees the separate images rear-projected to two 4-inch square panels in the front of its compartment. It makes its discriminative response to the stimuli by pushing either of the panels. Whether or not the response is correct (rewarded by food delivery) is determined by a second pre-punched code number. Selection of the stimulus for the next discrimination trial is contingent upon the response. If the response is correct a primary slide is selected. An alternate slide is selected following an incorrect response.

A flow-chart of the electrical sequence appears in Figure 1[5]. With column *3* of the *punch card* at the punch station, and column *4* of the *read card* at the read station of the 526, the cards will not move, nor the stimulus be projected until the animal inserts its head into the mask, breaking a photobeam. This causes opening of the shutter and projection of the stimuli. It also causes unblocking of the column-*3* emit pulse, causing card-escape and punch-out of the column-*3* time digit. The column-*3* emit pulse also picks the *A*-selector relay. At approximately this time, the column-*4* read pulse travels through the sense-pin driving through the pre-punched hole in the read card, and after passage through the *A* selector picks the tens-digit relay of the primary index (i_p) for the next slide. The selector relays, since each filters several separate read pulses, are relatively slow and require double-pulsing to insure picking.

Punch-out of the column *4-6* time digits and delivery of the remaining *A* and *B* selector pick-pulses is automatic, since nothing blocks the column 4-6 emit pulses. The units-digit relay of the primary index (j_p) for the next slide is also automatically picked by the column-*6* read-pulse.

In punch-column *7*, the column-*7* emit pulse is blocked, causing the cards to stop, until the animal makes its discriminative response. When unblocked, the column-*7* emit pulse causes punch-out of the first response-time digit, with subsequent automatic punch-out of the remaining time-digits and the response code (*0* or *1*). The *C* and *D* selectors are picked by emit-pulses *7-8*, and *9-10*, respectively, while the tens and units relays for the alternate index (i_a,j_a) are picked by column-*8* and-*10* read pulses, respectively. The column-*11* and-*12* emit pulses must travel through a correct-incorrect net whose condition is determined by comparison of the discriminative response with the pre-punched code (x or y) in columns *8-11* of the read card. If the comparison is positive (response correct), these pulses exit through the primary index relays (i_p, j_p), while if it is negative exit is through i_a, j_a. This causes indexing of the slide drum to the appropriate position for the next trial, and punch-out of the corresponding numerical index in punch-columns *11* and *12*.

In punch-column *13*, a new trial begins.

---

[1]Constructed under grants G-6115 from National Science Foundation and M-2035 from National Institutes of Health.

[2]Sarkes Tarzian

[3]McConnell, D. G., Polidora, V. J., Friedman, M. P. and Meyer, D. R., "Automatic Reading and Recording of Digital Data in the Analysis of Primate Behavior", *IRE PGME Transactions, (Now being processed)*; 1959.

[4]Leitz

[5]Complete schematics available upon request.

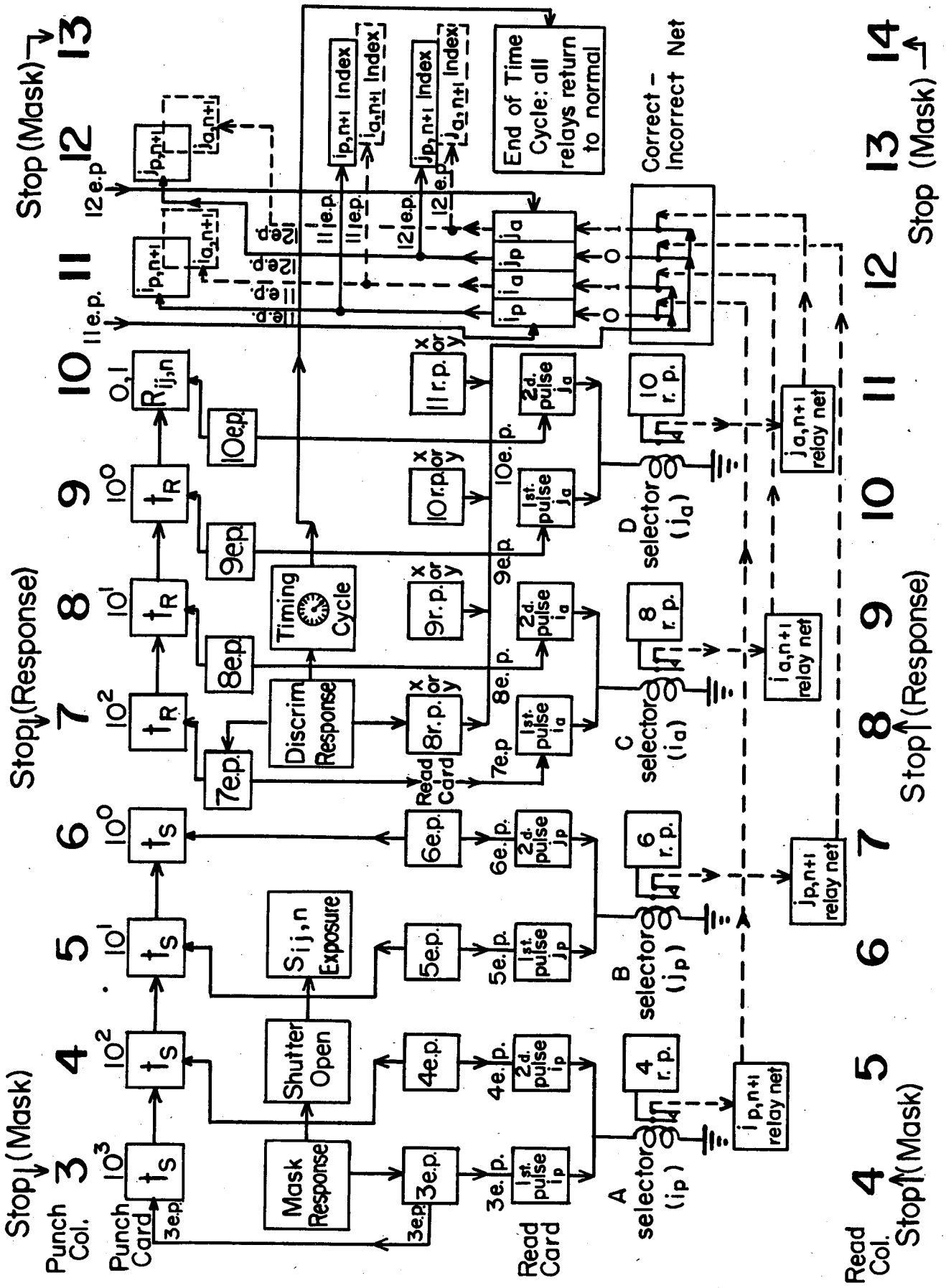

Figure 1—Automatic test apparatus (Mark II) flow chart. Notations are as follows: S_{ij} = ijth slide; t = time; n = trial number; i = tens index of projector, j = units index of projector; p = primary, a = alternate; x, y = response code for left or right; $R_{ij} = 0, 1$ = correct, incorrect.

SESSION X: General II

10.4: The Use of Punched Paper Tape in Animal Behavorial Testing

Murray E. Jarvik, Department of Pharmacology, Albert Einstein College of Medicine, Yeshiva University, New York, N. Y.

One of the Difficulties encountered in automatic testing of behavior in animals is that so much data are generated in a short space of time, that is both tedious and inaccurate to analyze by hand. Counters are cumbersome and limit the number of variables which can be measured simultaneously, particularly if time is an important variable (as in pharmacological studies). Pen-and-ink cumulative recorders suffer from the same defect. Both methods require interpretation involving human vision before further analyses can be made. The author has found the use of standard-5 level teletype paper tape an economical and convenient method for recording data in a form immediately amenable to automatic data analysis.

Responses of monkeys tested in a combined visual discrimination and delayed-response situation are coded via a relay network, and fed into tape punches.[1] The code is such that correct, incorrect, and premature responses, as well as the type of stimulus, plus the time may be indicated. In addition, the time elapsing between stimulus and response may be shown. The tape will accomodate 2^5 bits of information at a single punch, or 2^{10} for a double punch. Eight-level tape would accommodate more, but the punch equipment is correspondingly more expensive.

Two types of tape readers have been used to analyze the tapes, a standard teletype transmitter distributer which has been rewired to emit parallel rather than serial impulses, and a Wharf Mark II tape reader. The first reads 5 characters per second, and is connected to relay networks, counters, and a cumulative recorder. The second reads into an electronic and transistorized circuit at the rate of 60 characters per second. Examples of the use of this equipment will be given.

[1]Teletypewriter ARPE

Notes

SESSION X: General II

10.5: A Simplified Analog Storage and Averaging System for Electroencephalographic Responses

John F. Davis and W. R. D. Ross, Allan Memorial Institute of Psychiatry, McGill University, Montreal, Canada and H. A. Ferris, Sigma Technical Associates, St. Lambert, Quebec

THE MEASUREMENT of evoked electrical responses at the surface of the scalp involves problems which have absorbed the attentions of a number of investigators. At least a dozen systems have been developed in a half dozen centers. The difficulty of the problem is attested to by the fact that the search for a simple, yet accurate and reliable, method goes on.

It is known that almost any discrete stimulus is followed, after a characteristic lag, by a complex electrical response at the surface of the cortex (brain). This response is usually invisible at the scalp surface over such an area of cortex because of a high noise-to-signal ratio. To separate the very tiny, but predictable, signal from the unwanted and randomly related signals, including noise, the principle of integration is usually applied in some form. Well known names associated with systems utilizing this principle are *Dawson, Barlow, Rémond* and *Shipton*.

Our first system, described in 1957, consisted of two integrators, each gated to measure the response amplitude at a different point in time following the stimulus; we were interested in the ratio of responses at different time delays. Thus, for a given experiment (consisting of a series of 50 to 200 stimulations) only two points in the whole complex waveform could be plotted. It was soon realized that information about the whole response pattern was needed before the two points could be logically selected for comparison. The system to be described is intended to serve this function. It consists of a tape recorder for recording in reproducible form the stimulation series and the *EEG* responses. This tape is then made into a loop and played through a single gated integrator whose delay can be manually or automatically determined for the plotting of the average (integrated) response amplitude at any given point in time.

Figure 1 shows the scheme of the recorder. The repetitive stimulus is made random to avoid accidental synchronism with either line frequency or brain rhythms. The tape is dead (zero carrier) at the beginning of the test. First, the carrier is turned on, then after a 50-millisecond delay the stimulus is fired. The *EEG* signal is amplitude modulated onto the 1000-cps carrier and will contain the response to the stimulus. One of the functions of the pulse generator is to cut off the carrier for a fixed period just before each stimulus. This blank identifies the beginning of a new stimulus-response cycle. A limiter is inserted between the *EEG* amplifier and modulator to prevent accidental blanks in the carrier due to over modulation.

Figure 2 shows the tape, now in a loop containing the whole series of responses, playing back into a preamplifier and demodulator, thence through a gate relay to the integrator. The blanks in the carrier are identified by means of a limiter and detector and these start a variable run-down delay which eventually fires the gate pulse and operates the gate relay. This happens with each stimulus in the series. With each passage of the loop of tape, with its long blank at the loop joint, a motor is turned on to advance the variable run-down by one step. At the same time the integrator output is fed to the *Y*-axis of the *XY* recorder and the integrator is then discharged. *X*-axis information comes from the voltage setting of the run-down control. Thus, an automatic plot of the average of all the evoked responses on the tape is achieved.

It will be noted that, with recording at 3¾ ips and playback at 15 ips, the analysis proceeds at four times the speed of the original experiment. However, since as many as one hundred points may have to be plotted, the analysis can still run to several hours. Thus, there remains a need for techniques which will allow greater speed translation ratios to be used. At present, we are limited to a 4:1 ratio because of considerations of transient response and information bandwidth.

[1]Barlow, J. S. and Brown, R. M., "An Analog Correlator System for Brain Potentials", *Technical Report* 300, *Research Laboratory for Electronics, Massachusetts Institute of Technology;* 1955.
[2]Barlow, J. S., "A Small Analog Electronic Averager for Evoked Potentials of the Brain", *2nd International Conference on Medical Electronics*, Paris; 1959.
[3]Davis, J. F., "A Sensitive System for the Measurement of Brain Responses in the Intact Human", *IRE PGME Transactions*, 11:29; 1958.
[4]Dawson, G. D., "Cerebral Responses to Electrical Stimulation of Peripheral Nerve in Man", *J. Neurol. Neurosurg., Psychiat.*, 10:134; 1947.
[5]Rémond, A., "Au Sujet de L'intégration Progressive des Potentiels évoqués et de ses Variations Temporal Chez l'Homme", *J. Physiologie*, 50:484; 1958.
[6]Shipton, H. J., "A Simple Averaging Technique for the Study of Evoked Cortical Potentials in Man", *2nd International Conference on Medical Electronics*, Paris, France; 1959.

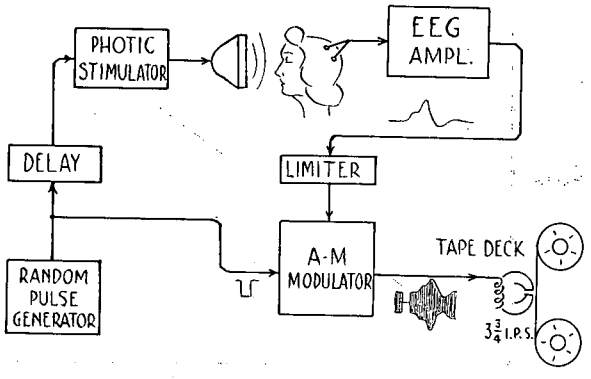

Figure 1—Amplitude-modulation tape recorder capable of recording *EEG* signals with a bandwidth of *dc* to 200 *cps* (1000-cps carrier).

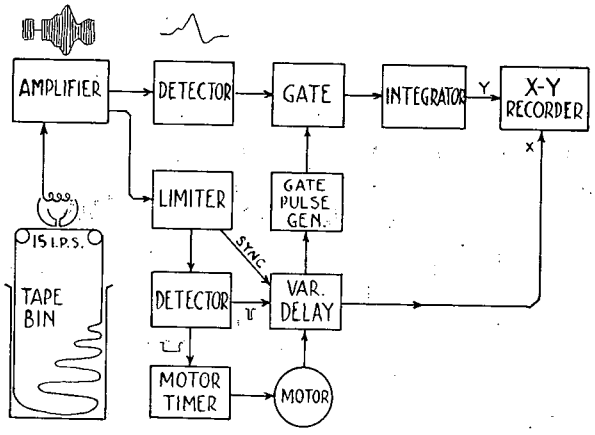

Figure 2—Demodulation, gate generation and integration system for averaging up to 200 responses to serial stimulation. Gate advances automatically with each cycle of the tape loop. Response outline is plotted automatically.

SESSION X: General II

10.6: A Transistorized Bio-Tachometer

Harve M. Hanish, Litton Industries, Los Angeles, Calif.

BIO-TACHOMETRY is the technique of automatically measuring time relationships of quasi-periodic biological signals.

Due to the nature of direct-writing oscillographs, amplitude is displayed on the *Y* or vertical axis as a function of time on the *X* or horizontal axis. Usually, we are primarily interested in the amplitude variations, but often we are interested in interval changes as well. The foregoing physical arrangement is convenient and conventional for the display of waveform amplitudes, but gives rise to difficulty in attempting to reduce visually or quickly reduce the data. This difficulty is caused by the relative inability of the human being to compare many parametric variations if they follow one another in a series arrangement; Figure 1*a*. It is much easier and faster if the variations of interest are turned 90° so that they may be compared side by side, Figure 1*b* and 1*c*. Knowing this frailty in our built-in, human, data-reduction system, techniques have been developed which automatically perform the conversion from serial variation to a parallel comparison display.

Regardless of what configuration the equipment might eventually take, the basic design approach is essentially the same. That is, the periodic variation is impressed upon a function whose amplitude varies linearly with time; Figure 2. It is thus readily seen that our parameter (variation of time) has been shifted from the horizontal axis to the vertical axis, where ease of comparison is enhanced.

Such instrumentation is not intended to supplant conventional techniques of recording analog bio-parameters such as the EKG. It is, however, intended to supplement these conventional methods to allow:

(*1*) Faster data reduction
(*2*) More information from the same signal in "real time."

There are ways of generating a function which varies linearly with time, as is required for a bio-tachometer. It must be remembered, however, that any such function must be capable of being returned to its zero level at any time. This consideration negates approaches such as the motor-driven potentiometer. One successful design has been the use of a simple series *RC* network which is charging to a relatively high potential; Figure 3. The incoming signal is utilized as a trigger to activate a mechanism which discharges the capacitor thus returning the output level to zero. In some cases the charge on the capacitor is merely sampled by another parallel capacitor, and then the network is discharged. Whatever the method, the voltage at any instant is proportional to time elapsed. It is obvious that this method fulfills three predominant design criteria for medical equipment; it is simple, cheap — and it works.

The drawbacks to this simple approach lie in the inherent non-linearity, Figure 3, of *RC* networks, (except over a narrow range). To utilize this design, one must either recalibrate the usual linear graph paper on a direct writer to correct for this non-linearity, or operate the system at a very low level over the relatively linear part of the charging curve.

It was felt that a unit could be designed and constructed which would utilize state of the art developments in electronics and still result in a simple, low-cost, reliable, and linear bio-tachometer. Basically, the design approach uses a 2-transistor ramp generator in a *Miller* integrator configuration. The incoming signal is clipped to remove the negative portions and then amplified to trigger the ramp generator back to its zero state. If the signal is of a sinusoidal nature (such as respiration), instead of periodic spikes, an optional zero-crossing detector can be used first to generate the necessary waveform. A front-panel control adjusts the clipping level in such a manner that lower amplitude signals (which are unwanted and might have a tendency to trigger the unit) are rejected. The resultant linear ramp is coupled from an emitter follower which is part of the integrator circuit. Such an emitter follower coupling has several distinct advantages. It supplies a very low-impedance output which makes signal contamination unlikely; and simultaneously gives a healthy power gain which is capable of driving a typical galvanometer pen motor directly.

The output of this system is a series of sawtooth waveforms whose amplitude is proportional to the time interval between signals. In EGK interval measurements, a *qrs* spike of 1 volt is sufficient to trigger reliably the bio-tachometer. A typical system diagram is shown in Figure 4.

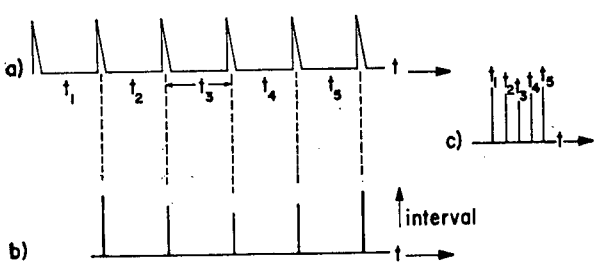

Figure 1—(*a*) Simulated *QRS* spike of the *EKG*. Note difficulty in discerning difference in intervals t_1, t_2, etc. (*b*) Interval converted to amplitude. Notice ease in discerning changes. (*c*) Same as (*b*) above, except recording speed is reduced for greater readability.

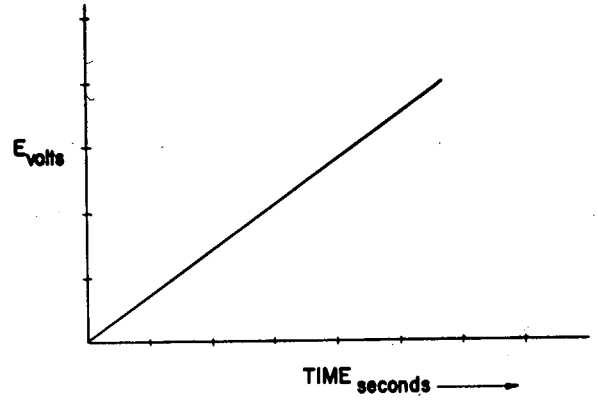

Figure 2—Linear function of voltage versus time.

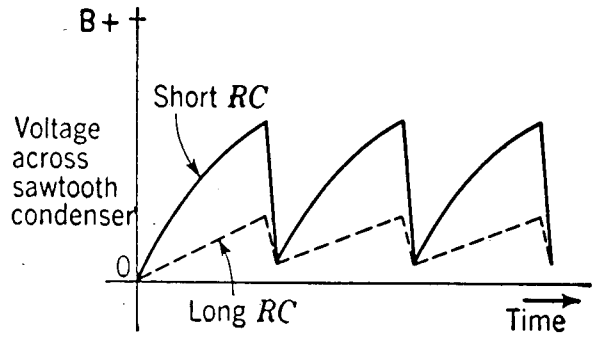

Figure 3—Typical curves showing voltage as a function of time across the capacitor of a series *RC* network. Shorter time constant gives higher amplitude, but poor linearity. Longer time constant allows better linearity, but lower amplitude.

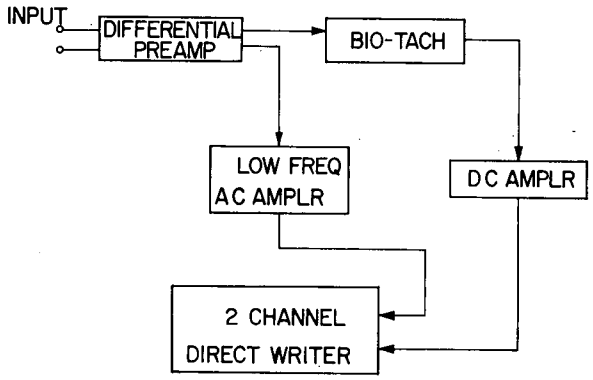

Figure 4—Typical installation block diagram of instrumentation using bio-tachometer. A zero-crossing detector can be inserted in series between preamp and tachometer if necessary.

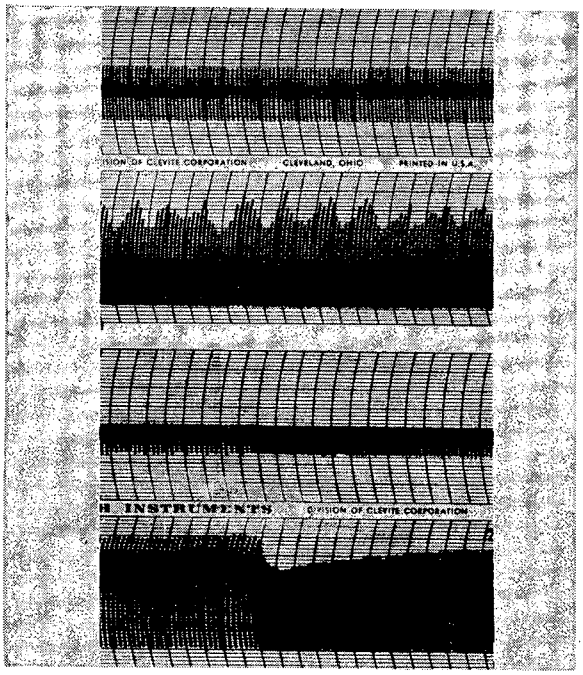

Figure 5—Tracings from system described in Fig. 4. Traces *1, 3* are *EKG; 2, 4* are tachometer output. Traces *1* and *2* were taken on a resting gopher snake, showing changes in cardiac rate due to respiratory activity (approx. 20 beats/minute over respiratory cycle). Traces *3* and *4* were taken on a Pacific rattlesnake suddenly stimulated by lighting his totally darkened cage. The rattlesnake consistently experienced an increase of 15 to 30 beats per minute upon stimulation.

(Tracings courtesy H. S. McDonald, Dept. of Zoology, UCLA.)

SESSION XI: Infrared Radiation II

Chairman: J. D. Hardy,

School of Medicine, University of Pennsylvania

11.1: The Predictability of Thermally-Induced Epidermal Injury

F. C. Henriques, Technical Operations, Inc., Burlington, Mass.

In 1947, *Henriques* and *Moritz* showed through hot water and hot-air exposure of both human and pigskin that a knowledge of the time-temperature history (T_t) of the basal-epidermal layer, due to an exposure to heat, suffices to predict the threshold criteria for transepidermal necrosis. This prediction is expressed quantitatively by what has now become known as the skin-damage integral, namely

$$\beta = 3.1 \times 10^{98} \int_0^t e^{-\Delta E/RT_t}\, dt$$

where ΔE = the activation energy, 150,000 cal/mol; R, the gas constant, = 2 cal/mol-°K; and T_t is the temperature in degrees *Kelvin* of the basal epidermal cells at the time (t) in seconds measured from the initiation of the hyperthermic episode. The quantity, β, is a quantitative measure of thermal cutaneous injury, such that:

when $\beta < 0.5$ there is no occurrence of irreversible epidermal injury,

and when $\beta > 1.0$ there is occurrence of irreversible transepidermal injury.

In 1952-54, *Pierce, Mixter,* etc., of the University of Rochester Medical School, developed the experimental equipment required to produce reproducible flash-burns in pig. The skin-damage integral was then extended to predict quantitatively their data. In order to make these predictions T_t had to be computed for pigskin subjected to flash-burns. This calculation required judicious estimates of the numerical values of two constants necessary to solve the complicated unsteady-state heat equations.

Recently, *Ross, Moritz,* et al, of the Institute of Pathology of Western Reserve University, managed to measure experimentally the thermal gradients in skin of pigs and rats during and following flash-burns. From these data the numerical values of the same two constants can also be derived. The values so calculated check remarkably well with those previously used to predict epidermal injury.

SESSION XI: Infrared Radiation II

11.2: The Temperature Response of Skin Exposed to Penetrating and Non-Penetrating Radiation*

Thomas P. Davis, Department of Radiation Biology, University of Rochester School of Medicine and Dentistry, Rochester, N. Y.

THE DETERMINATION of the temperature response of skin to a specified exposure is a problem of considerable importance in the investigation of the radiant energy burn. Such information is necessary for the study of the kinetics of thermal injury. This response is determined as soon as the details of a given radiant exposure have been translated into the equations which describe the transient flow of heat through skin, and the interactions of the tissue with the impinging radiation and with its environment. The numerical values of the constants appearing in the various equations are most directly evaluated by temperature response measurements under conditions such that analytical solutions of the governing equations can be obtained. It is not difficult to make exposures which approximate the following idealized conditions:

(1) The receiver is a passive, isotropic, semi-infinite solid; *(2)* Initially, this solid is at uniform temperature throughout; *(3)* The surface of the solid is exposed uniformly to the incident radiation; *(4)* The surface of the solid is insulated against all heat losses. With an additional assumption concerning the tissue-energy interaction, analytical solutions can now be obtained.

Non-Penetrating Case: Opaque Solid Model

In this case, it is assumed that the radiation is either reflected or absorbed at the mathematical surface of the solid; Figure 1. There are two constants, the "thermal" constants, to be determined. The thermal inertia *(1)*, μ, can be found from the surface response, while the thermal diffusivity, α, is evaluated from subsurface measurements; Figure 2.

The experimental work in this laboratory *(2)* was performed on young, anesthetized Chester White pigs, exposed to radiation from a carbon-arc image furnace. The skin was made opaque by painting it with India ink. Temperatures were measured with 50μ diameter silver-palladium thermocouples. The average thermal constants of pig skin were found to be:

Thermal inertia, $\mu = 11.7 \times 10^{-4}$ cal^2 cm^4 deg^{-2} sec^{-1}

Thermal diffusivity, $\alpha = 8.4 \times 10^{-4}$ cm^2 sec^{-1}

From these may be calculated:

Thermal conductivity, $k\,(=\sqrt{\mu\alpha}) = 10 \times 10^{-4}$ cal cm^{-1} deg^{-1} sec^{-1}

Heat capacity per unit volume, $v\ (=\sqrt{\mu/\alpha}) = 1.2$ cal cm^{-3} deg^{-1}

Penetrating Case: Diathermanous Solid Model

Here it is assumed that the radiation penetrates the solid and is absorbed only in depth. It is now necessary to specify the energy absorption per unit volume of material as a function of depth. For a highly scattering and complex structure such as skin, this not a simple problem. Further, for heterochromatic radiation, it is not possible to obtain a completely generalized solution (Figures 3 and 4). However, under the above assumptions, the energy absorption per unit volume at any depth can be determined directly from the initial time rate of change of temperature at that depth, and the data can be tested rigorously for their validity; Figure 5.

Experiments similar to those described were performed, omitting the India ink coating. The experimentally determined values were found to be seriously in error. The cause of this error was almost certainly the direct heating of the thermoelements by the penetrating radiation.

Conclusions

For the case of non-penetrating radiation heating, predicted and measured temperature responses of skin are in good agreement, and the thermal constants of this tissue are known. It follows that reasonably reliable temperature data are available for the study of the kinetics of thermal damage to opaque skin.

For the case of penetrating radiation heating, the accurate prediction of temperature response in skin is not yet possible. Much remains to be done on the problems of temperature measurements in a scattering diathermanous material and in the investigation of radiant energy absorption within such a medium.

---

*This paper is based on work performed under contract with the Atomic Energy Commission at the University of Rochester Atomic Energy Project, Rochester, New York.

[1]The term "thermal inertia for surface heating" was coined by J. D. Hardy. See Lipkin, M. and Hardy, J. D., "Measurement of Some Thermal Properties of Human Tissues", *J. Appl. Physiol.* 7:213; 1954.

[2]Davis, T. P. "A Theoretical and Experimental Investigation of the Temperature Response of Pig Skin Exposed to Thermal Radiation", *University of Rochester Atomic Energy Project Report UR-553*; 1959.

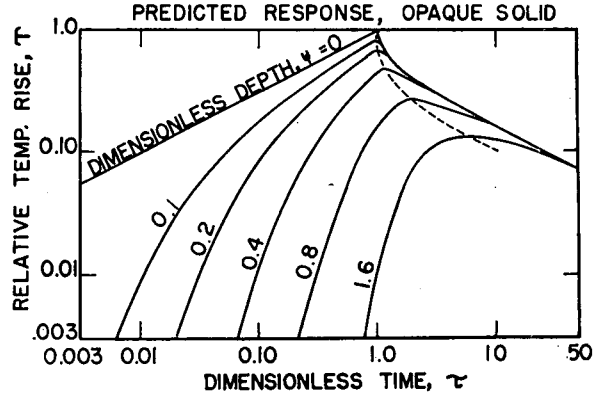

Figure 1—Relative temperature rise ($\Delta T\ \sqrt{\pi\mu}/2\ H_a\ \sqrt{\eta}$) of semi-infinite opaque solid for rectangular absorbed irradiance pulse, H_a, of duration η sec, as a function of dimensionless time (t/η) and dimensionless depth, ($x/2\ \sqrt{\alpha\eta}$); μ = thermal inertia and α = thermal diffusivity.

OPAQUE SOLID

RECTANGULAR IRRADIANCE PULSE, OF DURATION η sec

(A) SURFACE RESPONSE:

$$\frac{U(0,t)}{Ha\sqrt{\eta}} = \frac{2}{\sqrt{\pi\mu}}\sqrt{\frac{t}{\eta}}, \quad 0 \le \frac{t}{\eta} \le 1,$$

WHERE μ = THERMAL INERTIA,

(B) DEPTH RESPONSE,

$$\frac{x}{\sqrt{\eta}} = 2\sqrt{a}\left(\frac{\frac{t_{max}}{\eta}\left(\frac{t_{max}}{\eta}-1\right)}{2\ln\frac{\frac{t_{max}}{\eta}}{\frac{t_{max}}{\eta}-1}}\right)^{\frac{1}{2}}$$

WHERE a = THERMAL DIFFUSIVITY

Figure 2—Equations for the evaluation of thermal constants of "opaqued" skin. For surface response, U = temperature rise, H_a = absorbed irradiance, and t = time. In depth, x = depth for which temperature rise is maximum at time t_{max}.

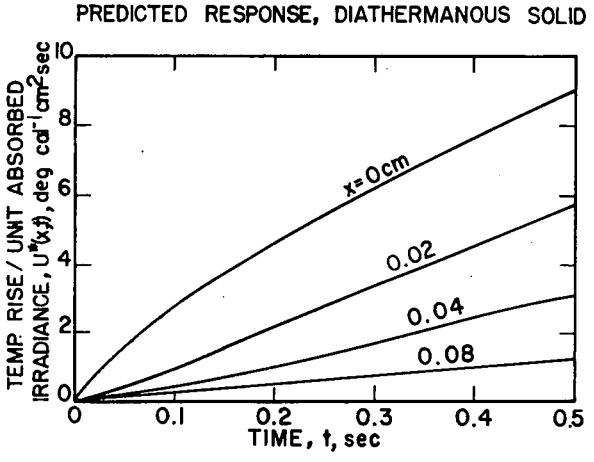

Figure 3—The predicted temperature-rise per-unit absorbed irradiance for the particular case of white pig skin exposed to an irradiance step function pulse from a carbon arc image furnace. Optical constants of skin from literature.[2]

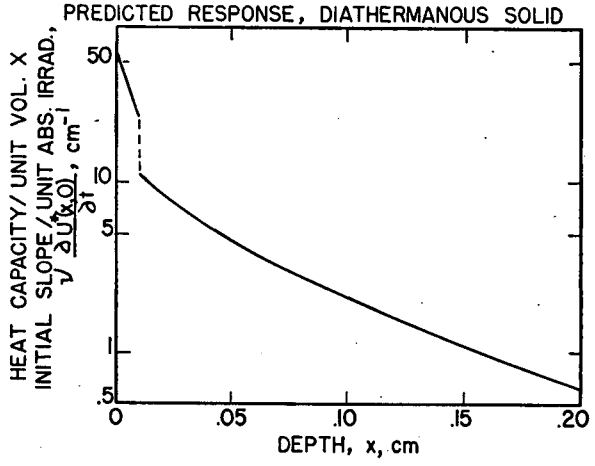

Figure 4—The product of initial time rate of change of temperature per-unit absorbed irradiance and heat-capacity per-unit volume as a function of depth. The particular conditions are as specified for Figure 3.

DIATHERMANOUS SOLID

STEP FUNCTION IRRADIANCE PULSE

(A) UNDER SUITABLE CONDITIONS:

$$\nu\left[\lim_{t\to 0}\frac{\partial U(x,t)}{\partial t}\right] = q'''(x),$$

WHERE q''' = POWER ABSORBED PER UNIT VOLUME

(B) FROM CONSERVATION OF ENERGY:

$$\frac{\nu}{Ha}\int_0^\infty\left[\lim_{t\to 0}\frac{\partial U(x,t)}{\partial t}\right]dx = 1$$

Figure 5—Under conditions described in reference,[2] the rate of energy absorption in skin exposed to penetrating radiation is proportional to the initial time rate of change of temperature rise, U. The measurements must satisfy energy conservation.

SESSION XI: Infrared Radiation II

11.3: Some Thermal and Optical Properties of Rat Skin

G. P. deLhery, W. L. Derksen and T. I. Monahan, Naval Material Laboratory, N. Y. Naval Shipyard, Brooklyn, N. Y.

The Naval Material Laboratory has employed albino rats as biological instrumentation in studying the protection of personnel against the thermal radiation of nuclear detonations. Since thermal damage is associated with the skin's temperature history during insult, an understanding of the heat flow processes associated with these burns demands a knowledge of such temperatures and, therefore, of the thermal and optical constants of the medium. The Laboratory has measured the $k\rho c$ product (k, conductivity; ρ, density; c, specific heat) and the effective extinction coefficient of anesthetized rat skin. Using experimental burn data for rat skin, the burn severity which a human may incur in a given situation may be estimated from the thermal and optical constants of both media.

Bare and blackened rat skin was exposed to square-wave pulses of carbon-arc and tungsten (3000°K) radiation for exposures ranging from 0.5 to 25 seconds. Radiant exposures causing maximum temperature rises less than those required to produce burns were normally employed. The temperature of the skin at the surface was measured before, during and after the exposures by means of fine-wire copper-constantan thermocouples. The rat skin was blackened through use of a suspension of graphite in oil.

The temperatures of the blackened rat skin are shown as function of time in Figure 1. Assuming that blackened rat skin behaves thermally as an opaque homogeneous semi-infinite solid, its temperature rise should be proportional to the square root of the exposure time. Using opaque solid theory, the $k\rho c$ product was computed for the temperatures corresponding to exposure times less than 10 seconds, giving an average value of 10.6×10^{-4} cgs units. For longer exposures the $k\rho c$ product increases, as shown in Figure 2, to 15×10^{-4} for the temperature rises for 24 seconds. The increase in $k\rho c$ could result from a variation in the skin's thermal properties with depth or it could result from a systemic reaction to temperature, involving a change type of heat flow for extended exposures. Most exposures of cloth-covered skin resulting in burns involve temperature histories longer than 10 seconds, even for very short thermal pulses. Rigorous application of the $k\rho c$ product to situations involving long exposures is questionable.

The temperature of the surface of bare rat skin for the carbon arc and tungsten sources are shown in Figure 3. The higher transparency for carbon arc radiation, with its greater proportion of visible to infrared energy, is apparent.

The $k\rho c$ value for rat skin, 10.6×10^{-4} cgs units, is significantly higher than the value, 8.6×10^{-4}, found for human skin. Consequently, for many burn situations the temperatures for human skin will be 10 per cent higher than those for rat skin. The temperatures in depth will have second-order differences caused by differences in thermal diffusivity ($k/\rho c$), as well as those resulting from difference in $k\rho c$.

Using the $k\rho c$ values and the relationship for the temperature rise in a semi-infinite diathermous solid, the effective extinction coefficients of rat skin were computed for the two sources in interest (Table 1); for the data for human skin from a previous investigation are included. The time variation of the effective extinction coefficient is most probably caused by the wavelength selectivity of rat skin to the penetration of carbon arc radiation, an effect similar to that observed for human skin. As the data show, the temperatures of the rat skin were higher for tungsten than for carbon-arc radiation. As the lower extinction coefficient indicate, carbon-arc radiation is relatively more penetration for rat skin than tungsten radiation, whereas it is less penetrating for human skin. Undoubtedly the difference in temperatures caused by the two spectra is caused by the higher penetration of radiation in the blue part of the visible spectrum, a fact which may be deduced from the high reflectance of rat skin over human skin in this spectral region.

Time	Rat Skin		Human Skin	
	Carbon-arc	Tungsten	Carbon-arc	Tungsten
sec	cm-1	cm-1	cm-1	cm-1
0.5			188	64
1	26	32	80	45
2	20	23	45	30
5	15	17	31	22
10	12	14	23	21
15	8	12		
20	7			26
35	5			

Table 1—The effective extinction coefficients, γ, are tabulated for human and rat skin. Notice that rat skin is more diathermous to the tungsten radiation than it is to carbon arc, while the opposite holds for human skin. However, on the whole rats are shown to be more diathermous than humans in all aspects.

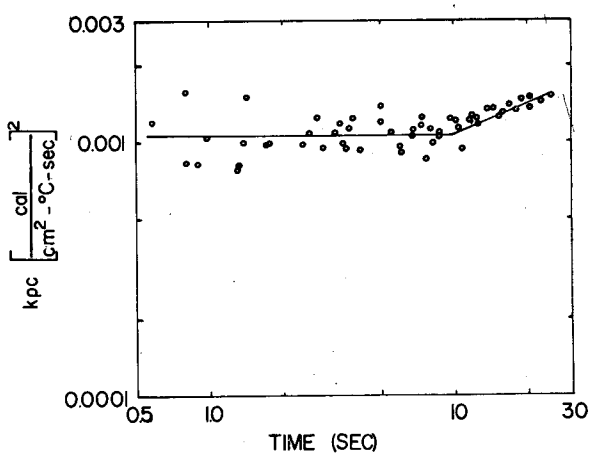

Figure 1—The apparent effect of time of exposure on the $k\rho c$ product of the anesthetized rat skin is illustrated in this graph. Each circle represents an experimental episode. Both abscissa and ordinate are logarithmic.

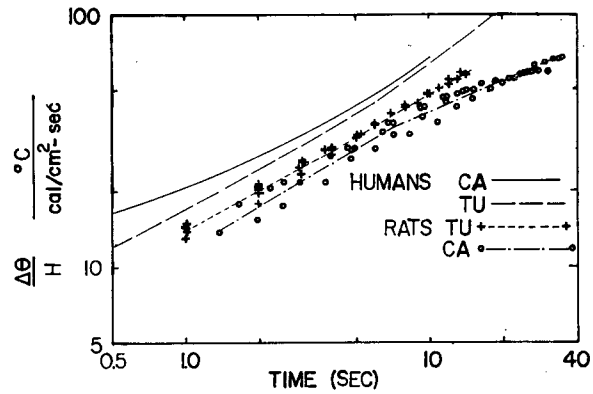

Figure 2—The temperature rise-per-unit irradiance as a function of reference time is illustrated here for bare rat and human skin. Circles represent exposure of rats to carbon-arc radiation while the crosses represent rat exposure to the tungsten lamp operated at 3000°K. In all cases the human temperatures are higher than those of rats for similar conditions. Coordinate are logarithmic.

SESSION XI: Infrared Radiation II

11.4: Skin Simulants Employed in Thermal Burn Studies

W. L. Derksen, G. P. deLhery, T. I. Monahan, Naval Material Laboratory, New York Naval Shipyard, Brooklyn, N. Y.

THE NAVAL MATERIAL LABORATORY conducts investigations on the protection of clothing against burns as part of its larger program on the effects of thermal radiation. To facilitate these investigations a skin simulant employing an inert material and relying on physical measurements has been developed.

In its present development the material consists of a hard, durable resin, urea formaldehyde, mixed with 40 per cent by weight of fine silica powder to attain the proper thermal conducting properties. The simulant is molded under pressure and at high temperatures.

The temperature history determined by an embedded fine wire thermocouple is employed as the physical parameter to be correlated with burn severity.

The thermal properties of trial materials and those of human skin were determined from the measured surface temperatures of the material or skin, when irradiated. The final proportion of ingredients for the skin simulant was chosen to make the surface temperatures correspond to those of skin when both are blackened. A $k\rho c$ product (χ, conductivity, ρc, volumetric specific heat) of 8.6 x 10^{-4} cgs units, matching that of skin, was determined from the surface temperatures shown in Figure 1. A value of 20.5 x 10^{-4} for the thermal diffusivity, $k/\rho c$, was determined from the depth temperatures. Figure 2 shows the normalized temperature histories at a depth of 0.05 cm in the skin simulant.

The skin simulant's diffuse spectral reflectance is shown in Figure 3.

The complexity of the temperatures of diathermous media resulting from exposure to thermal radiation is illustrated in Figure 4 by the temperature histories of the uncovered and unblackened simulant. Because of the selectivity of diathermancy with wavelength and the scattering properties of the skin simulant material the heat flow mechanism is complex and cannot readily be expressed with constant parameters. The surface temperatures, however, are very close to those of skin so that for many situations it is useful to employ the simulant temperatures, with slight corrections, to obtain a measure of bare human skin temperatures in a given situation.

The skin simulant in its present form has been employed successfully to study the protection given by clothing against thermal radiation burns. Because of the actual temperature measurement, the skin simulant gives quantitative and continuous response in complex situations. With the simulant we have determined the necessary control to be established on various parameters such as contact pressure, humidity and air supply for realistic reproducible experiments in clothing protection studies. The relative importance of the various heat transfer mechanisms causing burns under clothing has been determined, as well as the temperature histories of skin associated with burns caused by thermal radiation for uncovered as well as cloth covered skin. Skin simulants have been employed in the field during nuclear detonations to evaluate laboratory methods employed in studies of thermal radiation effects.

The inertness of the skin simulant constitutes a limitation in its use in that the simulant would indicate temperatures different that those of skin in situations in which skin would react by a mechanism such as increased blood flow. Its inertness, however, permits a quantitative measurement of the effect of such systemic reactions by comparing the measured temperatures of the skin and of the inert simulant in a given situation. The thickness of the simulant is 1.1 cm and, unless the mounting serves as a heat sink, exposures longer than 500 seconds are in error by more than 5 per cent. The thermocouple, while of negligible thickness to affect conducted heat, is opaque and intercepts a portion of the radiant energy which may enter the medium. The effect of this local absorption is not apparent except for exposures of less than 0.2 second duration. The startling effect of excessive temperature transients at local opaque layers can be seen in Figure 4 for the shortest exposure.

The skin simulant has proved to be a valuable tool for laboratory and field experiments. It is durable and gives precise and reproducible results.

Figure 4 (Right)—The temperature histories at 0.05 cm in the skin simulant for exposures from 0.2 to 20 seconds. These histories reveal the complex heat flow in a diathermanous scattering medium, by their differences from those of Figure 2. Abscissa = time (sec).

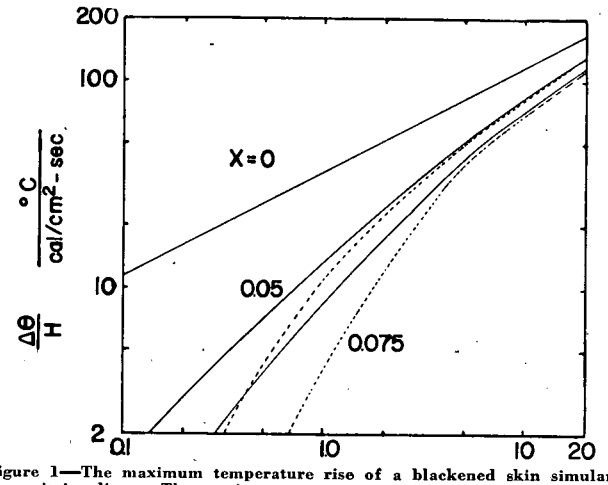

Figure 1—The maximum temperature rise of a blackened skin simulant for unit irradiance. The maximum temperature of the surface and at two depths is given. The dotted lines give the temperature at the cessation of irradiance. Abscissa = exposure time (sec.)

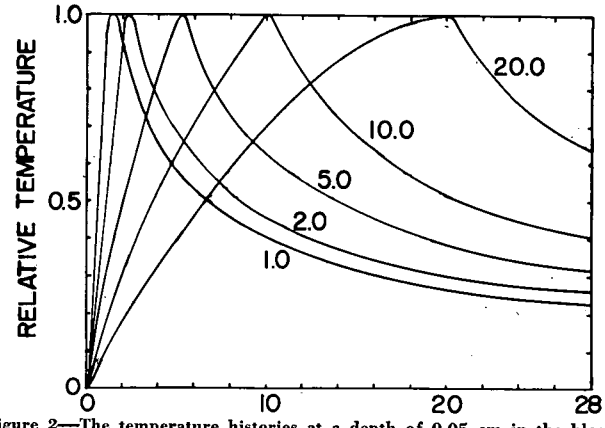

Figure 2—The temperature histories at a depth of 0.05 cm in the blackened skin simulant for exposure times from 1 to 20 seconds. These curves are precisely calculable from simple heat flow theory. Abscissa = time (sec.)

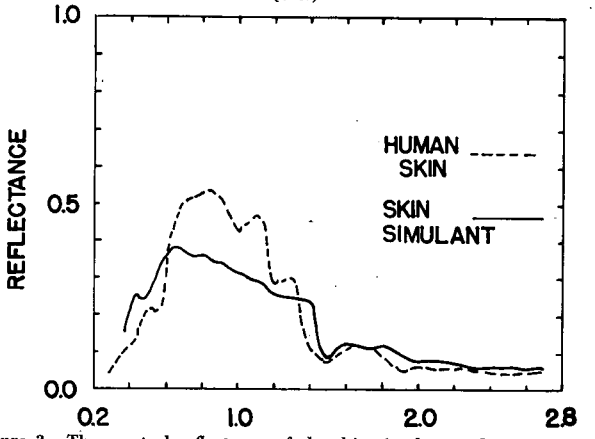

Figure 3—The spectral reflectance of the skin simulant and of an average human skin. The total absorptance for a carbon arc spectrum is 0.72, the same as that for human skin. Abscissa = wavelength (microns)

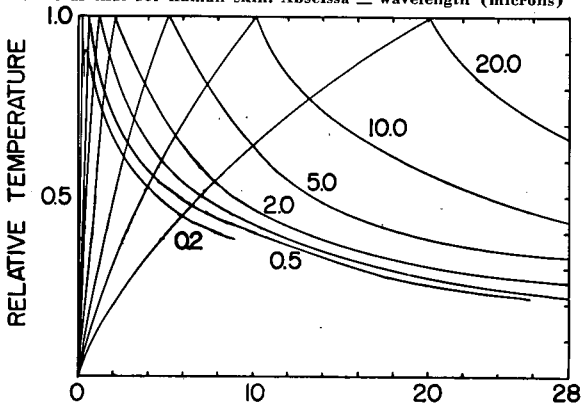

SESSION XI: Infrared Radiation II

11.5: The Effect of Intense Thermal Radiation upon Textile Materials

A. J. McQuade, U. S. Quartermaster Research and Engineering Center, Natick, Mass.

THIS PAPER will point out that in the evaluation of fibres suitable for military clothing there are three important qualities under consideration. These are as follows:

(a)—Resistance to energy transfer

(b)—Resistance to destruction

(c)—Physical properties of fibres required to make strong lightweight fabric suitable for hot weather wear.

The approach followed has been previously described and involves the use of a paper-making technique to cast fibres cut in short lengths in the form of a mat to approach the weight and thickness found in a 5 ounce-per-square yard cotton poplin fabric. The fibres are dyed whenever possible to attain equal energy absorption and reflectant.

In a previous report, data were presented showing the superiority, from the standpoint of resistance-to-energy transfer of flame-resistance cotton fibre, as well as a specific blend of nylon with cotton. Superiority shown was in comparison with several other existing synthetic and natural fibres.

The performance of materials such as these two has been considered by some to be related to the evolution of heat during their decomposition. This has not been fully subscribed to by others, including the author. Rather, the postulation was advanced that their good resistance to energy transfer was due to the fact that in their decomposition, a barrier layer of carbon-like fibre was formed, which resisted further decomposition and absorbed nearly all the energy applied.

With this thought in mind, it was logical to investigate carbon-like fibre. The first of this type investigated was introduced in 1953 and was formed by heat-treating fabric made from acrylonitrile fibre. Work at that time showed such a material to be highly resistant to destruction by radiant energy, but was highly conductive.

Using some of the fabric produced in 1953, in the outer layer in a space ensemble, it became apparent that this material was more resistant to decomposition than existing fibres. Also, it exhibited good resistance to the transfer of energy. Examination of the physical properties of this type of fibre showed that while its strength was of a low order, it might be adequate provided its elastic property were similar to that of wood.

Fibres, based upon graphite, showed similar results with the exception that their strength appeared to be lower than that found for heat-treated acrylonitrile material.

Other fibres investigated have been acrylics modified to impart flame resistance and those based upon glass. In the case of the modified acrylic there susceptibility to melting and thus forming a hole through which the incident energy could be readily transmitted was the first principal defect. Those of acysilica base provide good resistance to destruction when in an uncolored state. However, particularly those of glass have been destroyed when colored to 10% reflectance using carbon black.

In short, there do not exist today textile fibres with the three needed criteria.

SESSION XI: Infrared Radiation II

11.6: The Use of an Inanimate Skin Simulant in Evaluating Thermal Energy Transfer through Cloth to Skin

Nai-Yuen Chen, Department of Chemical Engineering, Massachusetts Institute of Technology, Cambridge, Mass.

RECENT STUDIES on the effect of high-intensity thermal radiation on skin and cloth-protected skin indicate that knowledge of the temperature history of the skin should contribute to the understanding of the energy transport processes governing the mechanism of thermal injuries to skin. Tests on live animals are expensive and time consuming. In addition, accurate measurement of the skin temperature in the region of interest is very difficult. Second-degree burns, for example, occur within 80 μ of the skin surface and the temperature gradient is consequently very great in this thin layer. An alternate approach which has been adopted by the author at MIT is to use an inanimate skin simulant in place of live animals.

For a given time-energy relationship, a material may be said to simulate skin when there is for every depth, L_s, below the surface of the skin, a corresponding depth, L_{ss}, in the simulant where the temperature history is identical. Two basic conditions must be met, i.e., *(1)* the steady-state thermal resistances of the two systems must be equal, or,

$$\frac{L_s}{k_s} = \frac{L_{ss}}{k_{ss}} \qquad (1)$$

and *(2)* the unsteady state requirement, the energy storage capacity of the two systems, must be equal, or,

$$L_s C_s \rho_s = L_{ss} C_{ss} \rho_{ss} \qquad (2)$$

Equations *(1)* and *(2)* yield the following relationship,

$$(kC\rho)_s = (kC\rho)_{ss} \qquad (3)$$

Thus, it is only necessary to match the product of k, C and ρ, not the individual quantities.

Equations *(1)* and *(2)* also show the relation between the corresponding depths in real and simulated skin. The ratio of the two is given the name "stretch factor, a" which is equal to:

$$a = \frac{L_{ss}}{L_s} = \sqrt{\frac{(k/C\rho)_{ss}}{(k/C\rho)_s}} \qquad (4)$$

A skin simulant of high stretch factor would allow one to measure the temperature distribution in a thick slab equivalent to that of a very thin skin layer without much difficulty.

Unfortunately, there are no known homogeneous materials which fulfill the condition prescribed by equation *(2)* while having a stretch factor of *10* or higher. The possibility of achieving such objectives can be realized, however, if one uses the combined properties of a metal (such as copper, which has high thermal conductivity and high volumetric heat capacity) and air (negligible thermal conductivity and heat capacity) in forming a heterogeneous skin simulant. If air is sandwiched between thin sheets of copper, the effective thermal conductivity and volumetric heat capacity of the combined system are reduced to:

$$k_{ss} = f\,k_{Cu}; \quad (C\rho)_{ss} = f\,(C\rho)_{Cu} \qquad (5)$$

Knowing the properties of copper, the volume fraction of copper, f, in a properly designed skin simulant depends on the value of $(kC\rho)_{ss}$, or,

$$f = \sqrt{\frac{(kC\rho)_{ss}}{(kC\rho)_{Cu}}} \qquad (6)$$

Figure 1 illustrates the general principles of skin simulation. The line of constant $kC\rho$, based on the value of 8.5 x 10^{-4} cal^2 - cm^{-4} - sec^{-1} - °C^{-2} agreed upon in the AFSWP conference at Technical Operations, Inc., as the value for standard human skin[1], is a straight line of slope equal to minus one on the logarithmic coordinates. A scale of stretch factor is constructed on this line ranging from *1* (skin) to *80*. The design values of f and a for the copper-air simulant have been calculated and plotted on the graph. It is seen that the copper-air skin simulant has a stretch factor of *28.4*.

An important limitation of the simulants made to date is that they are opaque semi-infinite solids, i.e., the diathermanous properties of human skin are not simulated. In addition, skin is assumed to possess constant, uniform physical properties; and on the basis of recent work by *Davis*[2] of Rochester this is considered a reasonable assumption for low level burns (such as second degree or less). Plainly, diathermancy cannot be a factor in the temperature distribution within irradiated skin if the latter is covered with opaque materials. One or more layers of closely-woven fabric adequately approximate this condition.

Figures 2 and 3 show two of the satisfactory designs of the copper-air skin simulant. To make these simulants truly semi-infinite solids, i.e., heat flows in one direction only, elimination of heat sinks and lateral heat flow in their design are of primary importance. Temperature measurement is accomplished by thermocouples consisting of fine constantan wires (0.001 inch in diameter) soldered to the copper element. Recently, the technique of electroforming the copper top plate onto the concentric copper cylinders has been perfected. With this improvement, the uncertainty in depth due to the presence of solder between the top plate and the cylindrical elements in the older models is eliminated.

The importance of using either live animals or properly designed skin simulants in evaluating the effectiveness of any protective covering for skin exposed to high-intensity thermal radiation will become clear after considering the following example. Suppose in one experiment, a layer of cloth is placed over an insulator such as a block of foam glass; while in another experiment, the cloth is placed over a conductor such as a block of copper. Under a given time-energy flux condition that would scorch the cloth in the first experiment, the cloth in the second experiment may remain completely intact. Thus, the behavior of the protective layer depends very much on the type of backing placed behind the test sample, and no meaningful data can be obtained if the backing does not adequately simulate the thermal properties of a backing of interest. The copper-air skin simulants described in this paper provide quick and simple means for allowing one to obtain the temperature history at various simulated skin depths under various exposure conditions. From these data, the effectiveness of the protective covering can be evaluated. Another possibility is to use the response of the skin simulant in deriving the mechanism of energy transport through the overlying layer to skin. This should be valuable for the eventual understanding of the governing processes in the complicated system, cloth-covered skin.

Nomenclature:

a=Stretch factor, dimensionless

C=Heat capacity, cal/gm -°C

f=Volume fraction of copper in the copper-air skin simulant dimensionless

k=Thermal conductivity, cal/cm-sec-°C

L=Thickness, cm

p=Density, gm/cm^3

Subscript:

Cu=Copper

s=Skin

ss=Skin simulant

[1]AFSWP Conference at Technical Operations, Inc., Arlington, Mass.; 1955.

[2]Davis, T. P., "A Theoretical and Experimental Investigation of the Temperature Response of Pig Skin Exposed to Thermal Radiation", *PhD Thesis*, University of Rochester; 1959.

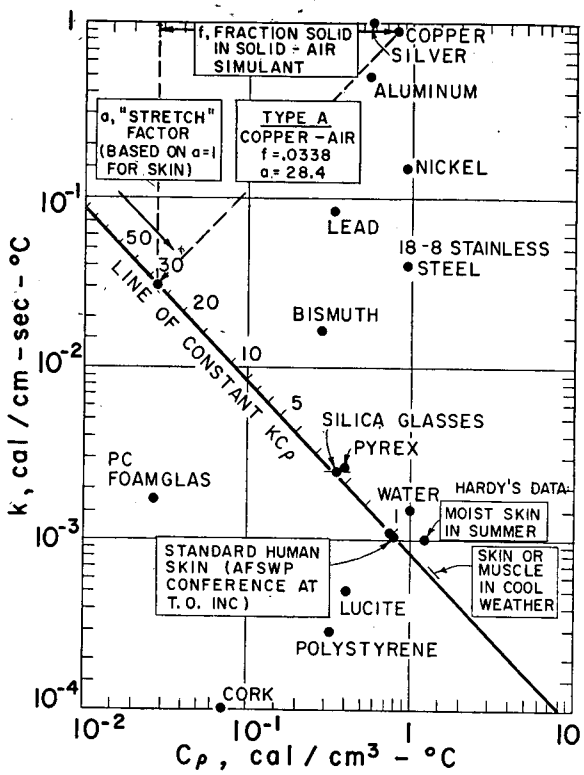

Figure 1—Graphical representation of the principles of skin simulation.

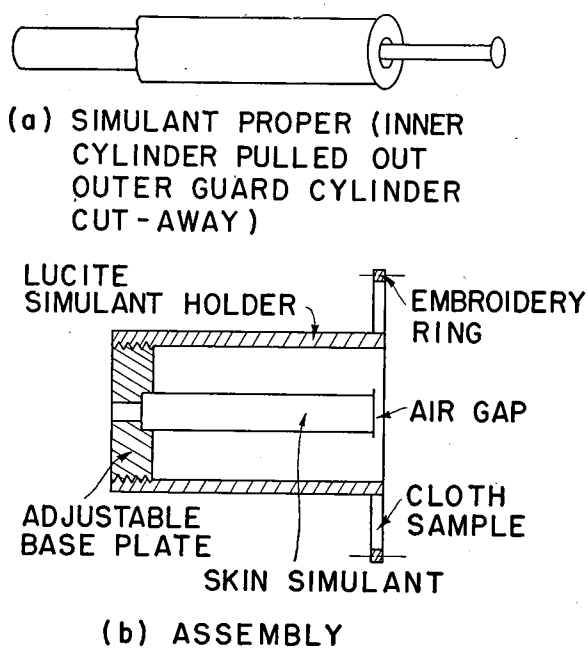

Figure 2—Skin simulant No. 10.

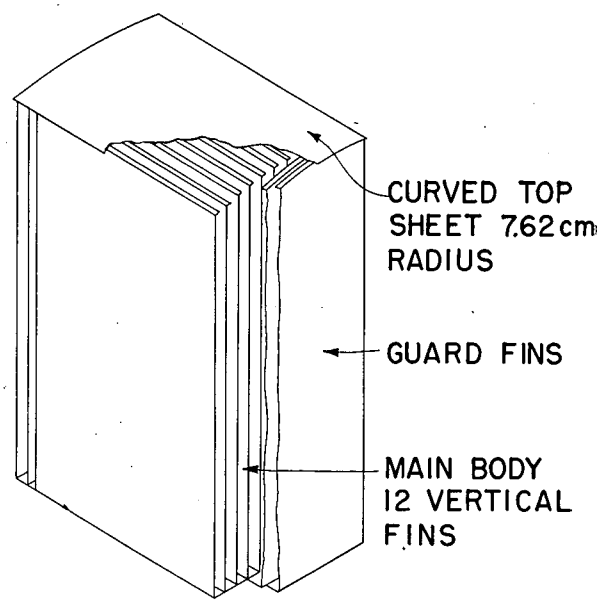

Figure 3—Skin simulant No. 11B.

12th Annual Conference on Electrical Techniques in Medicine and Biology

EXHIBITORS

Booth: *8* American Edelstaal, Inc.
350 Broadway, New York 13, N. Y.

On Display: Unimat-Miniature Machine Shop

In Attendance: *Ralph A. Heineman,* Sales Manager
Marvin Zweier *Ralph Pulliam*

Booth: *7* American Electronic Laboratories, Inc.
121 N. 7th Street, Philadelphia 6, Pa.

On Display: Cuvette Oximeter for Use with Whole Blood, Hemolyzed Blood and as a Densitometer for Fox Green Dye; Also on exhibit: Intracardiac Phonocatheters, High-Gain Wideband DC Amplifiers, Ultrahigh Impedance Wideband Amplifiers, Electronic Battery and Dual-Beam Oscilloscope

In Attendance: *R. D. Freedman,* Sales Manager
John Busser, Division Head, Instrumentation

Booth: *31a* American Institute of Electrical Engineers

On Display: AIEE Medicine-Biology Activity Reports, Institute Journals

Booth: *6* Baltimore Instrument Company, Inc.
716 West Redwood Street, Baltimore 1, Md.

In Attendance: *Eugene Heydemann,* President
Joseph deCastellane, Sales Manager
Waldemar Poppe, Sales Representative

On Display: Universal Stereotaxic Instrument—Operating Table for Animals — Microscopes and Microphotographic Equipment

Booths: *32a-33a* Bell Telephone Manufacturing Co.
1, Francis Wellesplein, Antwerp, Belgium

On Display: Counter Computer

In Attendance: *F. J. G. Van den Bosch*
Clyde Yost

Booth: *29a* Biophysical Electronics, Inc.
400 Northern Boulevard, Great Neck, N. Y.

On Display: Continuous Blood Pressure and Pulse-Rate Monitors, Wide-Range Electronic Timers, Data-Processing Equipment

In Attendance: *J. Malverne Benjamin, Jr.,* President
William Halpern, Vice President
Daniel Berger, Engineer

Booth: *5a* The Decker Corporation,
45 Monument Road, Bala Cynwyd, Pa.

On Display: Blood Pressure-Pulse Wrist Pick Up, Ophthalmic Pulse Pick Up (Electronic Goggles), Cardiodynameter, Fetal Heart Pick Up

In Attendance: *Theodore Kaslow, Vice President—*
Engineering
Betty Brown, Chief, Biology Dept.
Livingston Morris, Project Engineer

Booth: *1* Diapulse Manufacturing Corp. of America
350 Fifth Avenue, New York 1, N. Y.

On Display: Diapulse Unit and Oscilloscope; Historical Exhibit of Ideas Concerning Application of High-Frequency Currents to Living Organism

In Attendance: *Jesse Ross,* President
Bernard O. Siler, General Sales Manager
Mathilde N. Shapiro, Director of Professional Relations

Booth: *30a* Lester A. Dine Company
Levittown, New York

On Display: Clinical Photographic Equipment for Close-up Photography—Featuring Eastman Kodak Startech Camera

In Attendance: *R. Ussak,* Assistant Sales Manager

Booth: *4a* 4a Keithley Instruments, Inc.
12412 Euclid Avenue, Cleveland 8, Ohio

On Display: DC Research Amplifiers, Electrometers, Micro-microammeters, Micro-voltmeters, Static Meters

In Attendance: *Paul Saint-Amour,* Field Sales Manager
A. D. Oliverio, Dist. Mgr., Wash., D.C.

Booth: *9* Minneapolis-Honeywell-Heiland Division
5200 East Evans Avenue, Denver 22, Colo.

On Display: Direct-Recording Visicorder Oscillograph Medical Console

In Attendance: *Dean Trautner,* Engineer
Bill Ware, Field Engineer
Henry Rivitz, Field Engineer

Booth: *5* Institute of Radio Engineers

On Display: Professional Group, Medical Electronics Transactions, IRE Proceedings

Booth: *3* Laboratory of Technical Development
National Heart Institute, Bethesda, Md.

On Display: Liquid Flowmeter Based on Nuclear Magnetic Resonance Phenomena and Gas Chromatograph Detector Based on Measurement of Sound Velocity

In Attendance: *Vsevolod Kudravcev* *Robert L. Bowman*
Frank W. Noble

Booth: *2* Sanborn Company
175 Wyman Street, Waltham 54, Mass.

On Display: Advanced Design Electrocardiographs—Instruments for Diagnostic Applications; also Biophysical Research—Single and Multi-Channel Recording Systems, Monitoring Oscilloscopes, Physiological Transducers.

In Attendance: *L. A. Busenkell*
Don Coburn

Booth: *25a* Arthur H. Thomas Company
Third at Vine Street, Philadelphia 5, Pa.

On Display: Laboratory Apparatus

In Attendance: *D. E. King, Sales* *H. Schurr,* Sales
G. Kleinstuber, Sales

Booth: *24a* Yellow Springs Instrument Company, Inc.
P.O. Box 106, Yellow Springs, Ohio

On Display: Thermistor-Based Temperature Measurement and Control Instruments; also Psychophysiological Instruments and Blood-Gas Analysis Equipment

In Attendance: *Raymond I. Schiff,* Sales Manager
Hardy W. Trolander, President

Booth: *4* Electromedical Lab.
University of Pennsylvania

On Display: Transistorized Portable Electronic Hematocrit

Booths: *26a-27a* Veterans Administration
U. S. Public Health Service
G. Baum and I. Greenwood

On Display: Panoramic Visual Illustrating the Application of Ultrasonic Locating Techniques to Ophthalmology

12th ANNUAL CONFERENCE on ELECTRICAL TECHNIQUES in MEDICINE and BIOLOGY

CONFERENCE SCOPE

THE INTERACTION of non-ionizing forms of radiation with biological matter and advancements in electrical techniques in medicine and biology will be covered during the 11-session three-day program of the 12th Annual Conference on Electrical Techniques in Medicine and Biology. More than 40 papers will be presented in special sessions concerned with ultraviolet, infrared, microwaves and ultrasound. More than 20 additional papers will be concerned with cardiovascular techniques and instrument advances in the field of bio-medical electronics.

ADDITIONAL COPIES of the *Digest of Technical Papers,* priced at $4.00 per copy, may be obtained from H. G. Sparks, The Moore School of Electrical Engineering, University of Pennsylvania, 200 South 33rd St., Philadelphia 4, Pa. Remittance should be made out to the order of: 12th Annual Conference, Electrical Techniques, Medicine and Biology.

ALL TECHNICAL SESSIONS will start promptly at designated hours.

EXHIBITS

AN EXHIBITION AND DEMONSTRATION of the latest electromedical equipment and accessories are featured in the East Ballroom of the Hotel Sheraton.* Among those exhibiting are: Bell Telephone Manufacturing Company, Minneapolis-Honeywell Regulator Company (Heiland Division), Sanborn Company, Lester A. Dine Company, American Electronic Laboratories, Inc., Baltimore Instrument Company, Inc., Yellow Springs Instrument Company, Inc., Arthur H. Thomas Company, The Decker Corporation, Biophysical Electronics, Inc., American Edelstaal, Inc., Keithley Instruments, Inc., U.S. Public Health Service - Veterans Administration - G. Baum and I. Greenwood, Electromedical Division—Moore School of Electrical Engineering—University of Pennsylvania, National Heart Institute-National Institutes of Health.

SHOW HOURS ARE:

Tuesday,	Nov. 10	12:00 Noon—9:00 P.M.
Wednesday,	Nov. 11	12:00 Noon—9:00 P.M.
Thursday,	Nov. 12	9:00 A.M.—12:00 Noon

REGISTRATION . . . TOURS

CONFERENCE FEES ARE:

Registration	(General	$6.00
	(Student)	2.00
Cocktail-Buffet (Nov. 11)		2.00

TOURS:

Tuesday P.M. (Nov. 10)	
Air Crew Equipment Lab.....	$1.00
Wednesday P.M. (Nov. 11)	
Institute for Cancer Research.....	1.00
Thursday P.M. (Nov. 12)	
Electromedical Lab.—Johnson Foundation for Medical Physics, University of Pennsylvania	1.00
Friday—All Day (Nov. 13)	
RCA Labs—Princeton University, Princeton, N. J.	2.00
Friday—All Day (Nov. 13)	
Naval Air Devel. Center, Johnsville.....	2.00

CONFERENCE COMMITTEE

Chairman: Dr. Herman P. Schwan, University of Penna.
Secretary: Dr. Duncan A. Holaday, University of Chicago
Treasurer: George Barnes, Barnes Development Company
Program: L. E. Flory, RCA Laboratories
Publicity-Exhibits: Carl Berkley, Rockefeller Institute
Local Publicity: Joseph Fisher, Philco Corporation
Local Arrangements: John Reid, H. G. Sparks and Prof. O. Salati, University of Pennsylvania
Registration: Matthew Conrad, Consultant
Elizabeth Brown, Decker Corporation
Exhibits-Publication Manager: Lewis Winner, Consultant

JOINT EXECUTIVE COMMITTEE

Chairman: Dr. H. P. Schwan, IRE-AIEE
Vice-Chairman: Dr. R. L. Bowman, ISA
Secretary: Dr. D. A. Holaday, ISA
Members: Dr. Otto H. Schmitt, IRE
L. E. Flory, IRE
Carl Berkley, IRE
L. G. Cumming, IRE
R. S. Gardner, AIEE
G. C. Riggle, AIEE
H. S. Kindler, ISA

The Joint Executive Committee acknowledges with pleasure the support of the Conference by the Rome Air Development Center of the Air Research Development Command, U.S. Air Force.

*Presence of displays or products on Exhibit Floor does not constitute an endorsement of the Joint Executive Committee.

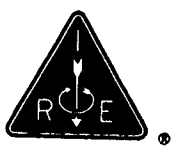
I
R E


A
E E
I


I
S A
INSTRUMENT
SOCIETY
OF
AMERICA